UNIVERSITÄT ZU LÜBECK

FROM THE INSTITUTE OF ANATOMY
OF THE UNIVERSITY OF LÜBECK
DIRECTOR: PROF. DR. MED. JÜRGEN WESTERMANN

PRENATAL EXPOSURE WITH ANTIBIOTICS DOES NOT INFLUENCE EXPERIMENTAL ALLERGIC ASTHMA IN MICE

Dissertation
for Fulfillment of Requirements for the Doctoral Degree
of the University of Lübeck

From the Department of Natural Sciences

Submitted by
Imke Lingel
from Elmshorn

LÜBECK, 2020

First referee: Prof. Dr. med. Peter König

Second referee: Prof. Dr. rer. nat. Jens Mittag

Date of oral examination: 26. January 2021

Approved for printing. Lübeck, 26. January 2021

Thore gewidmet

1 Summary

Analyzing the impact of prenatal antibiotics on asthma is of considerable interest, since life style changes known to change the microbiota were connected to an increased risk to develop asthma. Environmental factors that can influence the microbiota of the child are maternal diet, mode of delivery, formula feeding *vs*. lactation, and antibiotics exposure in pregnancy or early life. A study on prenatal antibiotics exposure and newborn immunity by the Deshmukh laboratory at the Cincinnati Children's Hospital Medical Center generated a prenatal antibiotics exposure mouse model and found that prenatal antibiotics exposure led to a high susceptibility of the mice to newborn pneumonia. The susceptibility was caused by a lack of gut microbiota-immune cell interaction, preventing protective immune cells from migration to the lungs. Using the same mouse model but an extended exposure duration to postnatal day 14, the Lewkowich laboratory in Cincinnati analyzed the impact of antibiosis on a well-established C57BL/6 HDM-driven asthma mouse model. Mice exposed to antibiotics until postnatal day 14 developed a severe asthma phenotype compared to the control mice, which included impaired lung function, increase in mixed T_H2/T_H17 responses associated with asthma severity, and neutrophilia. Given the knowledge that prenatal antibiosis induced changes in newborn immunity in terms of newborn pneumonia, we investigated for this study, if alterations induced by prenatal antibiosis persist long-term and can induce a severe asthma phenotype. Interestingly, naïve antibiotics-exposed mice showed a statistically non-significant increase in epithelial permeability. Epithelial barrier function has been shown to depend on microbiota and their metabolites. However, unlike postnatal antibiotics exposure, prenatal exposure did not lead to severe asthma: lung function and neutrophilia were comparable to the asthmatic control mice. At the same time, likewise to postnatal exposure, prenatal antibiotics exposure shifted the cellular immune responses towards a mixed T_H2/T_H17 response upon HDM-immunization, showing an increase in IL-17A$^+$ cells. The IL-17A$^+$ cells were identified as γδT cells. Although γδT cells have been shown to play a role in the resolution of inflammation in asthma, other published data support a proinflammatory role for γδT cells in experimental asthma. Given the increase in IL-17A$^+$ cells, an immunohistochemistry approach was established to analyze IL-17A-producing cells *in situ*. The subpopulations αβT cells, γδT cells, and innate lymphoid cells were identified. IL-17A-producing subpopulations localized to large and small airways and showed high contact rate with dendritic cells. However, localization and contact rate were comparable between asthmatic control- and antibiotics-exposed mice. Taken together, this study suggest that prenatal antibiotics do not alter long-term immunity in a way that postnatal antibiosis changed the severity of experimental allergic asthma.

2 Zusammenfassung

Die Rolle einer pränatalen Antibiose auf die Entwicklung von Asthma ist von großem Interesse, da verschiedene Veränderungen des Lebensstils der letzten Jahrzehnte, wie veränderte maternale Ernährung, Zunahme von Kaiserschnitten und der Einsatz von Muttermilchersatz, Mikrobiomveränderungen des Kindes hervorrufen können. Epidemiologische Studien legen eine positive Korrelation von Mikrobiomveränderungen mit einem erhöhten Asthmarisiko des Kindes nahe. Auch Antibiotikaeinnahme während der Schwangerschaft wurde mit erhöhtem Asthmarisiko in Verbindung gebracht. Das Deshmukh Labor im Cincinnati Children's Hospital Medical Center behandelte schwangere Mäuse mit Antibiotika und untersuchte die neugeborenen Mäuse bezüglich ihrer Anfälligkeit gegenüber Pneumokokkeninfektion. Die Jungmäuse zeigten eine erhöhte Anfälligkeit, die durch das Ausbleiben von Mikrobiom-abhängig in die Lunge migrierenden Immunzellen nach der Geburt bedingt war. Das gleiche Antibiotika-Mausmodell wurde durch das Lewkowich Labor in Cincinnati verwendet, mit einer Verlängerung der Antibiose um zwei Wochen postnatal, um den Einfluss der Antibiose auf das experimentelle Asthma von C57BL/6 Mäusen zu untersuchen. Im Vergleich zu den asthmatischen Kontrollmäusen, entwickelten diese Tiere ein schweres Asthma mit stark erhöhtem Atemwegswiderstand und Neutrophilie. Neben der unter allergischem Asthma zu erwartenden T_H2 Antwort zeigten die Mäuse eine verstärkte T_H17 Immunantwort in Form von vermehrten IL-17A$^+$ Zellen, die als Innate Lymphoid Cells identifiziert wurden. Wegen dieser Ergebnisse und der durch eine pränatale Antibiose verursachten Anfälligkeit gegenüber Neugeborenen-Pneumokokkeninfektion wurde für dieses Projekt untersucht, ob eine pränatale Antibiose langfristig veränderte Immunität im Sinne eines schweren experimentellen Asthmas verursachen kann. Dafür wurden die schwangeren Mäuse einer pränatalen Antibiose ausgesetzt und bei den Jungmäusen Asthma induziert. Interessanterweise zeigte sich bereits in den nicht-immunisierten Tieren eine erhöhte Permeabilität des Lungenepithels, die jedoch statistisch nicht signifikant war. Die Abhängigkeit intakter Epithelfunktion von kommensalen Mikroorganismen und deren Metabolite wurde zuvor durch verschiedene Studien gezeigt und eine erhöhte Permeabilität mit allergischem Asthma assoziiert. Trotz der erhöhten Permeabilität zeigte sich jedoch im Gegensatz zu der postnatalen Antibiose kein schweres Asthma: Die Mäuse entwickelten ähnlich schwere Atemwegswiderstände wie die asthmatischen Kontrollmäuse. Auch eine Neutrophilie konnte nicht festgestellt werden. Überraschenderweise entwickelten die Mäuse jedoch ähnlich zu den prä-/postnatal behandelten Mäusen eine gemischte T_H2/T_H17 Antwort, die sich durch vermehrte IL-17A$^+$ Zellen bei gleichbleibender T_H2 Antwort zeigte. Die IL-17A$^+$ Zellen wurden als γδT-Zellen identifiziert. Die

vermehrten IL-17A$^+$ Zellen wurden durch die Etablierung eines Mikroskopieansatzes genauer untersucht, um diese in der Lunge *in situ* nachzuweisen. Es zeigte sich eine Lokalisierung der Subpopulationen αβT-Zellen, γδT-Zellen und Innate Lymphoid Cells an großen und kleinen Atemwegen und zusätzlich eine hohe Kontaktrate mit Dendritischen Zellen. Im Rahmen der etablierten Mikroskopiemethode konnten jedoch hinsichtlich der Lokalisierung oder der Kontaktrate mit Dendritischen Zellen keine Unterschiede zwischen den asthmatischen Kontroll- und Antibiosemäusen festgestellt werden.

Zusammengefasst ergibt sich aus den Tierexperimenten zu pränataler Antibiose keine langfristig veränderte Immunität im Sinne eines schweren experimentellen Asthmaphänotypes.

3 Introduction

The following thesis work investigated the impact of changes to the maternal microbiota on the offspring allergic asthma development and phenotype. To understand the immune mechanisms underlying allergic asthma pathology, an understanding of pathogen elimination by the immune system is necessary. Therefore this introduction section includes factors and cell types involved in immune responses as they function in response to pathogens and during steady state. Next, the immune pathology of allergic asthma and severe allergic asthma with their phases of disease development are described. Finally, an introduction is given to microbial colonization and early life immune responses. In particular, a summary is given of how alterations to early life microbial colonization has been connected to the adequacy of immune responses and the immune pathogenesis in asthma later in life.

3.1 The innate immune system

The immune system functions in defense to microorganisms, foreign substances, and dysfunctional cells to maintain the body functions of the host. Common pathogenic organisms found in humans and mice are viruses, bacteria, fungi, and multicellular parasites like worms. [1] If pathogens overcome barriers like the skin or the mucosa, an immediate response of the innate immune system is initiated. If immediate responses cannot eliminate the pathogen sufficiently, antigen-specific immune responses of the adaptive immune system develop. [1] Although the innate and adaptive immune responses can be separated with regard to the cell types involved, both systems are linked tightly.

3.1.1 The non-cellular components of the innate immune system

The non-cellular components of the immune system are soluble proteins or peptides in the extracellular fluids that can function in communication between immune cells, detection of pathogens or have direct antimicrobial or antiviral properties. One of the most evolutionarily conserved pathogen sensing systems is the complement system. [2] In pathogen response, the inactive complement gets activated upon recognition of structures expressed by pathogens. [3] One of the many functions of complement is the opsonization of pathogens, which is the marking of a pathogen or pathogen products for phagocytosis by phagocytes and granulocytes. Opsonization often involves a combination of complement as a component of innate immune responses and immunoglobulins (Ig) as a non-cellular component of the adaptive immune responses. [4] Activated complement can also bind to receptors expressed by immune cells, inducing intracellular signaling and activation of these cells. Another non-cellular component of

the immune system are cytokines, which contribute to interaction between cells. [5] Cytokines are diverse peptides that mediate the communication between cells by binding receptors expressed by the same or other immune cells. The binding of a cytokine to the corresponding receptor activates intracellular signaling cascades that depend on the type, the combination of cytokines, and on the cell type expressing the specific receptor. [5] Cytokines that are secreted in response to pathogens are proinflammatory cytokines.

3.1.2 The cellular components of the innate immune system

The innate immune system is comprised of myeloid-derived cells, which include macrophages and dendritic cells (DCs), and granulocytes, including neutrophilic and eosinophilic granulocytes, mast cells and basophil granulocytes. Other cellular components are lymphoid-derived cells like innate lymphoid cells (ILCs) and natural killer cells. [6] These cell types contribute to immediate inflammatory responses by their distinct expression of cytokines, receptors, phagocytosis capacities, and the release of toxic granules. [7] Expressing specialized pattern recognition receptors (PRRs), epithelial cells or circulating innate immune cells can recognize distinct pathogen-associated molecular patterns (PAMPs), which are components of bacterial cell walls, sugar molecules, peptides, and nucleic acids. [7] Activation of PRRs induces intracellular signaling, resulting in activation of transcription factors and protein expression. A large, evolutionary conserved group of PRR that recognizes numerous PAMPs are toll-like receptors (TLRs). [8] Nucleotide-binding oligomerization domain (NOD)-like receptors mainly sense intracellular pathogen-associated patterns. [9]

Phagocytes

Phagocytosis is the engulfment, internalization, and degradation of pathogens, pathogen-associated products, and dysfunctional cells. [10] One important group of phagocytes are macrophages, which can take up debris, apoptotic cells, and pathogens. [10] Phagocytosis of pathogens can be triggered by receptors like TLRs and NOD-like receptors. [11] While phagocytosis of harmless particles or apoptotic cells does not induce proinflammatory responses, sensing of PAMPS activates intracellular downstream signaling, inducing a type of macrophage that contributes to inflammation by phagocytosis and proinflammatory cytokine secretion. Once the macrophage has internalized a pathogen, the phagosome can fuse with an organelle called lysosome filled with reactive oxygen species (ROS) and enzymes that can hydrolyze the biomolecules of the pathogen. [12] A second group of phagocytes, dendritic cells (DCs), play an important role in the activation of adaptive immune responses due to their ability of taking up antigens and migrating to lymph nodes, where they present antigen fragments on major

histocompatibility complex (MHC) II to naïve T cells. [13, 14] DCs express TLRs, NOD-like receptors, and other PRRs for pathogen sensing. [15] TLR-activation that parallels the uptake of pathogens by DCs can induce DC maturation, including the upregulation of a lymph node homing receptor, upregulation of MHC II, downregulation of phagocytosis, downregulation of adhesion molecules, and upregulation of co-receptors that mediate T cell activation. [16]

Granulocytes

Granulocytes include eosinophilic and neutrophilic granulocytes, mast cells, and basophilic granulocytes. For the scope of this project the focus will be on eosinophils and neutrophils. Although not part of this project, mast cells are introduced because of their unique role in the pathogenesis of asthma.

Eosinophils and neutrophils express PRRs, which can be triggered by PAMPs as well as complement and Fc receptors. [17, 18] Differential expression of cytokine receptors mediate recruitment to the infection site. Neutrophils are recruited rapidly to the site of injury or inflammation, if cytokines like interleukin (IL)-8 are secreted. [19] Once recruited, neutrophils contribute to the pathogen elimination by phagocytosis, often followed by phagocytosis-induced cell death and phagocytosis by macrophages. [20] In response to larger pathogens, neutrophils can release granules, which are comprised of proteases, other enzymes, and ROS that degrade biomolecules of extracellular pathogens like fungi or bacteria. [21, 22] Eosinophil granulocytes are recruited to site of inflammation upon infection with helminths and extracellular pathogens. [23] Cytokines like IL-5 induce the upregulation of adhesion molecules on endothelial cells, which cause circulating eosinophils to infiltrate the site of inflammation. [24] If phagocytosis is not possible, the pathogen elimination by eosinophils is mediated by degranulation of major basic proteins, toxic to helminths. [23] Also ROS, prostaglandins, and eosinophil-derived neurotoxins are released during degranulation. [25]

Like eosinophils, mast cells can respond to multicellular parasites like helminths and to extracellular pathogens. [26] In the presence of IL-9, immature tissue residing progenitor mast cells become activated and proliferate. [27] If in response to pathogens full adaptive immune responses have developed, including antigen-specific B cell secretion of Igs such as the Ig isotype IgE, mast cells can bind the Fc region of IgE due to the expression of a high affinity Fcε receptor (R). [28] The antigen-recognition of several neighboring IgE bound to IgεR by pathogen, can induce the release of toxic granules. Among other contents, mast cell granules consist of histamines and prostaglandins, which can trigger smooth muscle cell contractions. [29]

Innate lymphoid cells

ILCs have a common lymphoid progenitor and similar cytokine expression profiles as T cells but do not express the T cell receptor (TCR) (section 3.2.2). ILCs commonly reside in tissues, while few numbers are found circulating in the blood stream. [30, 31] ILCs contribute to inflammatory responses and to tissue homeostasis mainly by cytokine release. [31, 32] Progenitor cells differentiate into three subtypes, ILC1, ILC2, and ILC3, although plasticity and heterogeneity within the groups is known. [33] ILC1 activation is induced by IL-12, predominantly secreted upon infection with viruses or intracellular pathogens. [34] The differentiation depends on the transcription factor T-bet. [34] ILC2 are activated in defense to helminths and other extracellular pathogens by IL-25, IL-33, and thymic stromal lymphopoietin TSLP, cytokines which are secreted by damaged epithelial cells. [35-37] ILC2 differentiation depends on the transcription factor GATA binding protein (GATA) 3. [34] Upon activation, mainly IL-5 and IL-13 are secreted by ILC2, activating effector cells like eosinophils. [36, 38] The third group of ILCs, ILC3 are mostly activated by IL-23 in response to infection with extracellular pathogens like fungi or bacteria. ILC3 differentiation depends on the transcription factor retinoid-related orphan receptor (ROR)γt. [39] Upon activation, ILC3 secrete cytokines such as IL-17 and IL-22. [40, 41]

3.2 The adaptive immune system

During evolutionary processes, adaptive immunity first appeared in vertebrates. The evolutionary advantage of adaptive immune responses was the protection from unspecific cytotoxicity, which damages the host's tissue. [42]

3.2.1 Acquiring adaptive immunity

Upon phagocytosis of pathogens, some immune cells can present antigen in lymph nodes to naïve T cells and activate adaptive immune responses. Tissue-resident DCs are the major antigen-presenting cells that have the migratory capacities for lymph node homing. [43] DCs take up antigen from the extracellular fluids or spaces, process, and load fragments on specialized protein complexes, called MHC II. [44] The antigen fragments bound to MHC II are then presented on the cell surface. Upon additional activation by cytokines and receptors like TLRs, DCs undergo maturation processes and migrate to the draining lymph nodes, where interaction of the loaded MHC II and the TCR of naïve $CD4^+$ T helper (T_H) 0 cells occurs. [44, 45] If the TCR antigen-binding site of a T_H0 cell shows affinity to the antigen fragment presented on MHC II, the T_H0 cell becomes activated. [46] Additionally, the polarization of T_H0 cells to T_H1, T_H2, T_H17, and regulatory T (T_{Reg}) cells depend on the presence of certain cytokines and receptor-ligand signaling between the cells (section 3.2.2). [47, 48] Differentiated T_H cells proliferate and infiltrate the site of inflammation where

they contribute to pathogen elimination by cytokine production. A distinct group of antigen-specific T cells remain in the lymph node, where they interact with B cells. [49] Naïve B cells express the B cell receptor (BCR), a bound version of Ig. [50, 51] Upon antigen recognition by the BCR, antigen is taken up and antigen-fragments are presented on MHC II. If a T cell and a B cell that recognize the same antigen interact, the B cell proliferates and the antigen-binding site of the BCR undergoes somatic hypermutation, which is the introduction of mutations to the genes that encode for the antigen-binding region of the BCR, resulting in generation of new variants of the BCR binding site. B cells that show high affinity of the BCR to the antigen, receive survival signals. [52, 53] Igs are secreted by B cells, which are components of the non-cellular immune responses. An important function of Igs is the binding of the specific antigen for degradation by immune cells that express the corresponding FcR. In the presence of cytokines, B cells undergo changes, inducing class switch of the Ig isotype. Ig class switching is based on rearrangements of the genes that encode for the constant regions of the Ig. The isotypes that can form due to gene loci rearrangement are IgG, IgA, and IgE with several subisotypes specific for distinct responses to pathogens. [54]

3.2.2 T helper cell differentiation

Upon activation, T_H0 cells differentiate into the subsets T_H1, T_H2, T_H17, and T_{Reg} cells that play different roles in the defense of pathogens, control of commensal microbiota, and in tolerogenic responses. [47, 55] An overview of T cell differentiation is visible in Fig. 3.1. T_H1 differentiation is induced by IL-12 upon viral infections and intracellular pathogens. [56] The transcription factor T-bet determines T_H1 differentiation. Among the cytokines secreted by T_H1 cells are IFNγ and TNFα, which activate other immune cells and can exert direct antiviral properties. [57] T_H2 responses are activated in response to extracellular pathogens or infection with helminths in the presence of IL-4. [58, 59] Activation depends on the transcription factor GATA3. T_H2 cells can produce cytokines like IL-4, IL-5, IL-9, and IL-13. [60, 61] IL-5 contributes to eosinophilia, IL-9 to mast cell activation, and IL-4 can induce isotype class switch to IgE-producing B cells. [24, 62] T_H17 responses are induced by extracellular pathogens like fungi and extracellular bacteria by the cytokines IL-1β, TGF-β, IL-6, and IL-23. [63] T_H17 differentiation is dependent on the transcription factor RORγt. Cytokines released by T_H17 cells are IL-17A, IL-17F, and IL-22, contributing to the elimination of the pathogen by neutrophilia but also to tissue repair mediated by IL-22. [55, 64] T_{Reg} cells that differentiate in response to harmless biomolecules are induced by transforming growth factor (TGF)-β and retinoic acid. T_{Reg} cell differentiation is dependent on the transcription factor Forkhead-box protein (FoxP) 3. T_{Reg} cells suppress T_H cell differentiation and can also suppress antigen-specific T cells. [65]

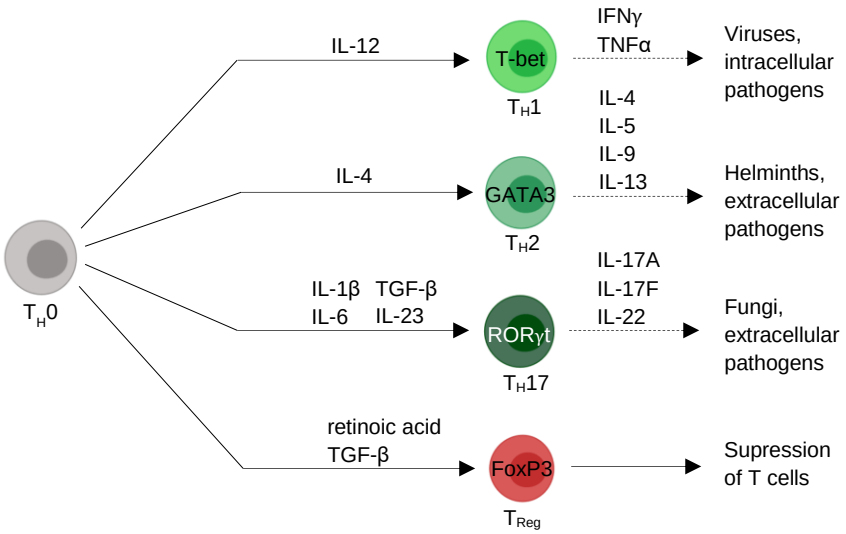

Fig. 3.1: Schematic overview of the T cell differentiation.
T cell differentiation is induced by cytokines. T_H1 differentiation depends on the transcription factor T-bet and is induced by IL-12. T_H2 differentiation depends on GATA3 and is induced by cytokines like IL-4. T_H17 differentiation depends on RORγt and is induced by cytokines like IL-1β, IL-6, TGF-β, and IL-23. T_{Reg} cell differentiation depends on the transcription factor FoxP3 and is induced by cytokines like retinoic acid and TGF-β. [56-62,64-65]

3.2.3 γδT cells

γδT cells are a minor group of T cells which express the γ and δ TCR chains instead of the α and β TCR chains. γδT cells rather contribute to innate immunity since they lack the ability to induce B cell activation the way αβT cells mediate adaptive immunity. [66] However, the recognition of specific antigens by the γδ TCR is possible. [67, 68] Recognition of pathogens by γδT cells is not only mediated by the γδ TCR but also by PRRs like TLRs. [69] Like cells of the innate immune system, following γδ TCR or TLR-mediated activation, γδT cells can rapidly respond to pathogens by cytokine secretion. [70] In terms of their cytokine profile, γδT cell subsets mirror αβT cell subsets T_H1, T_H2, and T_H17. [71] Regulatory functions of γδT cells are also known. [72]

While the first part of the introduction focused on the cellular and non-cellular components of the innate and adaptive immune system in their function to maintain homeostasis, the next part will focus on the dysfunction that occur in harmful immune responses found in allergic airway disease.

3.3 Anatomy of the lungs

For metabolic processes, body cells take up oxygen and in exchange as a product of cell metabolism release carbon dioxide. The body site that is responsible for the oxygen uptake are the lungs. Lungs are subdivided into lobes covered by the pleura. The airways are lined by epithelia covered by a mucus layer, directing the air flow through the trachea, which parts into the two main branches of the large bronchi leading to the bilateral lobes. An overview of a bronchial branch with a schematic cross section of an airway is visible in Fig. 3.2. The two main bronchi divide several generations, followed by several generations of bronchioles. Finally the airflow is directed to alveolar ducts and alveoli. The tight association of type II pneumocytes and the endothelial cells of the pulmonary capillaries provide a short diffusion distance for the exchange of O_2 and CO_2. [73] Pulmonary arteries that transport the deoxygenated blood for gas exchange run in parallel to the airways while pulmonary veins that transport oxygenated blood from the lungs run separately [73] Lymph vessels responsible for draining excessive tissue fluids, proteins, and immune cells also run close to airways and to blood vessels. [74, 75]

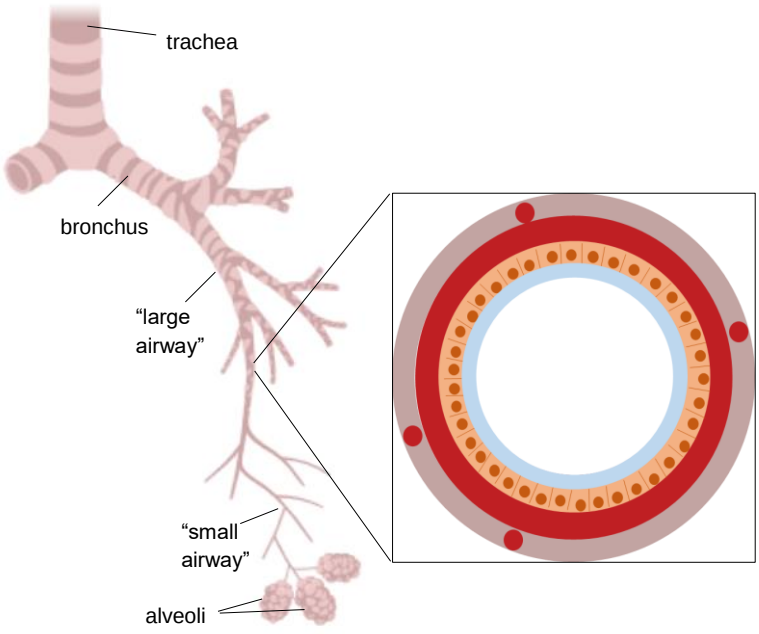

Fig. 3.2: Schematic overview of a bronchial branch and a cross section of an airway.
An overview of one bronchus, bronchioles, and alveoli is given (left). The schematic cross section of an airway is visible (right). The luminal side of the airway epithelium is covered by a mucus layer (light blue). A smooth muscle cell layer (red) surrounds the epithelium (yellow). Blood vessels run in close proximity to airways (small circles, red) and are surrounded by loose connective tissue (brown). [73]

3.4 Tolerance and lung immunity

Tolerance at mucosal sites such as the airways depends on an intact epithelial barrier, covered by a layer of mucus. One of the mucus functions is to keep potential pathogens at physical distance from the epithelium. Pulmonary immune tolerance involves mechanisms that prevent from inflammation to harmless particles or microbes, which would compromise the gas exchange. [76] The majority of immune cells found in the bronchoalveolar lavage (BAL) fluid of naïve mice are alveolar macrophages, functioning as first line sentinels during steady state. While the clearance of airborne particles and apoptotic cells is one important function, alveolar macrophages can also directly contribute to tolerogenic immune responses by secretion of cytokines that induce T_{Reg} cell differentiation. [77] Also a subgroup of DCs, $CD103^+$ DCs, have been reported to mediate pulmonary tolerance by secretion of TGF-β and retinoic acid and induction of antigen-specific T_{Reg} cells. [78] $CD103^+$ DCs mediate tolerogenic responses in other organs like the intestine. [32]

3.5 Allergic airway inflammation

Allergic asthma affects about 10 % children and 5 % adults in industrialized countries, after the prevalence has tripled over the last three decades. [79] Other, non-allergic types of asthma exist that include obesity-related and exercise-induced asthma. Symptoms of non-allergic and allergic asthma are wheezing, coughing, and shortness of breath. Although the symptoms are similar, the cause of allergic asthma is considered extrinsic, since the symptoms are caused by a non-adequate immune response to harmless, airborne particles.

3.5.1 Sensitization phase of allergic airway inflammation

Pollution, cigarette smoke, traffic exhaust, as well as other factors like viral infections were found to activate stress response by epithelial cells (Fig. 3.3). [80-86] Triggered by damage or pollution, epithelial cells release cytokines like IL-25, IL-33, and thymic stromal lymphopoietin (TSLP), which can contribute to DC maturation. [87] Epithelial cells can also be directly triggered by the allergen: some allergens like Der p1 protein found in house dust mite (*dermatophagoides pteronyssinus*) (HDM) have protease activity, interfering with the tight junction integrity of epithelial cells. [88, 89] IL-25, IL-33, and TSLP released from epithelial cells can activate ILC2, which contribute to the inflammation by releasing T_H2 cytokines like IL-5 and IL-13. [36, 90, 91] The uptake of antigen by DCs in addition to the activation by proinflammatory cytokines like IL-25, IL-33, and TSLP, induce the maturation of DCs and the migration to the draining lymph nodes where DCs can present antigen fragments on MHC II to naïve T_H0 cells. [92] In the presence of IL-4, T_H2 differentiation is initiated. [93] Differentiated T_H2 cells contribute to the inflammation by cytokine secretion of IL-4, IL-5, and IL-13 and can activate antigen-specific B cells, including the induction of isotype class switch of

activated B cells to IgE-producing plasma cells in the presence of T_H2 cytokines like IL-4 (Fig. 3.3). [94-96]

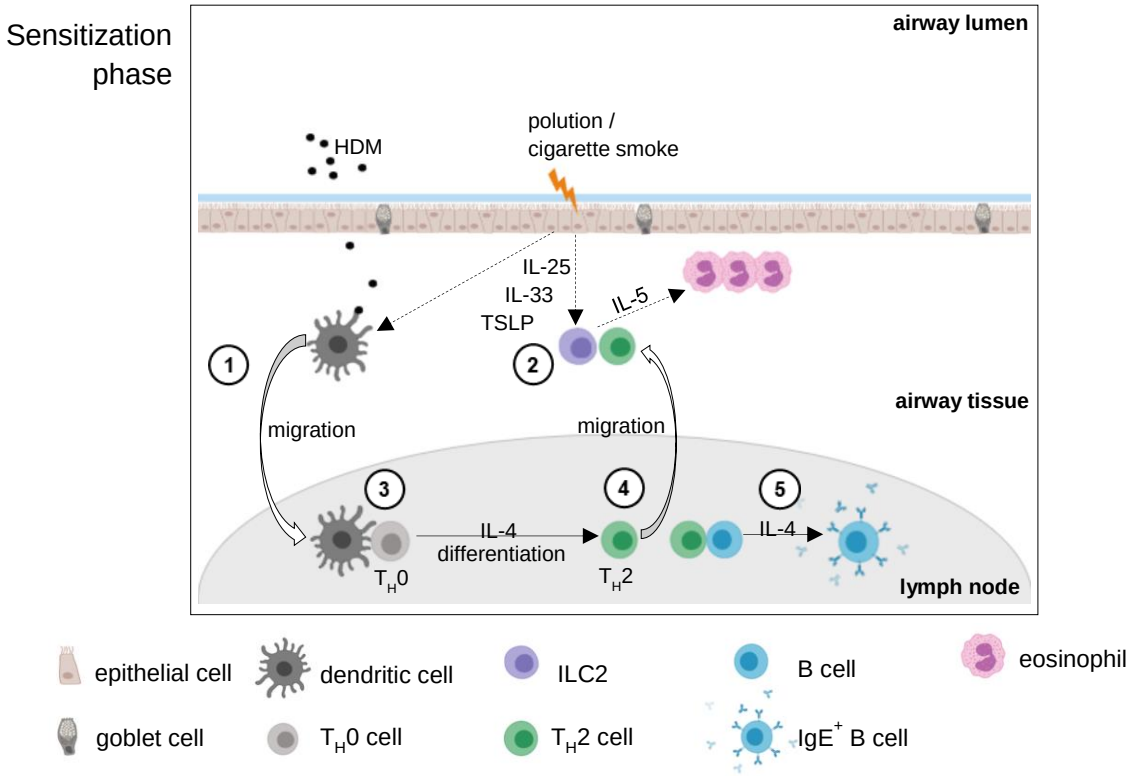

Fig. 3.3: Schematic overview of the sensitization phase of allergic asthma.
Upon HDM allergen uptake and receiving cytokine signals from damaged epithelial cells, DCs migrate to lymph nodes (1). Signals released by epithelial cells can also contribute to ILC2 activation (2). In lymph nodes, DCs can present antigen fragments to T_H0 cells (3). T_H2 differentiation is induced by T_H2 cytokine IL-4 (4). Differentiated T_H2 cells can activate B cells, secreting IgE in the presence of T_H2 cytokines like IL-4 (5). [81-97]

3.5.2 Effector phase of allergic airway inflammation

A subtype of T_H2 cells can activate mast cells by secretion of IL-9. [27, 97, 98] When reexposed to the allergen, IgE bound to the FcεR expressed by mast cells can become crosslinked. If bound IgE are crosslinked by the allergen, mast cells can release histamines, heparin, proteases, prostaglandins, and cytokines. [99-106] The granules released by mast cells damage the tissue and trigger contraction of smooth muscle cells (Fig. 3.4). [107, 108] Even long after allergen exposure has occurred, symptoms like wheezing and shortness of breath can persist that are caused by the remodeling and constriction of the airway smooth muscle layer. Long living B and T cells and

mast cells that bind IgE contribute to the chronicity of allergic asthma. Also the structural changes that are induced by the inflammation contribute to the chronic symptoms: epithelial cell layer hypertrophia contributs to the narrowing of the airway, as well as the increase in smooth muscle cells. [109] Goblet cell hyperplasia and mucus hypersecretion contribute to the narrowing of the airway. [110] The two main mucins found in the mucus layer covering the airway epithelium are mucins (Muc) 5B and Muc5AC. [111, 112] While Muc5B rather contributes to airway clearence during steady state, Muc5AC and goblet cell hyperplasia contribute to mucus plugging in chronic asthma. [113, 114] The T_H2 cytokine IL-13 can induce the transcription of the chloride channel accessory 1, also known as Gob-5, resulting in goblet cell proliferation and increased Muc5AC production. [115-117] The structural changes seen in chronic inflammation of the airways also include changes in vascularity and nerve tissue: asthmatics have a more dense network of sensory neurons that contribute to bronchoconstriction. [118] Increased number, size and density of blood vessels are also found. [119] Fig. 3.5 shows a schematic cross sections of a healthy and an asthmatic airway.

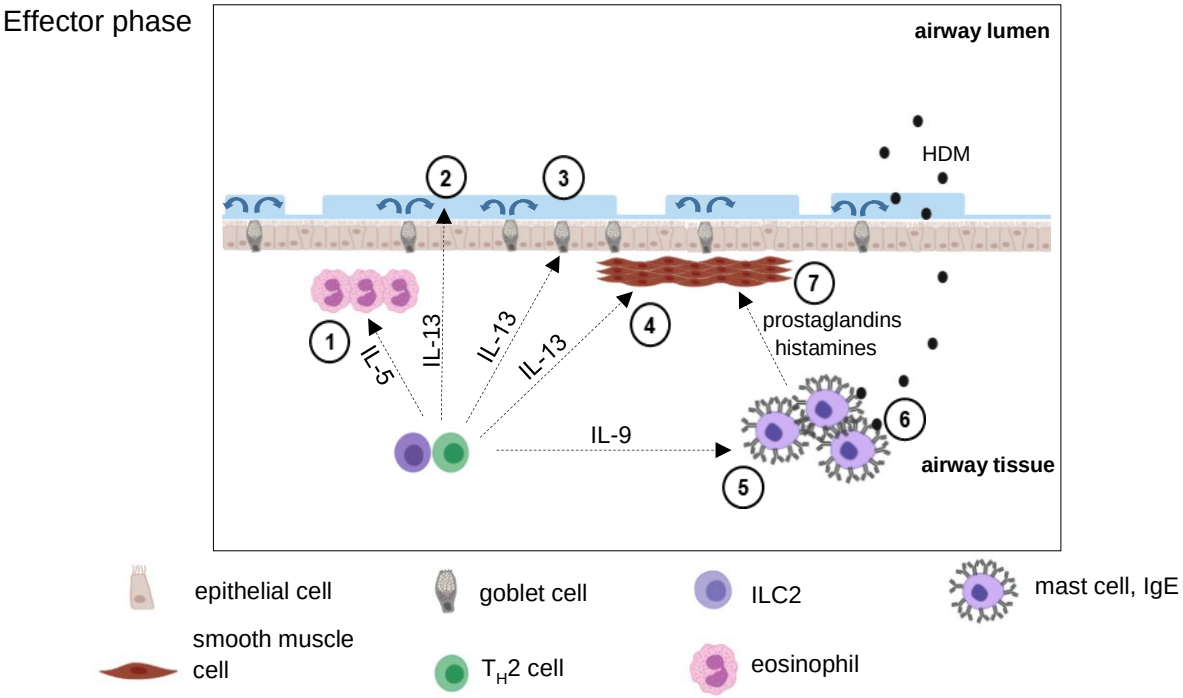

Fig. 3.4: Schematic overview of the effector phase of allergic asthma.
During the effector phase, T_H2 cytokines like IL-5 recruit eosinophils (1), IL-13 can induce mucus secretion (2), goblet cell hyperplasia (3), and smooth muscle cell hyperplasia (4). A subpopulation of T_H2 cells can secrete IL-9, activating mast cells (5). Granule release from mast cells is triggered by crosslinkage of IgE by the allergen (6), mast cell granule contain histamines and prostaglandins, causing contraction of smooth muscle cells (7). [97-118]

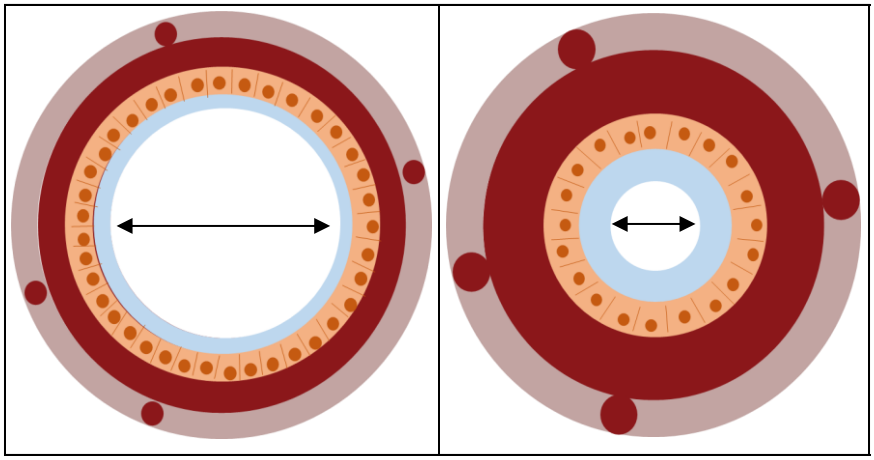

Fig. 3.5: Schematic overview of cross sections of a healthy *vs.* an inflamed airway.
In contrast to healthy airways (left), the inflamed airway undergoes changes in mucus secretion (blue), epithelial cell hypertrophy (yellow), increase in smooth muscle cells (red), and vasodilatation (small circles, red). The changes cause narrowing the airway lumen indicated by the arrows. [110-118]

3.5.3 Severe allergic airway inflammation

Severe asthma found in about 5-10 % of asthmatics is defined by intensified clinical symptoms like airway obstruction and the resistance to therapy with glucocorticoid steroids. [120, 121] For these patients an alternative pathogenesis was suggested to be responsible: while mild and moderate asthma was associated with T_H2 cytokines and eosinophilia, severe asthmatics were found to present with mixed T_H2/T_H17 responses and elevated IL-17A cytokine production, as well as high neutrophilic counts. [122-126] Also cytokines for T_H17 differentiation like IL-6 and TGF-β were found to be elevated in these patients. [127-129] In a mouse model of severe asthma, IL-17A was found to enhance IL-13 responses. [130] The same study found that IL-17A responses were mediated by complement C3a, while complement C5a negatively correlated with IL-17A levels. [130] Vroman *et al.* (2015) suggested that the mode of asthma development is dependent on activating factors: while TSLP, IL-25, and IL-33 determine T_H2 differentiation, factors like C3a and also serum amyloid A were suggested to contribute to T_H17 differentiation. [126] Synergistic effects of IL-13 and IL-17A were supported by the finding that intracellular IL-13R signaling was enhanced by IL-17A. [131] Like T_H2 responses, IL-17A can contribute to airway remodeling and mucin expression by goblet cells. [132] Another feature of IL-17A contribution to more severe asthma is the enhanced recruitment of neutrophils to the site of inflammation. [133] IL17A can recruit neutrophils by induction of IL-8 production of epithelial cells [134, 135] Additionally, IL-17A was found to enhance neutrophil proliferation from progenitor bone marrow cells. [136] A schematic overview of mixed functions of T_H2/T_H17 responses in severe asthma is given (Fig. 3.6).

Since mouse models are important for the investigation of allergic airway disease, the next section will briefly introduce the asthma mouse model.

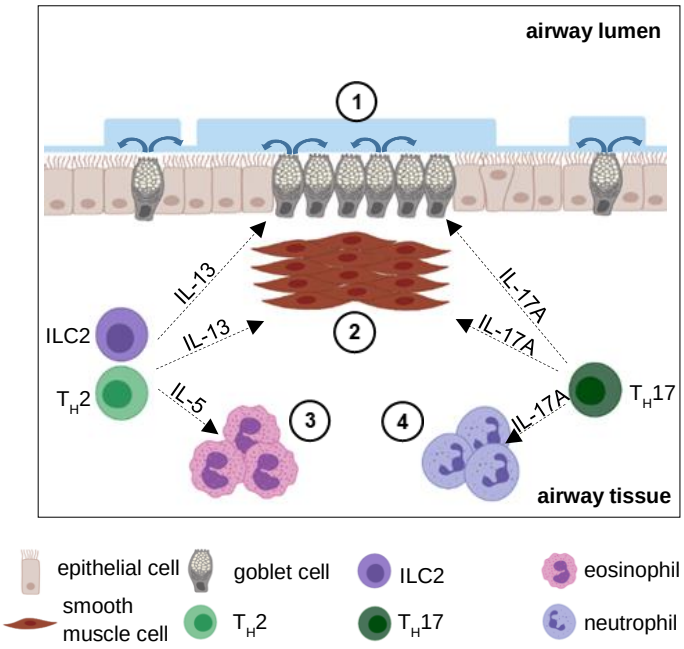

Fig. 3.6: Schematic overview of mixed T_H2/T_H17 responses associated with severe asthma. Both cytokines, IL-13 and IL-17A contribute to goblet cell hyperplasia, mucin expression by goblet cells (1), and smooth muscle cell hyperplasia (2). Eosinophils are recruited by T_H2 cytokines like IL-5 secreted by ILC2 and T_H2 cells (3), while IL-17A contributes to recruitment of neutrophils (4). [110-118,123-126,133-136]

3.5.4 Mouse models of allergic asthma

In mice, chronic inflammation is commonly induced by repeated allergen challenges. Allergens administered for the immunization of mice are ovalbumin (OVA), HDM extract, and less commonly cockroach extract or fungal allergens. [137] OVA is a commonly applied allergen for induction of experimental airway inflammation, although it is not commonly found in human asthma. [138] Because up to 85 % asthmatics are allergic to HDM-associated allergens and because the inflammation resembles human asthma, HDM has become a more commonly used allergen for experimental allergic asthma. [139, 140] The repeated topical *intratracheal* (*i.t.*) administration route of HDM is chosen for BALB/c mice, while C57BL/6 mice have decreased susceptibility to developing allergic airway inflammation by topic application of the allergen. [141-143] Therefore a systemic *intraperitoneal* (*i.p.*) sensitization phase prior to the topical *i.t.* HDM challenge is necessary. [144] The immune responses of several mouse strains resemble human allergic asthma with profound T_H2 inflammation, including eosinophilia and elevated levels of allergen-specific IgE. Also goblet cell hyperplasia, smooth muscle cell hyperplasia, and inducible contraction of the

airways by the muscarinic receptor agonist methacholine are found in mouse models of allergic asthma. [145-147] A major difference to human asthma is that mice do not develop acute bronchoconstriction in response to the allergen. Therefore the asthmatic phenotype can be investigated by the response to muscarinic receptor agonists like methacholine: mice with high airway hyperresponsiveness show increase in bronchoconstriction at lower doses of methacholine.

The next part of the introduction will focus on the early life microbiota and the influence of microbial disruption on asthma development.

3.6 Microbiota and asthma

During birth, microbiota from the mother's vaginal and gastro intestinal tract are transferred to the baby. [148] Soon after birth, skin contact and breast feeding introduces more microbiota to the child. [149] Coming from the rather sterile environment of the uterus, human babies reach a total of about 1^{13}-1^{14} microbes/mL of feces during the first year of life. [150] During the first two to three years of life, the microbiota consortium of the child is highly variable, depending on the ingested bacteria species. [151] During this time, a "climax consortium" is established that may remain similar for the rest of the life. [151, 152] The immune system of the newborn is strongly challenged by the large amount of ingested microbiota. Several ways in which the immune system reacts to rapid colonization after birth have been shown (section 3.6.2). Epidemiological and animal model data indicate a critical time window for developing adequate immune responses to commensal microbiota after birth. **[153] [154]**

3.6.1 Microbiota Hypothesis

In industrialized countries, allergic asthma prevalence has tripled over the last three decades, [155] suggesting that environmental factors contribute to the increased prevalence. In the 1990s it was assumed that exposure to common infections is associated with a smaller risk to develop atopic diseases during childhood. [156, 157] The idea that a lack of infections is associated with an increased risk to develop allergic diseases, resulted in the "Hygiene Hypothesis". [158, 159] However, subsequently the importance of beneficial commensal bacteria and microbial diversity, shaping adequate immune responses of the child was discovered and the "Microbiota Hypothesis" was acknowledged. [158, 160] Environmental risk factors for atopic disease and allergic asthma were identified to lower the diversity and amount of microbiota of the child. [43, 161] Risk factors included caesarian section, [162] high fat diet, [163] formula feeding, [164] and antibiotic use. [165-170] *Vice versa*, protective factors identified included vaginal delivery, [171] lactation, [172] high fiber diet, [173] older siblings, [174] pets, [175] and a farming environment. [176]

3.6.2 Pre- and postnatal immune development

The maternal-fetal barrier is highly restricted in terms of transfer of molecules from the mother to the fetus. While small molecules like chemicals can pass the maternal-fetal barrier by diffusion, larger components have to pass the barrier by active transport. [177-179] Recent data suggest that maternal microbiota can be transferred to the fetus. The suggestion was based on the finding of microbial DNA found in the uterus and in the newborn meconium of human babies and mice. [180, 181] The studies were supported by the finding that labeled bacteria given to pregnant mice were also found in the newborn meconium. [182] However, other studies did not support this finding. [183] A way of active transport of microbial fermentation products by maternal IgG was shown by Gomez de Aguero *et al*. (2016): maternal IgG known to be selectively transferred to the fetal endothelium by FcR expressed by trophoblasts were found to bind bacterial fermentation products, which co-migrated with maternal IgG. In the fetus, the microbial products activated ILCs, which subsequently expressed a receptor that can sense microbiota and microbial metabolites, called aryl hydrocarbon receptor (AhR). After birth, the activation of AhR receptor, which is upstream of IL-22 transcription, led to significantly more IL-22$^+$ ILCs in the newborn's intestine in comparison to control mice. IL-22$^+$ ILCs mediated the first immune responses to microbiota by preventing DCs from presentation of commensal microbial antigens in mesenteric lymph nodes, limiting proinflammatory responses. [184, 185]

While it is possible that the microbiota or microbial products translocate to the fetus, the vast influx of microbiota takes place after birth. [150] The colonization of the intestine is accompanied by a profound increase in immune cells of the intestinal lamina propria and gut-associated lymphoid tissues. [186, 187] Certain bacterial families or species have been described to be beneficial for the development of adequate immune responses. For example, vaginal birth in humans is linked with protective taxa like *Lactobacillus* and *Prevotella*. [188, 189] Lactation is associated with taxa like *Lactobacillus* and *Bifidobacterium* that can ferment human milk oligosaccharides to short-chain fatty acids (SCFAs) like butyrate, propionate, and acetate. [188] Bacterial fermentation products like SCFAs have been identified as beneficial for the health status of the child: Roduit *et al*. (2019) found that high serum levels of the SCFAs butyrate and propionate in children were protective in terms of allergic asthma. [190] Trompette *et al*. (2009) found that mice were protected from experimental allergic asthma, if their mothers received high fiber diet during pregnancy. High fiber diet provides the non-digestible carbonates that are fermented by intestinal microbiota. The protective effects seen by Trompette *et al*. were due to SCFA-mediated induction of bone marrow-derived macrophages and DCs that had high phagocytic capacity but low ability to promote T cell differentiation. [191] A way of shaping the newborn's microbiota before adaptive immune responses

to microbiota have fully developed are maternal Igs transferred to the child *via* breast milk. IgA^+ B cells can accumulate at mammalian glands, where IgA is secreted. In the newborn's intestine, maternal IgA can contribute to the shaping of the intestinal microbiota. [192, 193] Anti-inflammatory IgA responses to microbiota include keeping the microbiota at physical distance from the epithelium and also preventing from presentation of microbiota antigens in lymph nodes. [194] Innate and adaptive immune responses develop subsequently after birth. While some developments are independent to microbial colonization, others depend on the microbiota. Mao *et al.* (2018) showed that colonization of mice with Segmented Filamentous Bacteria (SFB) led to microbiota-dependent activation of IL-22^+ ILCs that prevented the commensal SFB from overgrowth. Around weaning time, IL-22^+ ILC activation and regulation of commensal microbiota was replaced and dominated by T_H17 cells. Mice that lacked T_H17 cells, showed constant activation of IL-22^+ ILCs even in adulthood, which had adverse effects on the mice, including upregulation of several cytokines and metabolic disadvantages. [64] T_H17 differentiation has been shown to be induced by SFB previously: colonization of germ-free mice with the murine commensals led to T_H17 differentiation. [55]

A good example of the importance of the microbiome to development of sufficient adaptive immune responses can be found in germ-free mice: secondary lymphoid tissues necessary for adaptive immune responses do not develop in germ-free mice. [195] Therefore germ-free mice show severely reduced immune cell frequencies, including IgA^+ B cells. [195] Overall, germ-free mice show disadvantages when it comes to pathogen responses that require adaptive immunity. [196]

3.6.3 Early life antibiotics and allergic asthma

Large cohort studies like the Canadian birth cohort study or the UK General practice data base correlated early life antibiotics and asthma development later in life. [165, 166] Although a few smaller studies failed to provide the link, large cohort studies with more than 10,000 and up to 250,000 children provided a positive correlation and found that the risk was highest when more than four courses of antibiotics were administered to the young child. [165-167, 170] Some studies included maternal antibiotics treatment during the last trimester of pregnancy and observed positive correlation of prenatal antibiotics with allergic asthma development. The highest correlation was found when more than four courses of antibiotics were given to the mother. [165, 170]

3.7 Previous results that led to the aims of this thesis

Being interested in maternal microbiota disruption and susceptibility to newborn pneumonia, the Deshmukh laboratory at Cincinnati Children's Medical Center (CCHMC) exposed pregnant mice from embryonic day (E) 15 to postnatal day (P) 0 to a mixture of antibiotics targeting a wide variety

of species. In these experiments, the same mouse strain and antibiotics were used, and the experiments were performed at the same facility as the project of this thesis. Increased susceptibility to pneumonia was found for the newborn mice along with alterations in intestinal bacterial composition during the first two weeks of life. The mechanism by which the control mice and mice that received a microbial reconstitution were protected from newborn pneumonia was found to be a gut microbiota-dependent influx of IL-22$^+$ ILC3 into the lungs of the newborn mice. IL-22$^+$ ILC3 protected the control mice from newborn pneumonia, while antibiotics-exposed mice did not show the IL-22$^+$ ILC3 influx to the lungs and were more susceptible to newborn pneumonia. [197] The study by the Deshmukh laboratory showed that maternal microbiota changes can alter immune responses of the offspring.

The Lewkowich laboratory in Cincinnati used the same antibiotics exposure mouse model as the Deshmukh laboratory but extended the duration of antibiotics exposure of the dams from E15 to P14 and analyzed the asthma phenotype of these mice. HDM-driven experimental asthma induced in antibiotics-exposed offspring mice led to a severe asthma phenotype, including increased respiratory system resistance (R_{RS}) at baseline and upon HDM-immunization, as well as increased frequency of IL-17A-producing cells, and increased frequencies of neutrophils. Notably, these mice did not show increased T_H2 responses. (unpublished data, Lewkowich laboratory) Due to the observation that antibiotics exposure until birth already led to increased susceptibility to newborn pneumonia and due to the increased asthma phenotype seen in P14 mice, we hypothesized that part of the increased asthma severity in offspring is already induced when antibiotics treatment of mothers is stopped immediately after birth.

4 Aims of the thesis

The results from the Deshmukh and the Lewkowich laboratories and the literature on epidemiological data not only link antibiotics-exposure in early childhood but also maternal antibiotics exposure to altered immunity. [165, 170] Because already very early microbiota disruption may impact the offspring's long-term immunity, the hypothesis is that a completed course of antibiotics by the time of birth might alter the basic lung function and experimental asthma development. To address this hypothesis, the same experimental approach as previously for the newborn pneumonia study was chosen, exclusively exposing mice to prenatal antibiotics and analyzing the phenotype.

To assess whether prenatal antibiotics impact the basal lung function and the asthma phenotype, the following steps were addressed**:**

- Measurements of epithelial permeability at baseline
- *In vivo* measurements of R_{RS} at baseline and during inflammation
- Assessment of BAL fluid cell counts at baseline and under inflammation
- Analysis of the production of T_H2 and T_H17 cytokines and intracellular cytokines
- Analysis of gene expression of mucus genes and other genes related to severe asthma
- Reversibility of the symptoms by IL-17A cytokine blockade
- Analysis of IL-17A-producing cells *in situ*, identified by the surrogate RORγt, with the specific focus on altered patterns of localization at large and small airways, and altered interaction with DCs

An overview of the expected changes in lung function and asthma phenotype hypothesized to occur due to maternal microbiota disruption is visible in Fig 4.1.

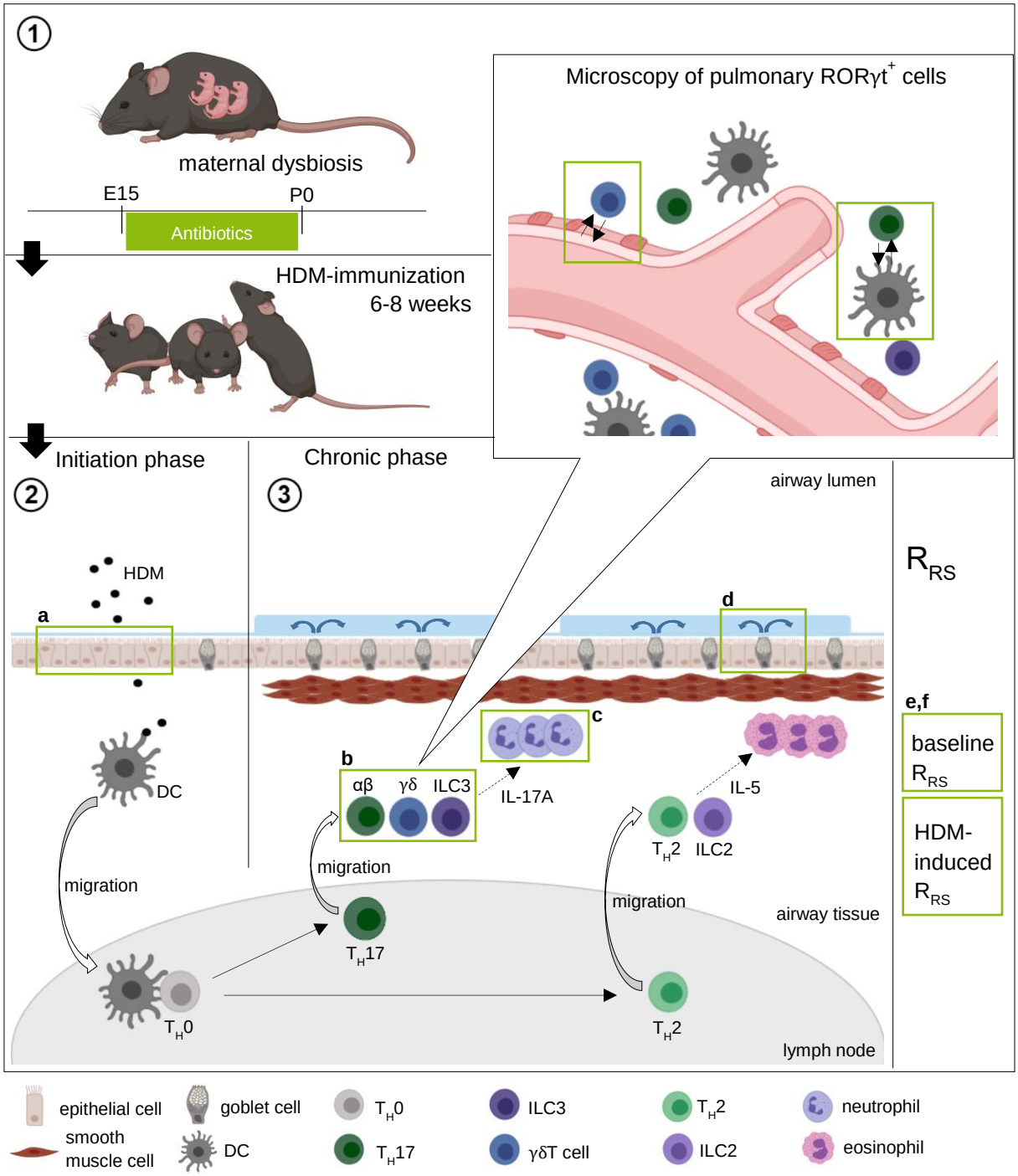

Fig. 4.1: Schematic overview of the working hypothesis adapted from Vroman *et al*. (2015). [126] Maternal antibiotics exposure (1) influence the immunity of the offspring mice immunized with HDM (2). Offspring mice develop immune responses to HDM allergens with differentiation of T_H2/T_H17 responses (3). Based on the results from previous experiments on P14 mice and adding more investigations, the hypothesized alterations for P0 mice are indicated by the green frames. These include increase in epithelial permeability at baseline [a], increase in IL-17A$^+$ cells [b], neutrophilia [c], increase in mucus-related gene expression [d], and increase in baseline and HDM-driven R_{RS} [e,f]. No increased T_H2 responses were expected. Additionally, the localization and the contact rate of RORγt$^+$ cells *in situ* were analyzed (upper right subfigure). (Elsevier license number: 4846630931634). [91-94, 110-118, 123-126, 133-136]

5 Materials and Methods

5.1 Materials

5.1.1 Chemicals and reagents

Table 5.1: Chemicals and reagents.

Reagent	Exact designation, company
Ampicillin	Sodium Ampicillin, USP Grade, Gold Biotechnology Inc., St. Louis, US
Brefeldin A, 1000x	eBioscience™ Brefeldin A Solution, Thermo Fisher Scientific Inc., Waltham, USA
Chloroform	Chloroform, Thermo Fisher Scientific Inc., Waltham, USA
Cytoseal	Thermo Scientific™ Richard-Allan Scientific™ Cytoseal™ 60, Thermo Fisher Scientific Inc., Waltham, USA
DTT	Dithiothreitol (DTT), 0.1 M Solution, USP Grade, Thermo Fisher Scientific Inc., Waltham, USA
Ethanol	Ethanol, 70 %, Blaze lab solutions Inc., Torrance USA
First strand buffer, 5x	First Strand Buffer Thermo Fisher Scientific Inc., Waltham, USA
Gentamicin	Gentamicin Sulfate, USP Grade, Gold Biotechnology Inc., St. Louis, USA
Glucose	D-(+) Glucose, Sigma-Aldrich Inc., St. Louis, USA
Glycerol	Glycerol for Fluorescence Microscopy, Merck KGaA, Darmstadt, Germany
HCL	Hydrochloric acid, Carl Roth GmbH, Karlsruhe, Germany
HEPES	4-(Hydroxyethyl)piperazine-1-ethanesulfonic acid, Sigma-Aldrich Inc., St. Louis, USA
Hoechst 33342	Hoechst 33342, Trichloride 10 mg/mL, Thermo Fisher Scientific Inc., Waltham, USA
Ionomycin	Ionomycin Calcium Salt from *Streptomyces conglobatus*, Sigma-Aldrich Inc., St. Louis, USA
Isopropanol	2-propanol, Sigma Aldrich Inc., St. Louis, USA
Ketamine	2-(2-Chlorphenyl)-2-(methylamino)cyclohexan-1-on, provided by the veterinary services, CCHMC, Cincinnati, USA

Continued

LM agarose	Low Melting Point Agarose, Universal Medical Inc., Oldsmar, USA
Methacholine	(2-Acetoxypropyl)trimethylammonium chloride, Sigma-Aldrich Inc., St. Louis, USA
Monensin,1000x	eBioscience™ Monensin Solution, Thermo Fisher Scientific Inc., Waltham, USA
Mowiol	Mowiol® 4-88, Sigma-Aldrich Inc., St. Louis, USA
NaCl	Sodium chloride, Carl Roth GmbH, Karlsruhe, Germany
$NaHCO_3$	Sodium hydrogencarbonate, Carl Roth GmbH, Karlsruhe, Germany
NaOH	Sodium hydroxide, Carl Roth GmbH, Karlsruhe, Germany
Pancuronium bromide	1,1′-[(2β,3α,5α,16β,17β)-3,17-bis(Acetyloxy)androstane-2,16-diyl]bis(1-methylpiperidinium) dibromide, provided by the veterinary services, CCHMC, Cincinnati, USA
Pen/Strep/L-Glut,100x	Penicillin Streptomycin L-Glutamine Gibco Life Technologies Corp., Carlsbad, USA
PMA	Phorbol 12-myristate 13-acetate, Sigma-Aldrich Inc., St. Louis, USA
PFA	Paraformaldehyde, 16 % solution (10x10ml), Agar Scientific Ltd., Stansted, UK
RNase Out	Murine RNase Inhibitor RNase Out, New England BioLabs Inc., Ipswich, USA
Sodium pentobarbital	(±)-5-Ethyl-5-(1-methylbotyl)-barbitur acid, provided by the veterinary service, CCHMC, Cincinnati, USA
β-mercaptoethanol	2-Sulfanylethanol, Thermo Fisher Scientific Inc., Waltham, USA
Sucralose	1´,6´,6´-Trichloro sucrose, Sigma-Aldrich Inc., St. Louis, USA
Sucrose	D(+)-Saccharose, Carl Roth GmbH, Karlsruhe, Germany
Super Aqua blue substrate	2,2′-Azino-di-(3-ethylbenzthiazolin-6-sulfon acid), Super AquaBlue Invitrogen™, Invitrogen Inc., Carlsbad, USA
Tris	Tris (hydroxymethyl)-aminomethan, Carl Roth GmbH, Karlsruhe, Germany
Triton	Triton® X-100, Thermo Fisher Scientific Inc., Waltham, USA

Continued

Trizol reagent	TRIzol™ Reagent, Thermo Fisher Scientific Inc., Waltham, USA
Trypan blue solution	Trypan Blue Solution, 0.4 %, Thermo Fisher Scientific Inc., Waltham, USA
Tween 20	TWEEN® 20, Sigma-Aldrich Inc., St. Louis, USA
Vancomycin	Vancomycin Hydrochloride, USP Grade, Gold Biotechnology Inc., St. Louis, US
Vetbond	Vetbond™ Tissue Adhesive, 3M Science Inc., Maplewood, USA
Viability dye	BD Horizon Viability Dye V500, Becton Dickinson Inc., Franclin Lakes, USA
Water, deion. sterile-filtered	CCHMC, Cincinnati, USA
Water, deionized, sterile	Ampuwa® Plastipur®, Fresenius Kabi GmbH, Bad Homburg, Germany
Water, drinking water, sterile	CCHMC, Cincinnati, USA
Water, sterile, nuclease free	Nuclease-Free Water, Stemcell Technologies Inc., Vancouver, Canada
Xylazine	2-(2,6-Dimethylphenylamino)-5,6-dihydro-4H-thiazin, provided by the veterinary services, CCHMC, Cincinnati, USA

5.1.2 Biological reagents and enzymes

Table 5.2: Biological reagents and enzymes.

Reagent	Exact designation, company
Avidin-HRP	eBioscience™ Avidin Horseradish Peroxidase, Invitrogen Inc., Carlsbad, USA
BSA	Bovine Serum Albumin Fraction V, Sigma-Aldrich Inc., St. Louis, USA
DNase I	DNase I , Roche AG, Basel, Switzerland
dNTP mix	dNTP Mix (10 mM), Thermo Fisher Scientific Inc., Waltham, USA
FBS	Fetal Bovine Serum, Thermo Fisher Scientific Inc., Waltham, USA
FITC-Albumin	Albumin-fluorescin Isothiocanate Conjugate, Sigma-Aldrich Inc., St. Louis, USA

Continued

HDM	Mite, House Dust *D. Pteronyssinus*, Greer Laboratories Inc., Lenoir, USA
IgG Fc block	Purified Rat Anti-Mouse CD16/CD32, Mouse BD Fc Block™, Becton Dickinson Inc., Franklin Lakes, USA
Isotype control antibody	*InVivoMab* Mouse IgG1 Isotype Control Bio X Cell Inc. Lebanon, USA
Liberase	Liberase™ Research Grade, Sigma-Aldrich Inc., St. Louis, USA
Normal donkey serum	Normal Donkey Serum Control, Jackson ImmunoResearch Laboratories Inc., West Grove, USA
Normal mouse serum	Normal Mouse Serum Control, Invitrogen Inc., Carlsbad, USA
Normal rat serum	Normal Rat Serum Control, Linaris Biologische Produkte, Dossenheim, Germany
Random primers	Random Primers, Invitrogen Inc., Carlsbad, USA
Recombinant mouse IL-4	Mouse IL-4 Recombinant Protein, eBioscience™, Invitrogen Inc., Carlsbad, USA
Recombinant mouse IL-5	Mouse IL-5 Recombinant Protein, eBioscience™, Invitrogen Inc., Carlsbad, USA
Recombinant mouse IL-13	Mouse IL-13 Recombinant Protein, eBioscience™, Invitrogen Inc., Carlsbad, USA
Recombinant mouse IL-17A	Mouse IL-17A Recombinant Protein, eBioscience™, Invitrogen Inc., Carlsbad, USA
Superscript II	Superscript™ II Reverse Transcriptase, Invitrogen Inc., Carlsbad, USA

5.1.3 Antibodies used for ELISA, flow cytometry, and IHC analyses

Table 5.3: Antibodies used for ELISA, flow cytometry, and immunohistochemistry analyses. The table provides information on antibodies, concentrations, and dilutions. APC-Cy7=Allophycocyanin-Cy7, BV=Brilliant Violet, AF=Alexa Fluor, pAb=polyclonal antibody, PE=Phycoerythrin.

Antibody	Clone	Conjugate	Manufacturer	Isotype	Dilution
anti-GFP pAb		-	Invitrogen Inc., Carlsbad, USA (# A11122)	rabbit IgG	1:1000
anti-mouse CD3e	eBio500A2	APC-Cy7	Invitrogen Inc., Carlsbad, USA	syr. hamster IgG	1:300

Continued

anti-mouse CD3	17A2	AF 488	BioLegend Inc., San Diego, USA	rat IgG2b	1:100
anti-mouse CD4	RM4-5	BV 710	BioLegend Inc., San Diego, USA	rat, IgG2b	1:300
anti-mouse CD11c	N418	AF 647	BioLegend Inc., San Diego, USA	arm. hamster IgG	1:200
anti-mouse CD90.2	53-2.1	BV 605	BioLegend Inc., San Diego, USA	rat IgG2a	1:300
anti-mouse GATA3	HG3-31	AF 647	Santa Cruz Inc., Dallas, USA	mouse IgG1	1:200
anti-mouse IL-4	11B11	-	Invitrogen Inc., Carlsbad, USA	rat IgG1	1:500
anti-mouse IL-4	BVD6-24G2	biotin	Invitrogen Inc., Carlsbad, USA	rat IgG1	1:500
anti-mouse IL-5	TRFK 4	-	Invitrogen Inc., Carlsbad, USA	rat IgG2a	1:500
anti-mouse IL-5	TRFK-4	biotin	Invitrogen Inc., Carlsbad, USA	rat IgG2a	1:500
anti-mouse IL-13	eBio13A	-	Invitrogen Inc., Carlsbad, USA	rat IgG1	1:500
anti-mouse IL-13	eBio13A	biotin	Invitrogen Inc., Carlsbad, USA	rat IgG1	1:1000
anti-mouse IL-13	eBio13A	APC	Invitrogen Inc., Carlsbad, USA	rat IgG1	1:150
anti-mouse IL-17A	eBio17CK15A5	-	Invitrogen Inc., Carlsbad, USA	rat IgG2a	1:2000
anti-mouse IL-17A	eBio17B7	biotin	Invitrogen Inc., Carlsbad, USA	rat IgG2a	1:500
anti-mouse IL-17A	eBio17B7	PE	Invitrogen Inc., Carlsbad, USA	rat IgG2a	1:150
anti-mouse IL-17A	17F3	-	Bio X Cell Inc. Lebanon, USA	mouse IgG1	*in vivo*
anti-mouse langerin pAb		-	BioLegend Inc., San Diego, USA (#E-17)	goat IgG	1:6000
anti-mouse αSMA	1A4	FITC	Invitrogen Inc., Carlsbad, USA	mouse IgG	1:3000
anti-mouse TCRβ	H57-597	AF 700	BioLegend Inc., San Diego, USA	arm. hamster IgG	1:300
anti-mouse TCRβ	H57-597	AF 488	BioLegend Inc., San Diego, USA	arm. hamster IgG	1:400

Continued

anti-rat IgG pAb		DyLight-549	Jackson ImmunoResearch Inc., West Grove, USA	donkey IgG	1:3000
anti-rat IgG pAb		AF 647	Jackson ImmunoResearch Laboratories Inc., West Grove, USA	donkey IgG	1:1600
anti-rbbt IgG pAb		AF 488	Jackson ImmunoResearch Laboratories Inc., West Grove, USA	donkey IgG	1:1600
anti-RORγt	AFKJS-9	-	Invitrogen Inc., Carlsbad, USA	rat IgG2a	1:100 1:800

5.1.4 Primers used for Real time-quantitative PCR

Table 5.4: Forward and reverse primers used for RT-qPCR.

Primer	Sequence
Gob5 forward	5´ ACT AAG GTG GCC TAC CTC CAA 3´
reverse	5´ GGA GGT GAC AGT CAA GGT GAG A 3´
Il17a forward	5´ CAG ACT ACC TCA ACC GTT CCA C 3´
reverse	5´ TCC AGC TTT CCC TCC GCA TTG A 3´
Il17f forward	5´ TGC CAG GAG GTA GTA TGA AGC TT 3´
reverse	5´ ATG CAG CCC AAG TTC CTA CAC T 3´
Il22 forward	5´ ACG CAA GCA TTT CTC AGA GA 3´
reverse	5´ AAC ATG AGT CCA GGG AGA GC 3´
Muc5ac forward	5´ CCA TGC AGA GTC CTC AGA ACA A 3´
reverse	5´ TTA CTG GAA AGG CCC AAG CA 3´
Muc5b forward	5´ TGT ACT GCC CCC AGG ATG GGC 3´
reverse	5´ AGC TCA GCT CTG CCT GAC CCT 3´
Mpo forward	5´ TCC CAC TCA GCA AGG TCT T 3´
reverse	5´ TAA GAG CAG GCA AAT CCA G 3´
S14 forward	5´ GAG GAG TCT GGA GAC GAC GA 3´
reverse	5´ TGG CAG ACA CCA AAC ACA TT 3´

5.1.5 Consumables and disposable equipment

Table 5.5: Consumables and disposable equipment.

Consumable	Exact designation, company
Adhesive plate cover	Sealing Tape for 96-Well Plates Thermo Fisher Scientific Inc., Waltham, USA
Cannula, 20 G	Vasofix® Safety B. Braun AG, Melsungen, Germany
Cell strainer, 70 µm	Falcon® 70 µm Cell Strainer Corning Inc., Corning, USA
Conical tubes, 15 mL, 50 mL	Falcon® Conical Centrifuge Tubes Corning Inc., Corning, USA
Cover glasses	Menzel Cover Glasses, 24x60 mm, thickness I, VWR International Inc., Radnor, USA
Cryostat blades	Low-profile Disposable Blades 819 Leica Biosystems GmbH, Wetzlar, Germany
Insulin syringes, 1 mL	Insulin Syringes Becton Dickson Inc., Franklin Lakes, USA
Liquid Blocker pen	Liquid Blocker PAP pen Daido Sangyo Ltd., Tokyo, Japan
Microscopy objective slides	SuperFrost Plus™ Objective Slides, Thermo Fisher Scientific Inc., Waltham, USA
Needle, 27 G 3/4	Sterican® Disposable Needle 27 G B. Braun AG, Melsungen, Germany
Parafilm	Parafilm® Laboratory Sealing Film Bemis Inc., Neenah, USA
PCR 96-well plate	LightCycler Plate Roche AG, Basel, Switzerland
PCR tubes and caps, 200 µL	0.2 mL 8-Tube PCR Strips and Domed Cap Strips Bio-Rad Inc., Hercules, USA
Pipette tips, 10 µL, 100 µL, 1000 µL	Eppendorf micropipette tips Eppendorf AG, Hamburg, Germany
Reagent reservoirs, 5 mL	5 mL Reagent Reservoir VitaScientific Inc., College Park, USA
Scalpel, disposable	Disposable Sabre Surgical Scalpels Swann-Morton Ltd., Sheffield, UK
Serological pipettes, 5 mL, 10 mL, 25 mL	Serological Pipettes Sarstedt AG, Nümbrecht, Germany
Serum tubes	BD Microtainer Tube Yellow Cap with Serum Separator Gel, Becton Dickinson Inc., Franklin Lakes, USA

Continued

Snap-cap tubes, 0.5 mL, 1,5 mL, 2 mL	Eppendorf Safe-Lock Tubes Eppendorf AG, Hamburg, Germany
Spatula	Wooden Disposable Spatula Laser physics Ltd., Cheshire, UK
Sterile vacuum bottle top filter, 0.22 μm	Stericup® and Steritop® Filter Units Sigma-Aldrich Inc., St. Louis, USA
Surgical suture	Non-Absorbable Suture A185 Ethicon Inc., Somerville, USA
Syringes, 1 mL, 2 mL	BD Plastipak™ Syringe Becton Dickinson Inc., Franklin Lakes, USA
Tissue cassette sponges	Tissue Embedding Sponge Carl Roth GmbH, Karlsruhe, Germany
Tissue cassettes	Histosette® I Biopsy Processing/ Embedding Cassette M498 (VWR International LLC, Radnor, USA)
6-well plates, flat bottom	Falcon® 6-well Flat Bottom TC-treated Multiwell Cell Culture Plate Corning Inc., Corning, USA
24-well plates, flat bottom	Falcon® 24-well Flat Bottom TC-treated Multiwell Cell Culture Plate Corning Inc., Corning, USA
96-well ELISA plates	Microplate Half Area Microlon® Greiner Bio One GmbH, Kremsmünster, Austria
96-well plates, black, flat bottom	Corning® 96 Well Black Polystyrene Microplate, Corning Inc., Corning, USA
96-well plates, flat bottom	Nunc™ MicroWell™ 96-Well Microtiter plate, Thermo Fisher Scientific Inc., Waltham, USA
96-well plates, round bottom	Nunc™ MicroWell™ 96-Well Round Bottom Microtiter plate, Thermo Fisher Scientific Inc., Waltham, USA

5.1.6 Kits used for experiments

Table 5.6: Kits used for experiments.

Kits	Exact designation, company
Fixation/permeabilization solution	Cytofix/Cytoperm™, Becton Dickinson Inc., Franklin Lakes, USA
Diff-Quick staining	RAL DIFF-QUICK™, RAL Diagnostics, Martillac, France
SYBR Green mix	Light Cycler 480® SYBR Green I Master Mix Roche AG, Basel, Switzerland

5.1.7 Buffer and media

Table 5.7: Buffer and media.

Buffer and reagents	Ingredients
ACK Lysing buffer	Ammonium-Chloride-Potassium Lysing buffer Lonza AG, Basel, Switzerland
ELISA blocking buffer	PBS-T BSA (1 % w/v)
ELISA coating buffer, pH 8.8	Water (deionized) Sodium carbonate 2.7 mM Sodiumhydrogen carbonate 8.9 mM
ELISA reagent diluent buffer	PBS-T BSA (0.1 % (w/v)
ELISA wash buffer	(see PBS-T)
Flow buffer	PBS BSA (0.5 % (w/v)
HBSS	Hank´s Balanced Salt Solution, Thermo Fisher Scientific Inc., Waltham, USA
IMDM	Iscove's Modified Dulbecco's Medium Thermo Fisher Scientific Inc., Waltham, USA
OCT media	TissueTek® O.C.T. Compound TM Science Services GmbH, München, Germany
PBS, 5x, pH 7.4	NaCl (685.0 mM) KCl (13.5 mM) NaH_2PO_4 x H_2O (50.0 mM) Na_2HPO_4 x H_2O (10.0 mM)
PBS-T / ELISA wash buffer	NaCl (137.0 mM) KCl (2.7 mM) NaH_2PO_4 x H_2O (10.0 mM) Na_2HPO_4 x H_2O (2.0 mM) Tween 20 (0.0005 % v/v)
PMA / ionomycin-based stimulation media	IMDM PMA (50 ng/mL) Ionomycin (500 ng/mL) Brefeldin (1x) Monensin (1x)
Permeabilization buffer, 10x	BD Perm/Wash Buffer Becton Dickinson Inc., Franklin Lakes, USA
PFA solution	PBS PFA (1 % v/v)

Continued

Ringer solution, pH 7.4	KCl (5.6 mM) NaCl (136.4 mM) $MgCl_2$ x 6 H_2O (1.0 mM) $CaCl_2$ x 2 H_2O (2.2 mM) Glucose (11.0 mM) HEPES (10.0 mM)
RPMI	RPMI Media 1640, Gibco Life Technologies Corp., Carlsbad, USA
RPMI culture media	RPMI 1640 FBS (10 % v/v) Pen/Strep/L-glut (1 % v/v) β-mercaptoethanol (0.1 % v/v)
RPMI digestion media	RPMI 1640 Liberase (1.5 mg/mL) DNase I (0.5 mg/mL) Pen/Strep/L-glut, 100x (1 % v/v)
RPMI wash media	RPMI 1640 FBS (10 % v/v) Pen/Strep/L-glut (1 % v/v) DNase I (0.5 mg/mL)
Sucrose solution	PBS Sucrose (20 % w/v, 30 % w/v)
Tris buffer, pH 8.5	Water, deionized, sterile Tris (0.5 M)

5.1.8 Mouse strains used for experiments

Table 5.8: Mouse strains and the origin of the experimental mice.

Mice	Origin
A/J wildtype mice	Colony Lewkowich, CCHMC
A/J RORC-GFP mice	Colony Lewkowich, CCHMC
C57BL/6 wildtype mice	Colony Lewkowich, CCHMC Colony Köhl, UzL

The CCHMC laboratory animal facility is a registered facility by the United States Department of Agriculture. Antibiotics experiments as described were permitted by the Institutional Animal Care and Use Committee (registration number: Lewkowich_2013-0180). Animal experiments in Lübeck included HDM-immunization of two C57BL/6 mice, permitted and registered by the state ministry of environment and agriculture of Schleswig-Holstein (registration number: 39(44-5/18)).

5.1.9 Non-disposable equipment and electronic devices

Table 5.9: Non-disposable equipment and electronic devices.

Equipment	Exact designation, company
Centrifuge	Centrifuge 5810 R, Eppendorf AG, Hamburg, Germany
Confocal laser scanning microscope (LSM)	Zeiss 710 meta, Carl Zeiss AG, Oberkochen, Germany
Cooling device (vibratome)	Ultratemp 2000, Julabo Labortechnik GmbH, Seelbach, Germany
Cryostat	Leica Biosystems Cryostat CM3050, Leica Biosystems GmbH, Wetzlar, Germany
Cytospin centrifuge	Shandon Cytospin™ 4 Cytocentrifuge, Thermo Fisher Scientific Inc., Waltham, USA
Cytospin clip	Shandon TM Cytoclip™ Stainless-Steel Slide Clip, Thermo Fisher Scientific, Waltham, USA
Cytospin funnel	Simport® Scientific CytoStep™ Funnel for Shandon™, Cytospin 4™ Centrifuges Thermo Fisher Scientific Inc., Waltham, USA
Ear punch	Ear Punch - Thumb Style, Braintree Scientific Inc., Braintree, USA
Electronic pipette	Original Portable Pipet-Aid Pipette Controler, Daigger Scientific Inc., Vernon Hills, USA
ELISA plate reader	BioTek™ Synergy™ 2 Multi-Mode Microplate Readers, BioTek Instruments Inc., Winooski, USA
FlexiVent	FlexiVent® System, Scireq Scientific Equipment Inc., Montreal, Canada
Flow cytometer	BD™ LSR II Becton Dickinson Inc., Franklin Lakes, USA
LightCycler	LightCycler® 480 Instrument II, Roche AG, Basel, Switzerland
Magnetic stirrer	Magnetic stirrer and hot plate, MR Hei-Tec, VWR International LLC, Radnor, USA
Micro centrifuge	Micro centrifuge 5430, Eppendorf AG, Hamburg, Germany
Microscissors	Microscissors, Stainless Steel, TDI International Inc., Tucson, USA
Microscope / cell counting	Microscope CKX53 Screening, Olympus Corp., Tokio, Japan
Microscope camera / cell counting	Microscope camera DP72, Olympus Corp., Tokio, Japan

Continued

Multichannel pipettes, 10 µL, 100 µL	Eppendorf Research Plus Multichannel Pipette, Eppendorf AG, Hamburg, Germany
Objective (confocal microscope)	EC-Plan-Neofluor 40x/1.30 Oil, Carl Zeiss AG, Oberkochen, Germany
NanoDrop	NanoDrop 2000 Spectrometer, Thermo Fisher Scientific Inc., Waltham, USA
Neubauer cell counting chamber	Neubauer chamber Improved cell counting chamber, VWR International LLC, Radnor, USA
Pipettes, 10 µL, 100 µL, 1000 µL	Single-Channel Pipette, Eppendorf AG, Hamburg, Germany
Precision scale	Precision Scale AD120, Scientific Industries Inc., Bohemia, USA
Surgical foreceps	Thumb Dressing Forceps, Roboz Surgical Instrument Co., Gaithersburg, USA
Surgical foreceps	Dumont 7 Forceps RS-4907, Roboz Surgical Instrument Co., Gaithersburg, USA
Surgical scissors	Dissecting Scissors, Streight, Ted Pella Inc., Redding, Canada
Tally counter	Tally Counter / Hand Clicker, Tally Counter Store, Leavenworth, USA
Tissue culture incubator	HERAcell® 240i CO2 Incubator, Terra Universal Inc., Fullerton, USA
Tube rodent holder	Tube Rodent Holder, Small, Kent Scientific Corp., Torrington, USA
Vibratome	Vibratome VT1200S, Leica Biosystems GmbH, Wetzlar, Germany
Vortex	Vortex Genie 2, Scientific Industries Inc., Bohemia, USA

5.1.10 Software used for data analysis

Table 5.10: Software used for data analysis.

Software	Company
BioTek Microplate reader and imaging software, version Gen 5	BioTek Instruments Inc., Winooski, USA
BioRender Scientific Illustrations	Science Suite Inc., Toronto, Canada
FlexiWare software, version 8.0	Scireq Scientific Equipment Inc., Montreal, Canada
FlowJo, version V10	Becton Dickinson Inc., Franklin Lakes, USA
GraphPad Prism, version 5	GraphPad Prism Software Inc., La Jolla, USA
Imaris software, version 6.4	Bitplane AG, Zürich, Switzerland
Microsoft Excel 2013	Microsoft Corp., Redmond, USA
Microsoft PowerPoint 2013	Microsoft Corp., Redmond, USA
Microsoft Word 2013	Microsoft Corp., Redmond, USA
Photoshop, version CS2	Adobe Systems Inc., San Jose, USA
ZEN software, version Zen lite 2011 (confocal microscope)	Zen Lite 2011 Carl Zeiss AG, Oberkochen, Germany

5.2 Methods

5.2.1 Maintenance procedures at the animal facility

All mice were kept under specific-pathogen free (SPF) conditions, only allowing certain murine, non-pathogenic microbes to be present. The SPF-conditions were controlled by the animal facilities. Sentinel mice housed in separate cages within the experimental mouse colony served in detection of pathogens. All actions that included handling and treatment of the mice within the mouse barrier were carried out under sterile conditions in a clean hood. Sterile food and drinking water were available at all times, as well as cotton nesting material. Mice were kept under constant observation by the animal facility staff, which included daily health checks and regular cage changes. Experimental interventions included oral administrations *ad libitum*, *i.p.* injections, *i.t*. treatments under general anesthesia, and *intravenous* (*i.v.*) injections.

5.2.2 Breeding and antibiotics treatment of pregnant mice

For breeding, one male and 2-3 female C57BL/6 wildtype (wt) mice were kept in one cage overnight. The next morning, the female mice were checked for mating plugs, indicating a possible pregnancy. On day 15 after the vaginal mating plug was observed, considered E15, pregnant mice were given drinking water *ad libitum*, containing the antibiotics ampicillin, gentamicin, and vancomycin (all at 1.0 mg/mL). To avoid dehydration, 0.5 % sucralose was supplemented to the drinking water, since the antibiotics solution tastes bitter. Control mice received 0.5 % sucralose in drinking water. After birth, considered P0, the antibiotic treatment was discontinued immediately. The offspring mice were kept with the dams for 3-4 weeks until separation by gender. The first treatment was performed at 6-8 weeks. Treatment groups equally consisted of female and male mice.

5.2.3 *In vivo* lung permeability studies

At 10-13 weeks, the offspring mice of antibiotics-treated mothers and sucralose control mothers were injected 200 µL FITC-albumin in saline solution (12.5 mg/mL) *i.v.*. Two hours later, mice were euthanized, BAL fluid and blood samples were collected and transferred to serum tubes. The serum tubes were centrifuged (10,000xg, 8 min). The serum samples were diluted 1:50, 1:100, 1:500, and plated in triplicates to black 96-well plates. The BAL fluid samples were plated in triplicates, undiluted. Fluorescence intensity was measured at 488 nm. The permeability index was assessed by dividing the BAL fluorescence intensity with the corresponding serum sample fluorescence.

5.2.4 Induction of asthma in offspring mice by HDM exposure

At 6-8 weeks, the offspring mice received an *i.p.* injection of 10 µg HDM extract in PBS (0.1 mg/mL) (experimental day 0) and another *i.p.* injection on experimental day 7. On experimental days 14 and 21, mice were treated *i.t.* with 100 µg HDM (1 mg/mL). i.t. treatments were carried out under general anesthesia with 120 mg/kg mouse weight ketamine and 8 mg/kg xylazine. The control mice received equal volumes of 100 µL PBS *i.p.* and 40 µL *i.t*. at the same time points. A cohort of mice received an *in vivo* blockade of IL-17A cytokine with 100 µL of antibody to murine IL-17A (2.5 mg/mL). The two other HDM cohorts received 100 µL isotype control antibody (2.5 mg/mL) at the same time. 72 hours after the last *i.t.* treatment, lung function measurements with the flexiVent system were performed.

5.2.5 *In vivo* lung function measurements

In order to perform *in vivo* lung function measurements, mice were anaesthetized with a sublethal dose of 70 mg/kg sodium pentobarbital and 10 mg/kg xylazine in saline solution. The body temperature was kept at 37° C during the measurements. The *in vivo* lung function measurements were performed, using the flexiVent system. First, the system was calibrated. After exposing the mouse trachea by surgical incision of the skin, submaxillary glands, and the muscles surrounding the trachea, a small incision was made between the tracheal rings to insert a blunt 20 G cannula. Cannula and trachea were kept airtight by surgical suture. The cannula was adjusted to the Y-tubing of the base. The system held a positive end-expiratory pressure of 3 cm H_2O. The flexiVent machine ventilated the mice at 150 breaths per minute with a volume that was automatically calculated based on the mouse weight. To avoid spontaneous inhalation, 1 mg/kg pancronium bromide was injected *i.p.*. Two total lung capacity perturbations were applied to recruit closed lung areas and standardize the lung volume history. Subsequently, three 1.25 s loops of single frequency forced exhalations were performed, followed by two deep inflations. PBS was aerosolized to evaluate the baseline resistance of the respiratory system (R_{RS}). Then, the dynamic R_{RS} was assessed by aerosolizing increasing concentrations of 12.5, 50, and 100 mg/mL methacholine. Methacholine stimulates the parasympathetic nervous system by acting as a non-selective muscarinic receptor agonist. If pre-existing hyperreactivity exists, increased R_{RS} are measured at lower concentrations of methacholine. If a maximum value was followed by three decreased data points, the measurements were discontinued and the next concentration of methacholine was administered. For data analysis, the maximum R_{RS} values measured were depicted. The mean of the maximum R_{RS} values per treatment group were graphed in a methacholine dose-response curve. For measurement points of the PBS aerosolization, the mean was calculated instead of depicting the maximum value.

5.2.6 Bronchoalveolar lavage fluid processing

After the lung function measurements, for collecting the bronchoalveolar lavage (BAL) fluid cells, lungs were rinsed three times with 1 mL ice cold HBSS buffer. The recovered volume was noted for the calculations of total cell numbers per mL. The collected BAL fluid was centrifuged (300 g, 6 min) and resuspended in ACK lysing buffer to remove erythrocytes. The lysing buffer was diluted with ice cold PBS, containing 5 % FBS and centrifuged (300xg, 6 min). The pellet was resuspended in PBS. Cells were counted, using the Neubauer chamber. Approximately 5-10x10^4 cells were transferred to objective slides by cytospincentrifuge (400 rpm, 4 min). Following the Diff-Quick staining, the cells were coverslipped, and 500 cells were differentially counted under the microscope, dividing monocytes/macrophages, eosinophils, neutrophils, and lymphocytes, according to their morphology. To assess absolute numbers per mL, the percentages were normalized to the corresponding total cell numbers per mL. Because of technical issues with pale Diff-Quick stainings a number of slides of low quality had to be discarded, explaining the limited overall number of data points.

5.2.7 Lung single cell suspension processing for *ex vivo* cytokine stimulation assays

After the lung function measurements and harvest of the BAL fluid cells, the chest cavity was exposed by surgical incision and the lungs were surgically removed. The postcaval lobe of the right lung was snap frozen for RT-qPCR analysis (sections 5.2.10, 5.2.11). The left lung tissue and the three remaining lobes of the right lung were minced with sterile surgical scissors and incubated in 7 mL RPMI digestion media (45 min, 37°C). The minced and digested lobes were then brought into single cell suspensions, using a 70 µm cell strainer, and centrifuged (400xg, 8 min). By addition of 1 mL ACK lysing buffer to the pellet, erythrocytes were lysed. The cells were washed and the pellet was resuspended for counting, using a Neubauer counting chamber. The volume was adjusted to 4x10^6 cells/mL. For the subsequent *ex vivo* cytokine stimulation assays, lung cell suspensions were plated: 1x10^6 cells per well were plated in a flat bottom 96-well plate for cytokine-stimulation assay and subsequent ELISA analysis (section 5.2.8). 2.5x10^5 cells per well were plated in a round bottom 96-well plate for the restimulation assay and subsequent flow cytometry measurements (section 5.2.9).

5.2.8 *Ex vivo* cytokine stimulation assay, ELISA

After single cell suspensions were processed, 1x10^6 cells per well were plated in a flat bottom 96-well plate and HDM was added to the media to a final concentration of 0.03 mg/mL. The plates were incubated in the humid chamber for 72 h (37°C), followed by harvesting the supernatants.

ELISA plates were coated with 50 µL of the diluted capture antibodies to IL-4, IL-5, IL-13, and IL-17A in coating buffer and incubated overnight at 4°C. The antibody dilutions are listed in Table 5.3. After washing with ELISA wash buffer, the plates were incubated with ELISA blocking buffer (2 h, 4°C). Meanwhile, the recombinant cytokines for the standard curves were titrated in a range of 5,000 to 4.88 pg/mL. After a plate wash, 50 µL recombinant standards and 50 µL samples were added to the antibody-coated 96-well plates and incubated overnight at 4°C. After a plate wash, the biotinylated detection antibody diluted in ELISA reagent diluent buffer was added (2 h, RT). HRP-Avidin diluted in ELISA reagent diluent was added after washing the plate (30 min, RT). The Super Aqua blue substrate was given into the wells after washing the plates, and once the standard curve had developed sufficiently, the optical density (OD) was measured with the BioTek plate reader. The table with OD values and the calculated concentrations based on the standard curve were exported and the mean values of concentrations of mice in one treatment group were graphed. The detection threshold was determined by noting the lowest concentration within the linear interval of the standard curve.

5.2.9 *Ex vivo* intracellular cytokine stimulation assay and flow cytometry measurements

After single cell suspensions were processed, $2.5x10^5$ cells plated in round bottom 96 well-plates were stimulated with 250 µL PMA/ionomycin-based stimulation media, containing Brefeldin A for inhibition of vesicle formation and trapping intracellular cytokines (4 h, 37°C). After stimulation, the cells were centrifuged (400 g, 3 min) and the pellet was resuspended in flow buffer, containing IgG FC block (15 min, 37°C). The cells were incubated with cell surface marker antibodies CD90.2, TCRβ, and CD3ε, diluted in flow buffer according to Table 5.3 (30 min, 37°C). CD4 was included but is not presented in the results section. After a wash, viability dye diluted in PBS was added, followed by incubation in darkness (15 min, RT). The cells were resuspended in 100 µL fixation/permeabilization solution for fixation and membrane permeabilization and incubated in darkness (60 min, RT). 100 µL IgG Fc block diluted in permeabilization buffer was added (15 min, 4°C). After a wash with permeabilization buffer, the cells were incubated with intracellular cytokine antibodies to IL-13 and IL-17A diluted in permeabilization buffer, according to the antibody dilutions listed in Table 5.3 (30 min, 4°C). After a wash, the cell pellet was resuspended in flow buffer. Flow cytometry measurements were performed using the flow cytometer LSR II. The data was imported to FlowJo software for manual compensation of overlapping fluorescence spectra and the gating of the cell populations analyzed (Fig. 5.1). The mean of the percentages of cytokine positive cells was determined and compared to the other treatment groups. For IL-17A$^+$ cells, the subpopulations expressing CD3 and TCRβ were further analyzed.

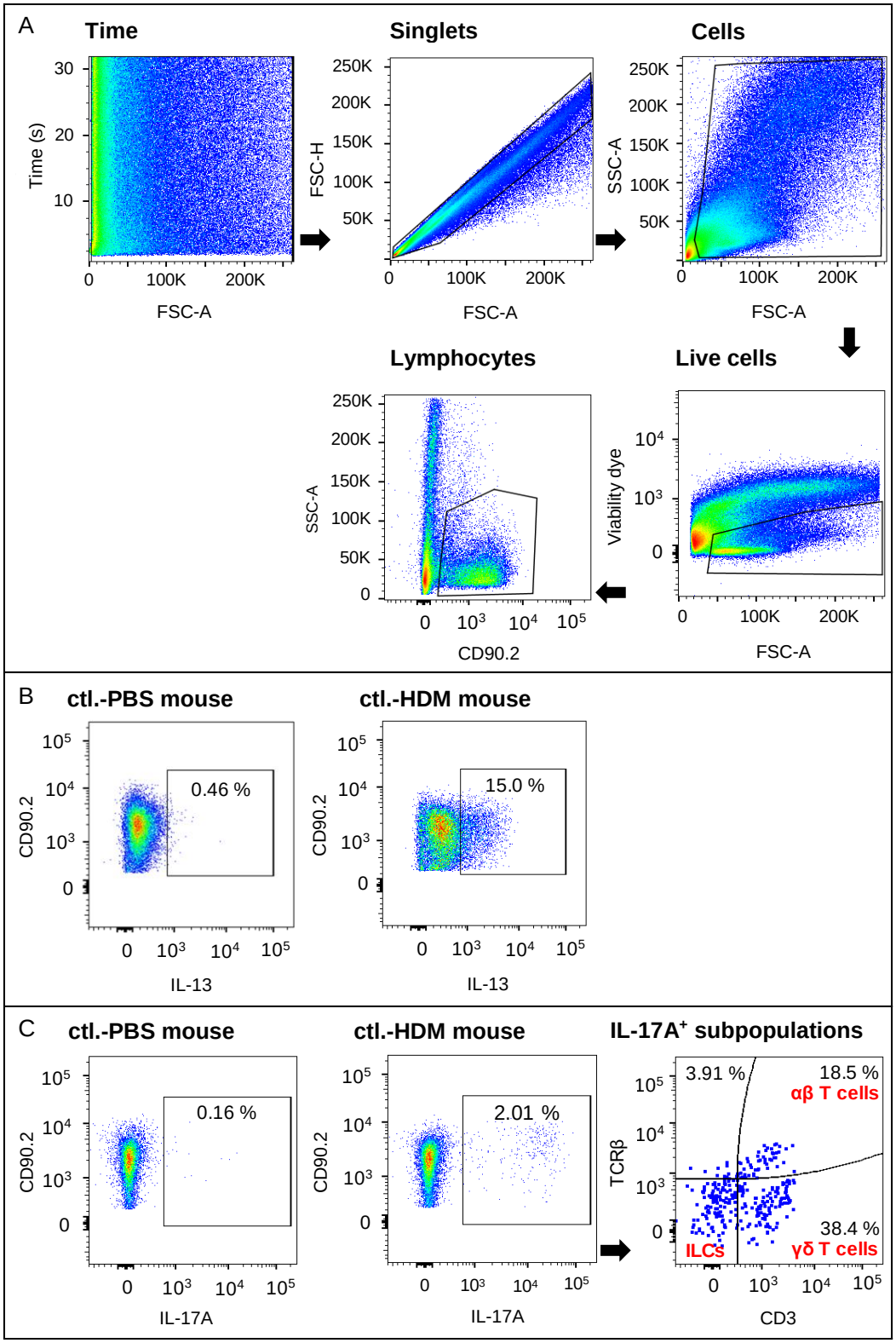

Fig. 5.1: Gating strategy for the analysis of intracellular cytokines. Lung tissue of C57BL/6 control or P0 mice treated with PBS or HDM was harvested and single cell suspensions were restimulated with PMA (50 ng/mL) and ionomycin (0.5 µg/mL) and stained for cell surface marker and intracellular cytokines. Pregating was performed as depicted [A]. CD90.2⁺ cells were gated for IL-13⁺ cells as visible for one dot plot of a control-PBS and a control-HDM mouse [B]. IL17A⁺ cells [C] were further analyzed for their expression of CD3 and TCRβ identifying the IL-17A⁺ subpopulations (right dot plot).

5.2.10 RNA extraction, cDNA synthesis

The postcaval lung lobe was lysed by adding 500 µL TRIzol reagent and vortexed (5 min, RT). 200 µL chloroform was added and mixed, followed by a short incubation, and centrifugation (12,000xg, 15 min, 4°C). The aquaeus phase was transferred to 500 µL isopropanol, containing glycogen (0.1 mg/mL) and incubated (10 min, RT). The samples were centrifuged (12,000xg, 10 min, 4°C). The supernatant was discarded and the pellet was washed with 1 mL 75 % ethanol and centrifuged (7,500xg, 5 min, 4°C). The supernatant was discarded and the pellet was dried for 30-60 min, before resuspension in 20-40 µL nuclease-free water. The samples were heated to 65°C and shortly centrifuged. The RNA concentration and quality were measured, using a NanoDrop. For cDNA synthesis, 300-1,000 ng RNA in 11 µL nuclease-free water and 2 µL master mix I were pipetted (Table 5.11). A cycle for primer annealing was run on the PCR machine (Table 5.12). After the reverse transcription PCR run, 7 µL master mix 2 (Table 5.11) were added to each reaction tube and the cycle of cDNA synthesis was started (Table 5.13). After completing the cycle, 100 µL nuclease free water were added to each cDNA sample.

Table 5.11: Master mix I and II for cDNA synthesis

cDNA master mix I		**cDNA master mix II**	
Random primer	1 µL	1st strand buffer (5x)	4 µL
dNTP mix	1 µL	0.1 M DTT	2 µL
		RNase Out	0.5 µL
		H_2O	0.5 µL
		Superscript II	0.25 µL

Table 5.12: Reverse transcription PCR cycle settings, primer annealing

Temperature (°C)	**Duration (min)**
65	5
4	1

Table 5.13: Reverse transcription PCR cycle settings, reverse transcription

Temperature (°C)	**Duration (min)**
25	10
42	50
70	15
4	hold

5.2.11 Real time-quantitative PCR

For RT-qPCR, the master mix was prepared, keeping the reagents on ice. 8 µL master mix were pipetted to LightCycler plates and 2 µL cDNA were added (Table 5.14). The plate was sealed and the RT-qPCR run was started (Table 5.15). After the run, the data were exported and the Crossing point (Cp) values were evaluated. The Cp value of the housekeeping gene Ribosomal protein (S) 14 served to determine the relative quantities of the target genes.

Table 5.14: Master mix for Real time-quantitative PCR

SYBR green master mix	5.0 µL
Primer forward	0.5 µL
Primer reverse	0.5 µL
H_2O	2.0 µL

Table 5.15: Real time quantitative PCR cycle settings

Step	Temperature (°C)	Duration	Cycles (n)
Denaturation	95	10 min	1
Amplification	95	5 s	45
	60	10 s	
	72	11 s	

5.2.12 Intestine removal and cryosectioning

For dissection of intestinal tissue, A/J wt and A/J RORC-GFP mice were injected *i.p.* with 100 µL sodium pentobarbital (65 mg/mL). The peritoneum of was exposed and the small intestine was removed from the mesentery and dissected behind the caecum. Approximately 10 cm of the small intestine were rinsed thoroughly with PBS until flow through came clear. The lumen was filled with 1 % PFA solution, coiled into a spiral, using forceps, and placed between two sponges in a tissue cassette. The intestine tissue was incubated in 10 mL fixation/permeabilization solution 1:4 with PBS at 4°C overnight, shaking. The solution was replaced by PBS (8 h, 4°C, shaking). The PBS was replaced by 30 % sucrose solution 1:1 with OCT media and incubated overnight at 4°C, shaking. The intestine tissue was embedded in OCT media and transferred to liquid nitrogen. The frozen tissue blocks were placed at -20°C for 1 h to reach optimal cutting temperature. 18 µm sections were generated with the cryostat, transferred to objective slides and dried for 2 h at RT. The sections were stored at -80°C. Before immunohistochemistry (IHC) incubation, the objective slides were defrosted and dried for 1 h and the tissue was circled, using a liquid blocker pen.

5.2.13 Lung removal and slicing of agarose-filled lungs for microscopy

For dissection of lung tissue, C57BL/6 wt mice were injected *i.p.* with 100 µL sodium pentobarbital (65 mg/mL). To remove the lungs, the chest cavity was exposed by surgical incision. The lungs were perfused *via* the right ventricle with 3 mL ice cold Ringer solution, containing 5 % heparin. The trachea was exposed, a surgical suture was loosely tied around the trachea, a small incision was made, and ~1.5 mL 3 % LM agarose in Ringer solution (37°C) was injected into the lungs. When the lungs were filled, they were removed, using micro scissors, and transferred to ice cold Ringer buffer. The left lobe or the large right lobe were attached to the vibratome block, using vetbond. 300 µm sections were sliced by the vibratome and collected in ice cold Ringer buffer. The lung sections were fixed with 1 % PFA in PBS (15 min, RT, shaking), washed three times with PBS (15 min, RT, shaking), and incubated with 20 % sucrose solution overnight at 4°C. 300 µm sections were stored at -20°C in 20 % sucrose solution. A representative image of a 300 µm section of the left lung is visible in Fig. 5.2.

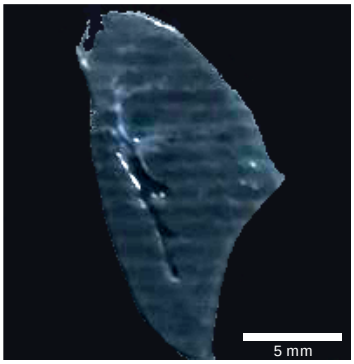

Fig. 5.2: Representative image of a section of the left lung generated by the vibratome.
Lungs were filled with 3 % LM agarose and 300 µm sections were sliced, using the vibratome. The sections were fixed with 1 % PFA and kept in 20 % sugar solution at -20°C until IHC staining was performed.

5.2.14 Immunofluorescence staining

300 µm lung sections or 18 µm intestinal sections were incubated with IHC blocking buffer (20 min, RT). Antibody dilutions were prepared in IHC blocking buffer as following: 18 µm intestine sections were incubated with 1:100 RORγt antibody overnight (4°C). 300 µm lung sections were incubated with 1:800 RORγt antibody solution (60 h, 4°C, shaking). Following the incubation, the sections were washed three times with PBS (10 min, RT). The sections were incubated with the secondary antibody diluted in PBS, containing 5 % normal serum of the host species (60 min, RT). The sections were washed three times with PBS and embedded in mowiol embedding media or

Hoechst-containing mowiol media (1 µg/mL). For the double-labeling of RORγt and αSMA, TCRβ, and CD11c, the antibodies were added to the RORγt antibody incubation. The dilutions are listed in Table 5.3. For the double-labeling with CD3, an additional blocking step with 10 % normal rat serum in PBS was performed (1 h, RT), followed by incubation with the CD3 antibody diluted in PBS (2 h, RT) and wash. The sections were embedded in mowiol media on objective slides.

5.2.15 Settings of the laser scanning confocal microscope

Z-stacks were generated, using the laser scanning confocal microscope (LSM) Zeiss 710 meta. With the laser and filter setups used, a combination of four fluorochromes of distinct excitation/emission wave lengths could be analyzed. These covered the spectrum of visible and invisible light, ranging from ultra violet (Hoechst), green (Alexa Fluor 488), red (DyLight 549), and far red light (Alexa Fluor 647). Before image acquisition, the mode was switched to “Location”, to visually detect regions of interest by fluorescence light. If an area of interest was detected, the mode was switched to “Acquisition” to record Z-stacks of that area. Before the scan was started, the laser power was adjusted for each channel. The “Smart setup” was used, simultaneously scanning the green and far red channels, while UV and red channels were scanned separately. Z-stacks of negative controls were acquired, using the same laser power and settings.

5.2.16 Identification of RORγt$^+$ cells in intestine and lung tissue

Z-stacks of intestine or lung sections were generated to identify and analyze RORγt$^+$ cells. The generated files were imported to Imaris software analysis and for the quantification of RORγt$^+$ cells by counting. Based on the knowledge that RORγt is a transcription factor and to our knowledge no description of RORγt as a structural component of pulmonary septae exists, we concluded that the RORγt antibody produced unspecific background staining. To reduce the background staining, the images were adjusted in terms of brightness and contrast.

RORγt$^+$ cells were counted at large and small airways, using labeling of α smooth muscle actin (SMA) for identification of airways and blood vessels. Because the tissue-intrinsic autofluorescence and the accumulation of immune cells were sufficient to identify large airways and small airways/blood vessels without the αSMA labeling, a large part of the images where analyzed without αSMA labeling. An example of a large airway and a small airway/blood vessel is visible in Fig. 5.3. Small airways/blood vessels were defined as less than 100 µm in diameter. Because small airways and blood vessels cannot be distinguished by autofluorescence, they were counted in one group. Large airways were defined by their diameter and by the accumulation of high numbers of immune cells in a relative large area as visible in the example. Structures that could not be categorized, were excluded from the analysis. RORγt cells were counted and the

percentages were determined. Generally, the total number of counted cells are given in the figure descriptions of the results.

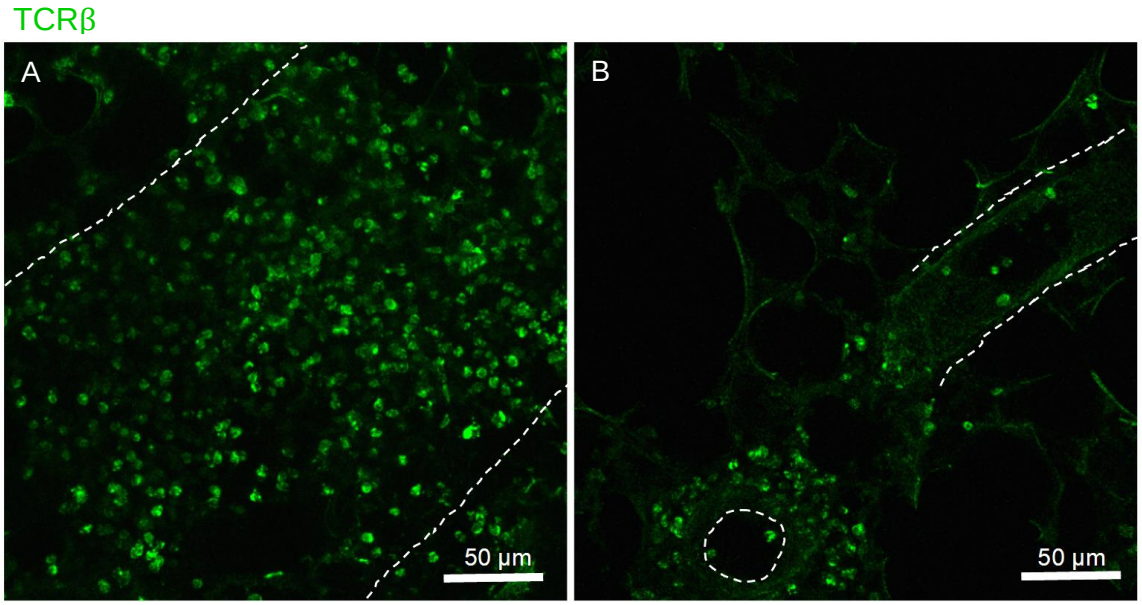

Fig. 5.3: Large and small airways/blood vessels identified by tissue-intrinsic autofluorescence and cell frequencies. Large airways were identified by tissue autofluorescence, the numbers of immune cells, and the size [A]. Small airways/blood vessels were identified by tissue autofluorescence, by immune cells visible, and by their size of <100 µm [B]. The white lines mark the border of the airways/blood vessel.

To analyze the localization of the RORγt subpopulations, the acquired Z-stacks for identification of the subpopulations were reanalyzed. Again, large airways were defined by the large cell numbers, tissue-intrinsic autofluorescence, and by the size of the diameter. To determine the contact rate of RORγt in relation to CD11c, the “Slice function” of Imaris was used, to scroll through the single planes of the Z-stack and analyze, whether the specific cell signal for RORγt and the signal for $CD11c^+$ were in close proximity as visible in a representative example (Fig. 5.4). Percentages of cells in contacts were determined.

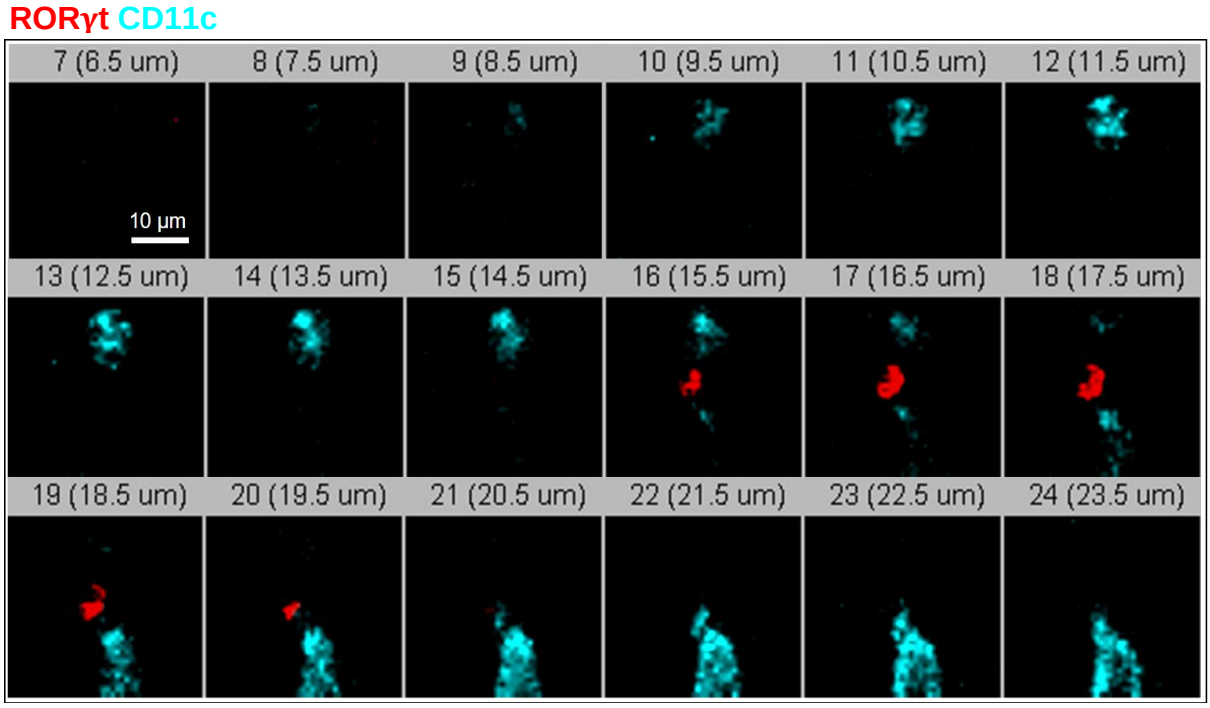

Fig. 5.4: Analysis of RORγt$^+$ cells in proximity to a CD11c$^+$ DCs. The proximity in the 3D setting was counted as positive, if cell-specific signal of RORγt (red) and CD11c (turquois) were detected in immediate proximity. The "Slice" function of Imaris software was used to scroll through the Z-stacks for a detailed analysis of contacts. "7"-"24" describe the single planes viewed in the "Gallery" mode.

5.2.17 Statistics

Data analysis and graphing were performed, using GraphPad Prism software. If outlier were found, a Grubbs test was performed for exclusion. For the comparison of multiple independent treatment groups, a one-way ANOVA was performed. The post hoc tests depended on the distribution of the measurement points: if a Gaussian distribution was found, which was analyzed by Kolmogorov-Smirnov test, a parametric analysis was chosen. For multiple parametric comparison, the Tukey post hoc test was chosen, the mean and the standard error of the mean (SEM) were included in the graph. If one parameter was dependent like a dose response curve, a two-way ANOVA was chosen, followed by the Bonferroni post hoc test, due to a grouped analysis of different concentrations per treatment group. For the comparison of two data sets that showed a Gaussian distribution, a Student T test was performed and the mean and SEM were included in the graph. The statistical comparison of two groups that did not show Gaussian distribution was analyzed by Mann-Whitney U test and the median and 10-90 percentile were graphed. Correlation analysis of measurement points with Gaussian distribution was performed by assessment of the Pearson correlation coefficient.

6 Results

Colonization of the newborn with commensal microbiota is initiated after birth. However, also prenatal antibiotics exposure has been linked to an increased disease developmental risk for asthma by epidemiological data. Therefore it is of interest to investigate, if prenatal disruption of the colonization with microbiota in a well characterized mouse model of HDM-immunization will change the asthma phenotype.

6.1 Exposure to prenatal antibiotics induces minor alterations to the basal lung physiology and to the asthma phenotype

Pregnant C57BL/6 dams were prenatally exposed to antibiotics together with sucralose from E15 to P0 ("P0 mice") or to sucralose alone ("control mice"). At six to eight weeks of age, the offspring mice were treated twice *i.p.* and twice *i.t.* with PBS, constituting the groups "control-PBS mice" and "P0-PBS mice". "Control-HDM mice" and "P0-HDM mice" were immunized with HDM *i.p.* and *i.t.*, according to the schematic overview (Fig. 6.1). One cohort, "P0-HDM / IL-17A mAb" received an additional systemic cytokine blockade of IL-17A.

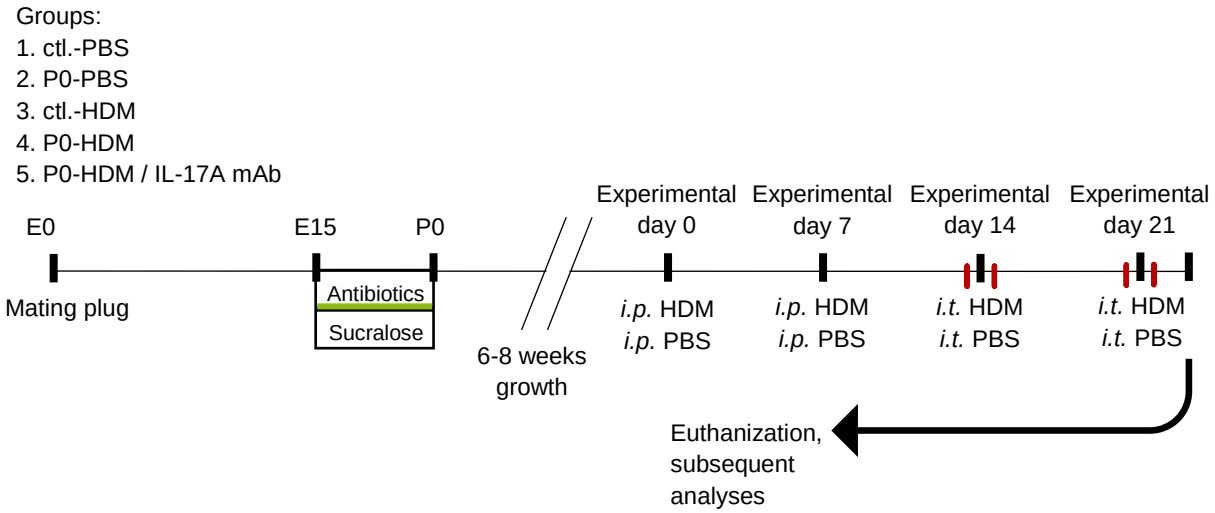

Fig. 6.1: Time line for antibiotics exposure and immunization steps.
Breeding pairs were set up and E0 was determined by vaginal mating plug. On day E15, dams received ampicillin, gentamicin, and vancomycin (each 1 mg/mL) in drinking water, containing 0.5 % sucralose until postnatal day (P) 0. During the same time span, control (ctl.) mice received 0.5 % sucralose in drinking water. After 6-8 weeks of growth, control- and P0-HDM mice were challenged twice *i.p.* with 10 µg HDM (experimental days 0, 7) and twice with 100 µg *i.t.* (days 14, 21). At the same time points, control- and P0-PBS mice received *i.p.* and *i.t.* treatments with PBS. The red marks indicate time points 24 hours before and after *i.t.* HDM challenge, when 250 µg IL-17A mAb was injected *i.p.*, while all other HDM mice received 250 µg isotype control. 72 hours after the last *i.t.* treatment, mice were euthanized.

6.1.1 Prenatal antibiotics trend to increase the pulmonary epithelial permeability

For maintenance of tolerance, epithelial barrier function plays an important role. To investigate the role of pulmonary epithelial barrier function under steady state conditions, the entry of vascular FITC-albumin into the airway lumen was measured, comparing control-PBS and P0-PBS mice. FITC-albumin in solution was injected into the tail veins, followed by BAL fluid and serum sample collection and photometric measurements. The medium percentage of BAL fluorescence intensity measured for control-PBS mice was 0.66 %, while mice exposed to prenatal antibiotics showed a percentage of 1.12 %. The difference measured was statistically not significant (p=0.145) (Fig. 6.2).

Taken together, mice exposed to prenatal antibiotics showed a trend of increase in luminal entry of vascular FITC-albumin.

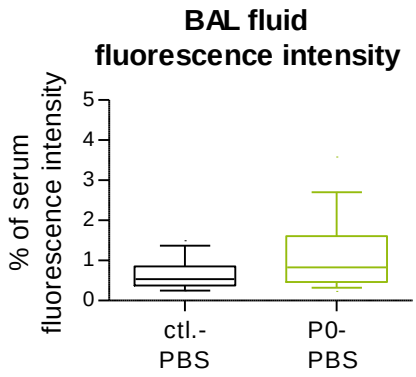

Fig. 6.2: Analysis of entry of intravascular FITC-albumin into the lung lumen.
C57BL/6 control (n=13) and P0 mice (n=18) treated with PBS were injected *i.v.* FITC-albumin solution (12.5 mg/mL). Two hours following the *i.v.* injection, BAL fluid and blood serum samples were collected. The extent of entry of intravascular FITC-albumin into the lung lumen was measured photometrically by determining the BAL/serum fluorescence ratio. Results of three independent experiments are shown. ctl.=control. Median and 10-90 percentile range are shown. Mann-Whitney U test.

6.1.2 Prenatal antibiotics do not enhance the respiratory resistance of HDM-immunized mice

After sensitization to an allergen, an increase in airway hyperresponsiveness is one of the cardinal symptoms of allergic airway inflammation. The underlying inflammatory responses cause changes in airway structure, contractibility, and in mucus production. To test airway hyperresponsiveness, challenge with aerosolized methacholine, a muscarinic receptor agonist, was performed, followed by measurements of the resistance of the respiratory system (R_{RS}). As expected, at baseline,

control-PBS mice showed only minor changes in R_{RS} in response to increasing concentrations of methacholine, reaching a maximum R_{RS} of 2.0 cm H_2O*mL/s at 100 mg/mL methacholine. Expectedly, the control-HDM mice developed a fourfold increase, the difference reaching statistical significance at 50 and 100 mg/mL methacholine and a maximum R_{RS} of 8.5 cm H_2O*mL/s (Fig. 6.3). Similar to control-PBS mice, lung function measurements of antibiotics-exposed P0-PBS mice showed a dose response curve with minor changes in response to increasing methacholine concentrations, reaching a maximum R_{RS} of 2.2 cm H_2O*mL/s. P0-HDM mice showed a fourfold increase in R_{RS}, reaching statistical significance at 50 and 100 mg/mL methacholine and a maximum R_{RS} of 8.9 cm H_2O*mL/s, which was essentially similar to control-HDM mice (Fig. 6.3). Blocking of IL-17A reduced R_{RS} to 5.32 cm H_2O*mL/s at 100 mg/mL methacholine.

Taken together, although the overall expected increase in R_{RS} under inflammation of the airways was observed, prenatal antibiotics exposure did neither enhance the baseline R_{RS}, nor the R_{RS} upon HDM-immunization.

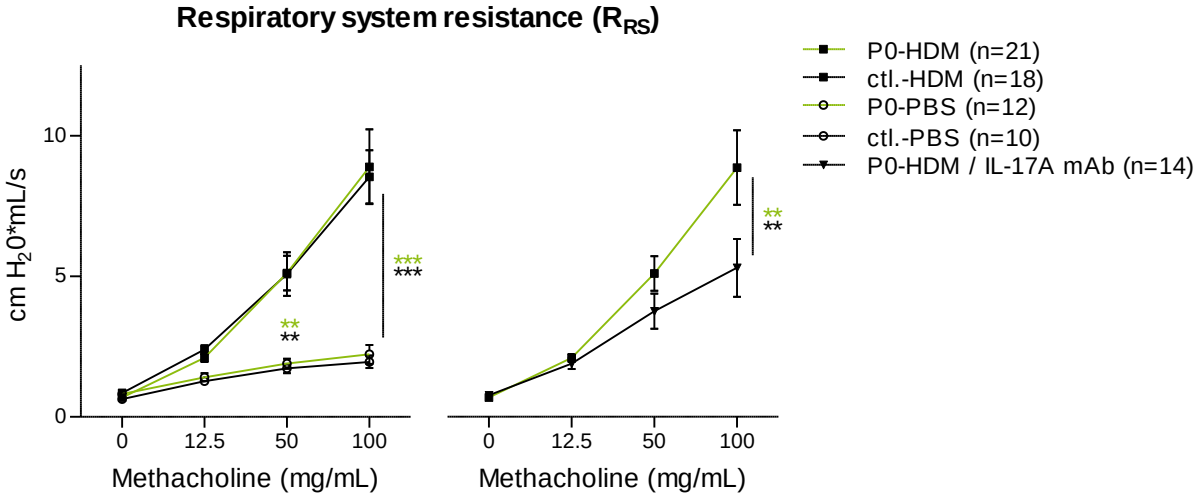

Fig. 6.3: Lung function analysis *via* respiratory system resistance measurements.
C57BL/6 control or P0 mice treated with PBS or HDM and P0-HDM mice that received IL-17A blockade underwent lung function measurements with the FlexiVent system. After setting an initial set of measurements nebulized PBS, increasing doses of 12.5, 50, and 100 mg/mL methacholine were administered through the nebulizer and the R_{RS} was determined. ctl.=control. Mean and SEM shown. Two-way ANOVA; Bonferroni test (** $p < 0.01$; *** $p < 0.001$).

6.1.3 Prenatal antibiotics do not change the total BAL fluid cell numbers or the BAL fluid cell composition

Next, the underlying inflammatory responses associated with increased R_{RS} seen under inflammation were analyzed. To this end, total BAL fluid cell counts and the cellular composition of BAL fluid cells were assessed. In terms of total BAL cell numbers, control-PBS mice showed total count of $0.37x10^6$ cells. As expected, the total cell numbers increased ninefold to $3.23x10^6$ cells for control-HDM mice ($p<0.001$) (Fig. 6.4 A). Comparable to control-PBS mice, antibiotics-exposed P0-PBS mice showed similar total BAL cell numbers with $0.23x10^6$ cells, which increased under inflammation twelvefold to $2.84x10^6$ cells, reaching statistical significance ($p<0.001$). In terms of the immune cell composition of control-PBS mice, expectedly, monocytes/macrophages were the largest immune cell population with $0.31x10^6$ cells. A tendency of increase to $0.88x10^6$ cells was observed under inflammation. The analysis of the immune cell composition of P0-PBS mice also showed the expected predominance of monocytes/macrophages with $0.15x10^6$ cells, which trended to increase under inflammation to $0.61x10^6$ cells. In contrast, upon HDM treatment, eosinophil granulocytes predominated the immune cell composition, increasing from $0.06x10^6$ cells at baseline 37-fold to $2.22x10^6$ cells upon HDM-immunization. P0-HDM mice showed an increase of eosinophils from $0.07x10^6$ cells at baseline 31-fold to $2.18x10^6$ cells. At baseline, $0.06x10^5$ neutrophil granulocytes were found for control-PBS mice. Under inflammation, neutrophils increased to $0.38x10^5$ cells. Neutrophil frequencies of P0-PBS mice were $0.04x10^5$ cells, which increased under inflammation non-significantly to $0.21x10^5$ cell. No lymphocytes were counted in the BAL fluid of control-PBS mice, while $0.82x10^5$ cells were found under inflammation ($p<0.05$). For P0-PBS mice, lymphocytes counted $0.04x10^5$, while under inflammation a tendency of increase to $0.34x10^5$ was found (Fig. 6.4 B-E). Statistically, no difference in composition of BAL cells was observed, comparing control-HDM and P0-HDM mice, although a statistically non-significant reduction especially of neutrophils and lymphocytes was observed for P0-HDM mice (Fig. 6.4 B-E). Blocking of IL-17A did not reduce the frequency of total cells or the composition of immune cell populations.

Summarizing the results in terms of total BAL cell numbers and BAL fluid cell composition, a substantial increase in total cells and differential composition was visible upon HDM-immunization, although statistical significance was not reached for all populations. Prenatal antibiotics exposure did not enhance the total cell number or the differential cells found in the airway lumen.

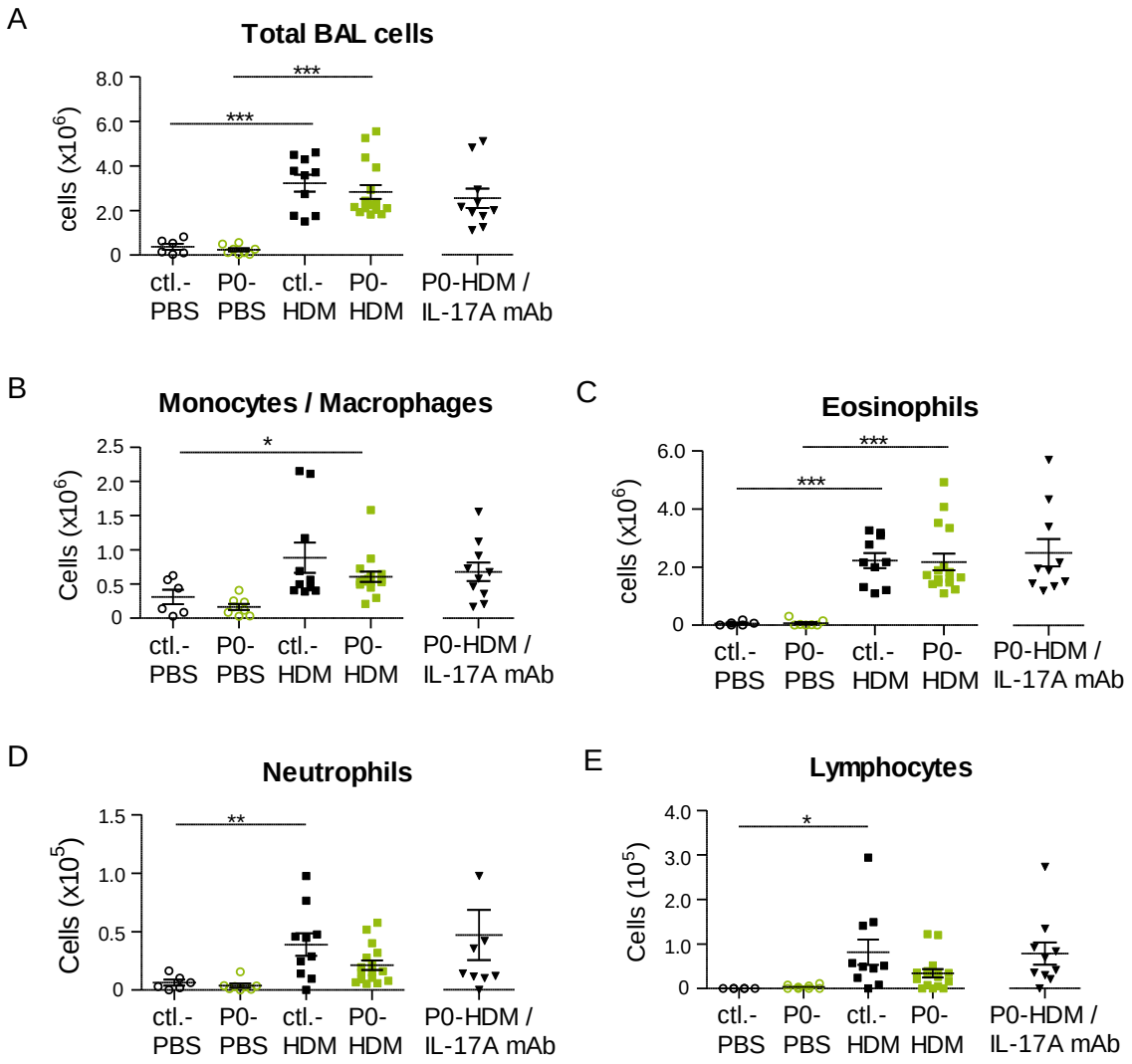

Fig. 6.4: Analysis of the immune cell composition of BAL fluid cells.
BAL fluid was collected from C57BL/6 control and P0 mice treated with PBS or HDM and P0-HDM mice that received IL-17A blockade. Total cell counts were determined [A]. The BAL fluid cells were cytospinned and stained with Diff-Quick staining. 500 cells were differentially counted by morphological criteria and cell numbers were determined, including monocytes/macrophages [B], eosinophils [C], neutrophils [D], and lymphocytes [E]. ctl.=control. Mean and SEM shown. One-way ANOVA; Tukey test (* $p < 0.05$; ** $p < 0.01$; *** $p < 0.001$).

6.1.4 Prenatal antibiotics do not influence the cytokine concentrations of T_H2 or T_H17 cytokines

To assess the levels of production of T_H2 cytokines IL-4, IL-5, and IL-13, as well as the T_H17 cytokine IL-17A, the cytokine concentrations in lung cell culture supernatants that had been restimulated with HDM was determined by ELISA. Restimulation was necessary, since unstimulated cells do not secrete cytokines, even if the mice had been immunized. For control-PBS mice, T_H2 cytokine concentrations were measured below the detection threshold, which was an expected result under steady state. In contrast, control mice immunized with HDM showed a substantial increase in T_H2 cytokine concentrations for IL-4 to 15.7 pg/mL, for IL-5 to $1.1x10^3$ pg/mL, and for IL-13 to $2.3x10^3$ pg/mL, reaching statistical significance for each of the three cytokines ($p<0.001$) (Fig. 6.5 A-C). Analyzing the effects of prenatal antibiotics exposure, P0-PBS mice showed T_H2 cytokine concentrations below the detection limit, essentially similar to control-PBS mice. Comparable to control-HDM mice, T_H2 cytokine concentrations of antibiotics-exposed P0-HDM mice substantially increased for IL-4 to 18.5 pg/mL, for IL-5 to $0.8x10^3$ pg/mL, and for IL-13 to $2.3x10^3$ pg/mL, reaching statistical significance for each of the three cytokines ($p<0.001$). No difference was observed when comparing control-HDM and P0-HDM mice (Fig. 6.5 A-C). Analyzing the T_H17 cytokine IL-17A, for control-PBS and P0-PBS mice the mean cytokine concentration was below the detection limit. A tendency of increased concentrations of 19.3 pg/mL was measured for control-HDM mice, while for P0-HDM mice a mean of 12.7 pg/mL was measured (Fig. 6.5 D). Blocking of IL-17A did not reduce the concentrations of T_H2 cytokines. The concentration of the T_H17 cytokine IL-17A was below the detection limit.

Taken together, HDM-immunization expectedly led to increased T_H2 cytokines. However, prenatal antibiotics exposure did not enhance the production of T_H2 or T_H17 cytokines.

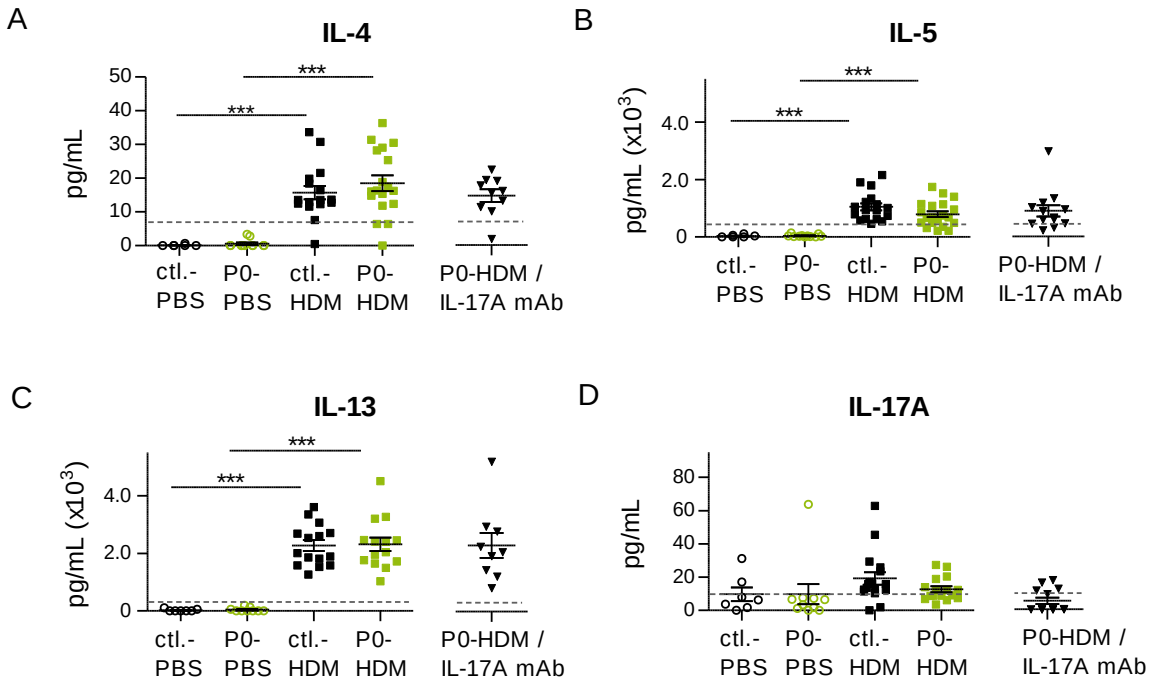

Fig. 6.5: Cytokine concentration analysis in supernatants of antigen-restimulated whole lung cells. Lung tissue of C57BL/6 control or P0 mice treated with PBS or HDM and P0-HDM mice that received IL-17A blockade was harvested and single cell suspensions were restimulated with HDM (0.03 mg/mL) for 72 h. Cytokine concentrations of IL-4 [A], IL-5 [B], IL-13 [C], and IL-17A [D] were measured in supernatants of restimulated single cell suspensions by ELISA. The dotted lines mark the detection limit. ctl.=control. Mean and SEM shown. One-way ANOVA; Tukey test (*** $p < 0.001$).

6.1.5 Prenatal antibiotics increase IL-17A$^+$ cells but not IL-13$^+$ cells

To measure the capacities of lung cells to produce certain cytokines, whole lung cell suspensions were restimulated with PMA/ionomycin and analyzed by flow cytometry. Stimulation by PMA/ionomycin is unspecific, which means that cytokine production is activated by potential cytokine producing cells, including cells that would not be restimulated by adding the antigen to the media. CD90.2 served as a marker for lymphocytes, further gating on IL-13$^+$ or IL-17A$^+$ cells. The gating strategies are visible in the methods section (Fig. 5.2). While for control-PBS mice the percentage of IL-13$^+$ cells was 0.4 %, a substantial increase in T_H2 response was visible for control-HDM mice, where the percentage of IL-13$^+$ lymphocytes increased to 11.8 % (Fig. 6.6 A). Similar to control-PBS mice, P0-PBS mice showed a percentage of 0.7 % for IL-13$^+$ lymphocytes, which substantially increased to 10.6 % upon HDM-immunization ($p<0.001$) (Fig. 6.6 A). In terms

of IL-17A$^+$ cells, control-PBS mice showed a percentage of 2.3 %, which, upon HDM-treatments of control-HDM mice slightly increased to 3.0 %, not reaching statistical significance (Fig. 6.6 B). For IL-17A$^+$ cells, P0-PBS mice showed a percentage of 2.7 %, which increased under inflammation to 4.4 %, reaching statistical significance ($p<0.05$). Comparing control-HDM and P0-HDM mice, an increase of IL-17A$^+$ was observed that showed statistical significance ($p<0.05$) (Fig. 6.6 B). Blocking of IL-17A reduced IL-13$^+$ cells to a mean of 5.69 % CD90.2$^+$ cells, while IL-17A$^+$ cell percentages remained similar for P0-HDM mice.

Given the significant increase in IL-17A$^+$ cells of P0-HDM mice, IL-17A-producing cell subpopulations were analyzed next. According to the expression of CD3 and TCRβ, the populations could be distinguished into αβT cells (CD3$^+$TCRβ$^+$), γδT cells (CD3$^+$TCRβ$^-$), and ILC3 (CD3$^-$TCRβ$^+$). In terms of IL-17A$^+$ subpopulations, a percentage of 62.1 % αβT cells, 14.1 % γδT cells, and 23.8 % ILC3 were identified for control-HDM mice. P0-HDM mice showed a percentage of 53.0 % αβT cells, 22.41 % γδT cells, and 25.6 % ILC3. In terms of IL-17A$^+$ γδT cells, the difference between control-HDM and P0-HDM mice was statistically significant ($p<0.05$) (Fig. 6.6 C). In the supplement section, the percentages of CD4-expressing αβT cells for both HDM groups are graphed to further identify αβT cells (Supplement Fig. 10.1).

Taken together, an expected increase in IL-13$^+$ cells was observed under inflammation. While IL-13$^+$ cells were not influenced by prenatal antibiotics exposure, IL-17A$^+$ cell frequencies increased. The IL-17A$^+$ subpopulation was identified as γδT cell population.

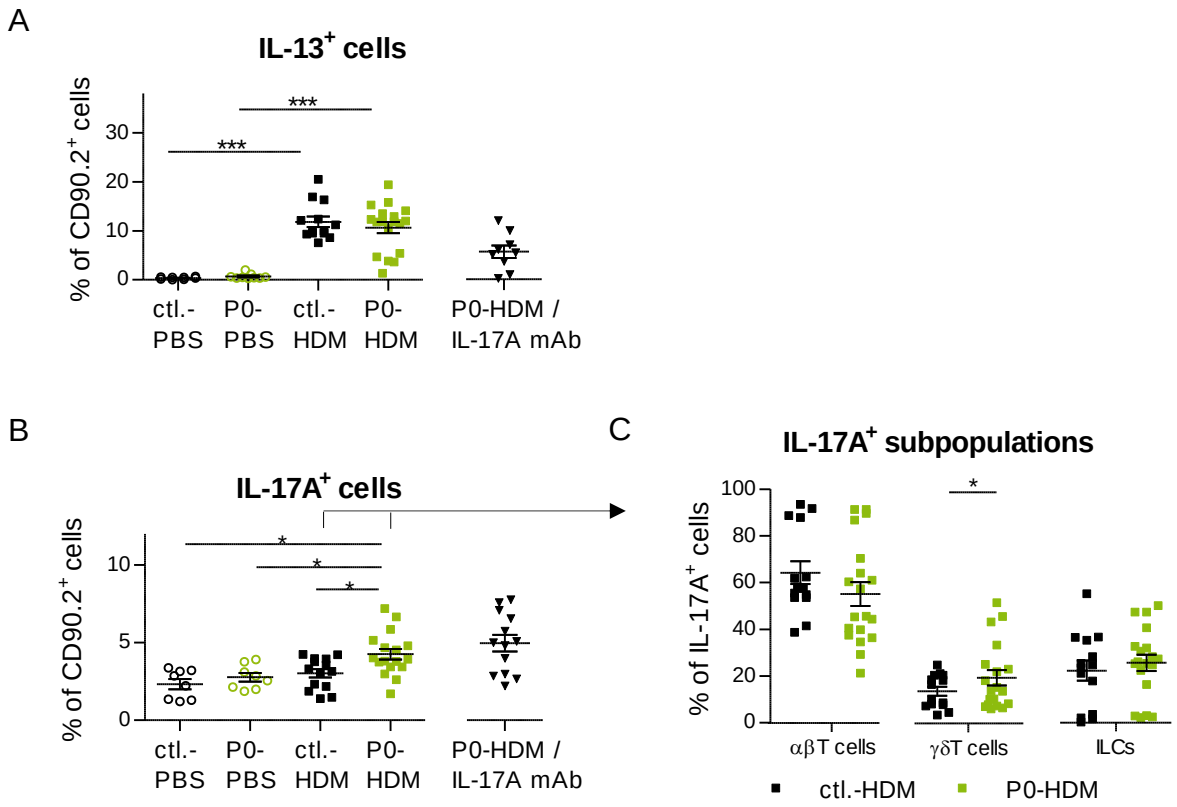

Fig. 6.6: Analysis of intracellular IL-13 and IL-17A in restimulated whole lung cell suspensions. Lung tissue of C57BL/6 control or P0 mice treated with PBS or HDM and P0-HDM mice that received IL-17A blockade was harvested and single cell suspensions were restimulated with PMA (50 ng/mL) and ionomycin (0.5 µg/mL), intracellularly stained for IL-13 and IL-17A. The cells were analyzed by flow cytometry. Lymphocytes identified by CD90.2 expression were analyzed regarding their IL-13 positivity [A] or IL-17A positivity [B]. To further differentiate IL-17A$^+$ populations of HDM-immunized mice, CD3 and TCRβ expression was analyzed to identify CD3$^+$TCRβ$^+$ αβT cells, CD3$^+$TCRβ$^-$ γδT cells, and CD3$^-$TCRβ$^-$ ILCs. ctl.=control. Mean and SEM shown. One-way ANOVA, Tukey test [A,B]; Student T test [C] (* $p < 0.05$; *** $p < 0.001$).

6.2 Mice exposed to prenatal antibiotics show higher variability in gene expression associated with severe asthma

Given the increase in IL-17A$^+$ cells, the gene expression of T_H17-related cytokines *Il17a*, *Il17f*, and *Il22* was analyzed in whole lung cell homogenates. A low overall gene expression of *Il17a*, *Il17f*, and *Il22* was measured. A trend of increased gene expression was visible upon HDM-immunization of control-HDM mice (Fig. 6.7). Similar to control-PBS mice, P0-PBS mice showed

a low gene expression of *Il17a*, *Il17f*, and *Il22*, essentially close to the detection limit. An increase in gene expression was visible for P0-HDM mice, reaching statistical significance for *Il17f*. For *Il17a*, some variability in gene expression was observed. No differences in gene expression of T_H17 cytokines were measured between control-HDM and P0-HDM mice. (Fig. 6.7). A tendency of reduced *Il17f* and *Il22* gene expression was observed, if IL-17A cytokine was blocked.

Taken together, a trend of higher gene expression of T_H17-related cytokines *Il17a* and *Il17f* was observed under inflammation. However, under exposure to prenatal antibiotics no further increase was observed.

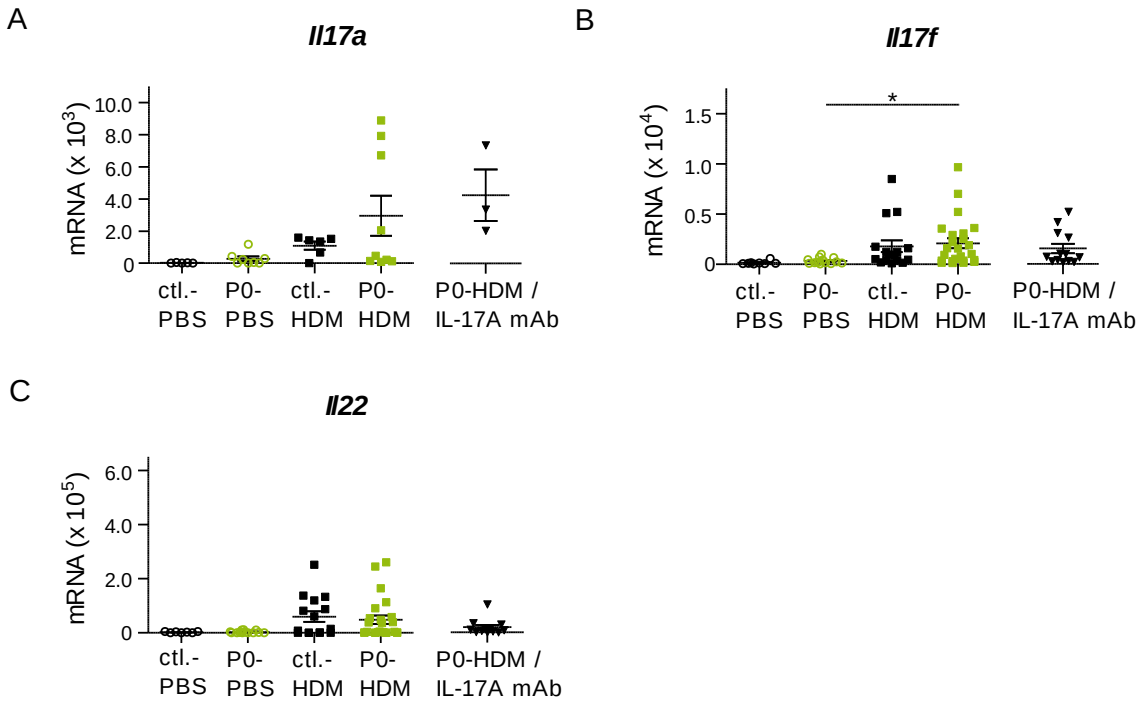

Fig. 6.7: Transcription analysis of T_H17-related cytokine gene expression.
The postcaval lobe of C57BL/6 control and P0 mice treated with PBS or HDM and P0-HDM mice that received IL-17A blockade were removed for RNA extraction, cDNA synthesis, and analysis of the gene expression by RT-qPCR. The gene expression T_H17 cytokines *Il17a* (IL-17A) [A], *Il17f* (IL-17F) [B], and *Il22* (IL-22) [C] was analyzed by normalization to the housekeeping gene *S14*. ctl.=control. Mean and SEM shown. One-way ANOVA; Tukey test (* $p < 0.05$).

Gene expression of the neutrophil granule enzyme myeloperoxidase (*Mpo*) was analyzed next to verify the results on BAL fluid neutrophils. As expected, *Mpo* gene expression of control-PBS mice was close to undetectable. For control-HDM mice, no increase in gene expression was visible. *Mpo* gene expression of P0-PBS mice was comparable to control-PBS mice. Increase in *Mpo* expression was observed for P0-HDM mice, showing some variability but not reaching statistical significance (Fig. 6.8). No difference in *Mpo* expression was observed between control-HDM and P0-HDM mice. IL-17A cytokine blockade did not alter the expression level of *Mpo* gene.

Taken together, no differences were visible in gene expression of myeloidperoxidase gene *Mpo*, although some variability in *Mpo* expression was visible in HDM-immunized mice that had been exposed to antibiotics.

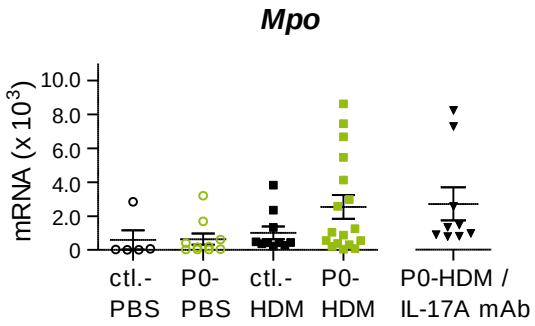

Fig. 6.8: Transcription analysis of neutrophil marker gene expression.
The postcaval lobe of C57BL/6 control and P0 mice treated with PBS or HDM and P0-HDM mice that received IL-17A blockade were removed for RNA extraction, cDNA synthesis, and analysis of the gene expression by RT-qPCR. The neutrophil marker expression of *Mpo* (myeloidperoxidase) was analyzed by normalization to the housekeeping gene *S14*. ctl.=control. Mean and SEM shown. One-way ANOVA; Tukey test.

As T_H2 responses are potent drivers of mucus expression, the expression of mucin-related genes *Muc5ac*, *Muc5b*, and the goblet cell marker *Gob*5 were assessed. Analyzing control-PBS mice, low levels of mucin-related gene expression were observed, which upon HDM-immunization increased non-significantly (Fig. 6.9). For P0-PBS mice, a similar mucin gene expression to control-PBS mice was observed. For P0-HDM mice, increase in gene expression of *Muc5b*, *Muc5ac*, and *Gob5* was visible, reaching statistical significance for *Muc5ac* and *Gob5*. Individual

P0-HDM mice showed higher gene expression compared to control-HDM mice (Fig. 6.9). If IL-17A was blocked, a robust reduction in gene expression of mucin genes was observed.

Because P0-HDM mice showed higher variability in gene expression, *Il17a* mRNA levels were correlated to mucin gene expression levels. A trend of positive correlation of *Il17a* with the three mucin genes was visible, although no statistical significance was reached (Supplement Fig. 10.2 A-C). The mucus-related gene expression, if correlated to each other, showed a strong positive correlation with high statistical significance (Supplement Fig. 10.2 D-F).

Taken together, under inflammation, increased gene expression of mucus-related genes *Gob5* and *Muc5ac* was observed. For P0-HDM mice, some variability in mucus-related gene expression was observed.

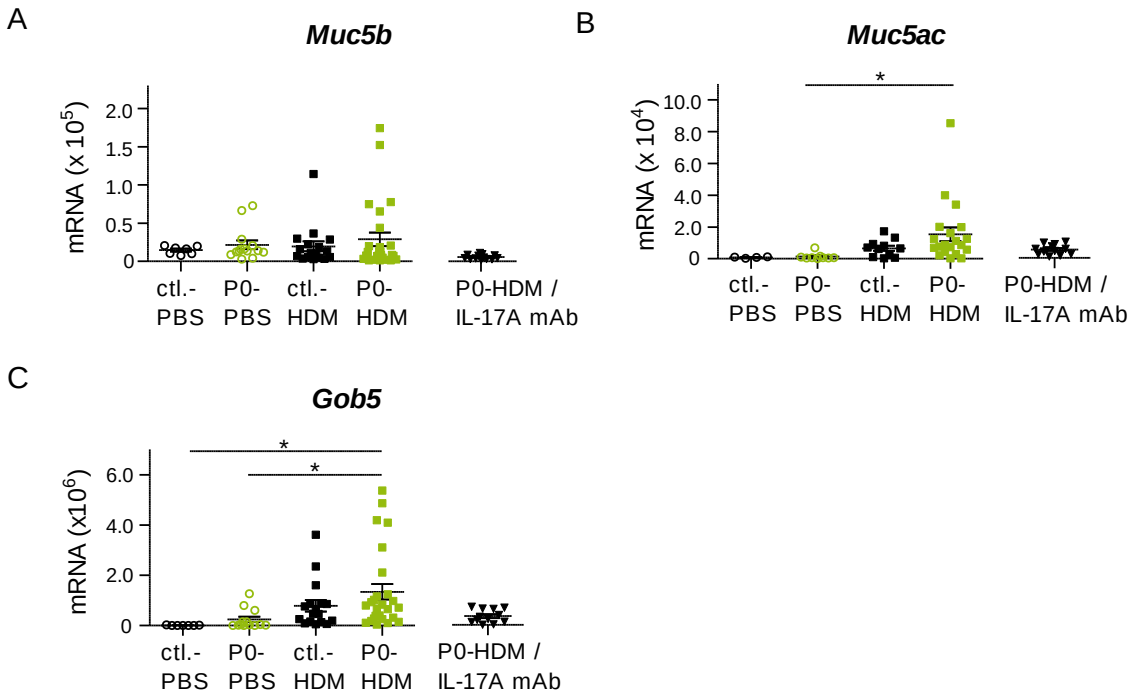

Fig. 6.9: Transcription analysis of mucus-related gene expression.
The postcaval lobe of C57BL/6 control and P0 mice treated with PBS or HDM and P0-HDM mice that received IL-17A blockade were removed for RNA extraction, cDNA synthesis, and analysis of the gene expression by RT-qPCR. The mucin-related genes *Muc5b* [A], *Muc5ac* [B], and the goblet cell marker *Gob5* [C] were normalized to the housekeeping gene *S14*. ctl.=control. Mean and SEM shown. One-way ANOVA; Tukey test (* $p < 0.05$).

6.3 Prenatal antibiotics do not change the localization of IL-17A$^+$ cells or the interaction rate with DCs

Given the result of increase in IL-17A$^+$ cells found upon antibiotics exposure of P0-HDM mice measured by flow cytometry, pulmonary IL-17A$^+$ cells were analyzed *in situ*. Thus far, little is known about the distribution of pulmonary IL-17A$^+$ cells. The IHC approach required the selection of a surrogate, since intracellular cytokine staining is not feasible for IHC. For the analysis of intracellular cytokines by flow cytometry, Brefeldin A was used for intracellular accumulation of the cytokines by inhibition of the externalization, which is not feasible for IHC. Therefore to detect IL-17A$^+$ cells with IHC, the transcription factor RORγt known to be the key transcription factor of IL-17A expression was chosen. [198] In order to establish an IHC protocol on pulmonary RORγt$^+$ cells, an additional step was taken by detecting RORγt$^+$ cells in the intestine, before focusing on the lung.

6.3.1 RORγt antibody labels GFP$^+$ cells localizing to cryptopatches in intestinal sections of RORC-GFP reporter mice

For establishing an IHC protocol, A/J RORC-GFP reporter mice were chosen. The RORγt antibody was tested on intestinal sections of A/J RORC-GFP mice, since published protocols for intestinal RORγt$^+$ cells exist. [64] A large proportion of small intestinal RORγt$^+$ cells are known to accumulate in structures called cryptopatches of the lamina propria. [64] Cryptopatches are distinguishable from intestinal villi by their crypt-like appearance (Supplement Fig. 10.3). Evaluating the sections of the small intestine of A/J RORC-GFP mice and A/J wt mice, the incubation with the RORγt antibody resulted in multiple fluorescence signals visible in cryptopatches. Double labeling of RORγt and GFP fluorescence signals was analyzed to see, if both antibodies label the same cells. While for A/J wt mice expectedly RORγt but no GFP signal was detected, strong overlap in signal was observed in sections of A/J RORC-GFP reporter mice (Fig. 6.10 A,B). The sole incubation of intestinal sections with the secondary antibodies did not result in positive signals (Fig. 6.10 C). The next step was to analyze the subcellular localization of RORγt, given the knowledge that RORγt is a transcription factor. Double labeling of RORγt and Hoechst DNA staining of nuclei was performed. The intestinal RORγt signal was found to colocalize with Hoechst, suggesting a nuclear localization of RORγt (Fig. 6.11).

Taken together, the RORγt antibody labeled cells in intestinal cryptopatches and double labeling of RORγt and GFP in sections of reporter mice showed an overlap of both signals. A double labeling with Hoechst showed a nuclear localization of the transcription factor RORγt.

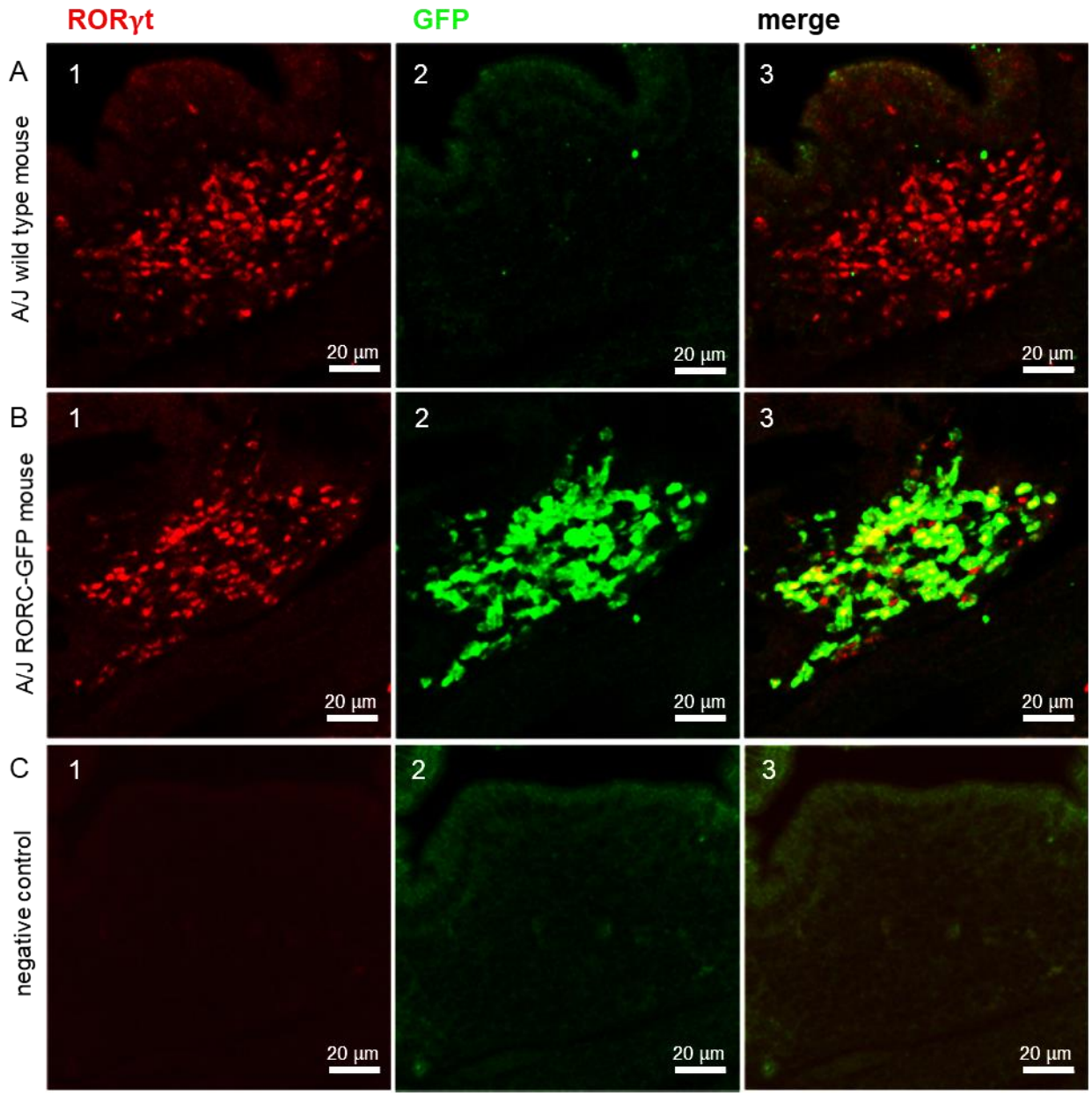

Fig. 6.10: Evaluation of RORγt IHC staining approach on intestinal sections.
18 µm intestinal cryosections of A/J wt mice (n=2) [A1-3], and A/J RORC-GFP reporter mice (n=2) [B1-3] were incubated with RORγt and GFP antibodies. Control sections were incubated with the secondary antibodies alone [C1-3]. Z-stacks were generated with the laser scanning confocal microscope and analyzed, using Imaris software. Representative images are shown.

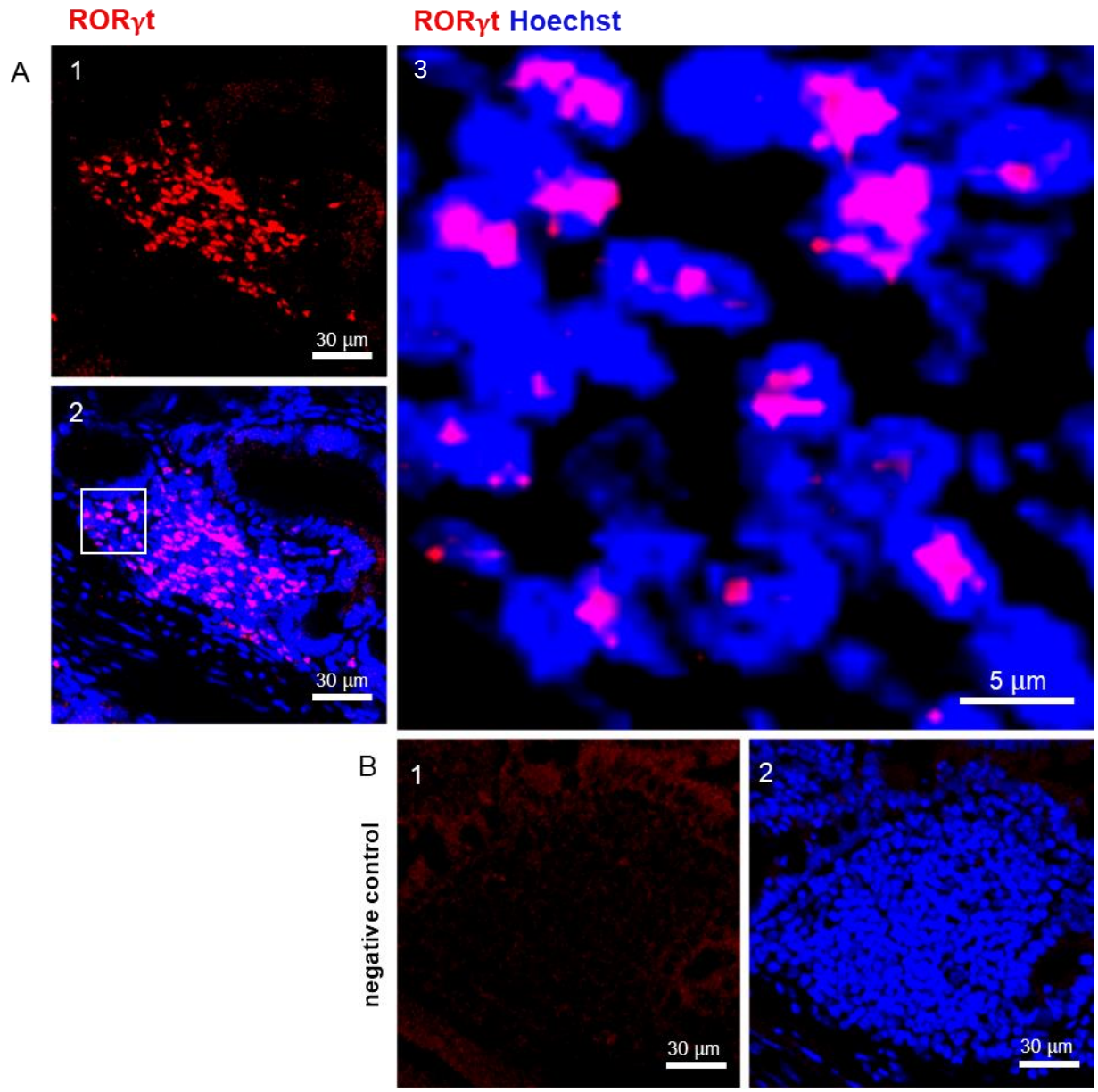

Fig. 6.11: Analysis of subcellular fluorescence signal of intestinal RORγt⁺ cells.
18 µm intestinal cryosections of A/J wt mice (n=2) were incubated with a RORγt antibody [A1] and Hoechst DNA dye was added [A2]. The frame indicates the magnified area in [A3]. Controls were incubated with the secondary antibody and Hoechst [B1-2]. Z-stacks were generated with the laser scanning confocal microscope and analyzed, using Imaris software. Representative images are shown.

6.3.2 Pulmonary RORγt$^+$ cells are rare in lung sections of naïve mice and frequent in lung sections of HDM-immunized mice

The next step was to transfer the IHC protocol to the lung. An adapted RORγt IHC protocol was established for lung sections (Methods section 5.2.14). For establishing a protocol, lung sections of three naïve mice and two HDM-immunized C57BL/6 wt mice were generated. Lung sections of naïve mice were incubated with the RORγt antibody and analyzed for fluorescence signal. As a result, expectedly, few cells were observed that were positive for the signal. These localized to large airways, as the example of RORγt$^+$ cells at a large airway shows, which is representative for naïve mice (Fig. 6.12 A). In contrast, upon HDM-immunization, RORγt cells were found frequently, especially localizing to large airways. A representative example of RORγt$^+$ cells at a large airway of an HDM-immunized mouse is visible in Fig. 6.12 B. The sole incubation of lung sections with the secondary antibody did not result in positive signals as visible in the negative control (Fig. 6.12 C). Next, the subcellular localization of the pulmonary RORγt signal was analyzed in a double labeling with Hoechst. Similar to intestinal RORγt signal, the fluorescence signal of RORγt colocalized with Hoechst staining (Fig. 6.13).

Taken together, the RORγt antibody stained cells in lung sections of naïve and, more frequently, of HDM-immunized mice. Double labeling with Hoechst showed nuclear localization of the transcription factor RORγt.

6.3.3 RORγt$^+$ cells co-express the T cell co-receptor CD3 and lack expression of the T_H2 transcription factor GATA3

In order to further evaluate the specificity of the antibody, the expectation that many RORγt$^+$ cells should express the T cell co-receptor CD3 was analyzed, since many cells should be T cells. As expected, the percentage of RORγt$^+$ cells expressing CD3 was 92 %**,** while 8 % did not express CD3 (Fig. 6.14 A,C). Additionally, the expectation was challenged that the master transcription factor of T_H2 differentiation GATA3 would not be expressed by the same cells. In contrast to the frequent double expression with CD3, no overlap of RORγt and GATA3 expression was observed (Fig. 6.14 B,D). Counting GATA3$^+$ and RORγt$^+$ cells showed that GATA3$^+$ cells were more frequent in comparison to RORγt$^+$ cells with a percentage of total cells of 93 **%** GATA3$^+$ cells, while only 7 **%** of the evaluated cells expressed RORγt$^+$. (Fig. 6.14 B,D).

Taken together, co-expression with CD3 in a majority of cells and a lack of GATA3 expression was observed, suggesting that the RORγt antibody was specific.

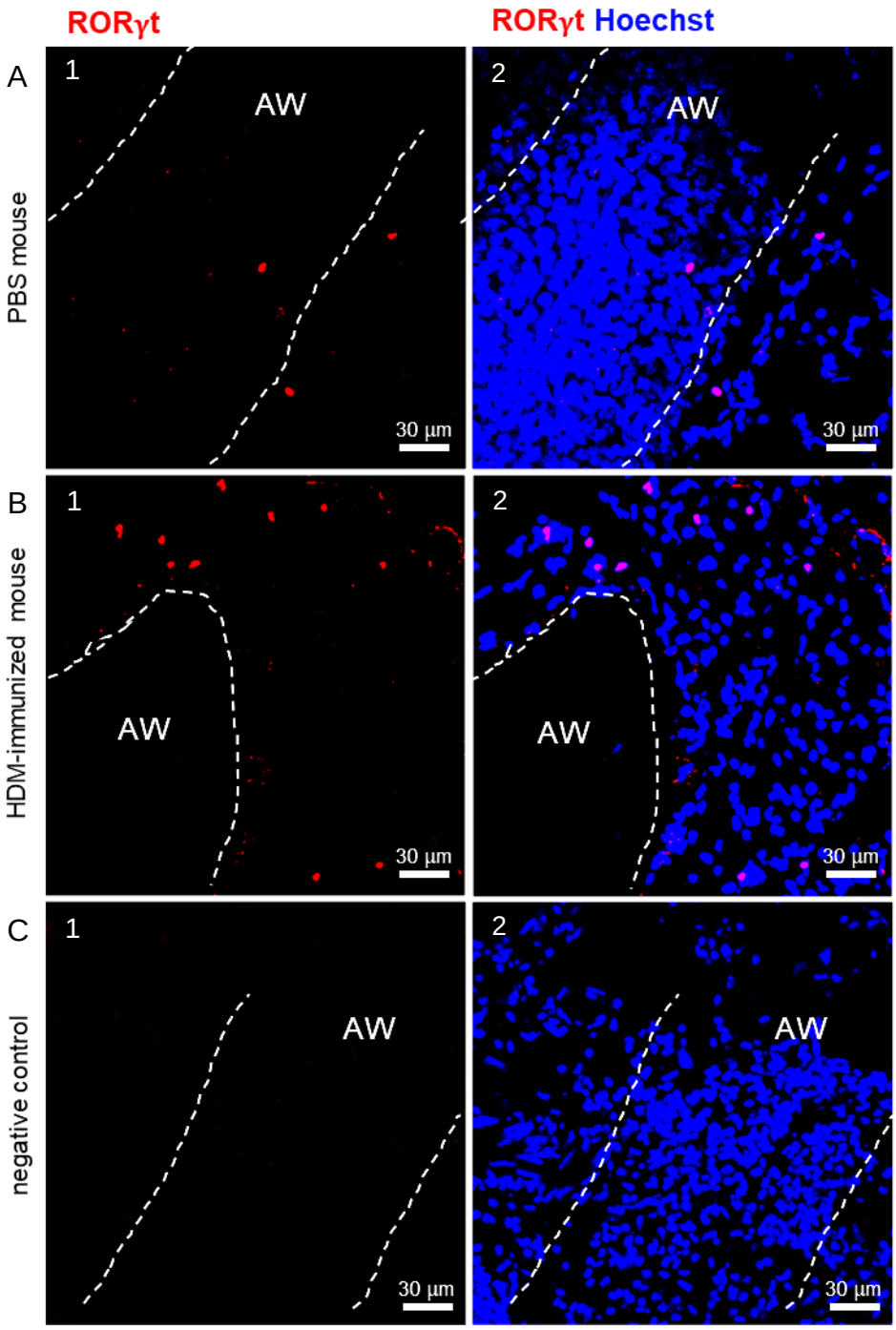

Fig. 6.12: Analysis of pulmonary RORγt⁺ cells, comparing steady state *vs*. inflammation.
300 µm lung sections of naïve C57BL/6 mice (n=3) [A] and HDM-immunized mice (n=2) [B,C] were incubated with a RORγt antibody [A,B] or with the secondary antibody for control [C]. Hoechst DNA dye was added to visualize nuclei [A2-C2]. Z-stacks were generated with the laser scanning confocal microscope and analyzed, using Imaris software. Representative images are shown. White lines mark the borders of the airways. AW=airway lumen.

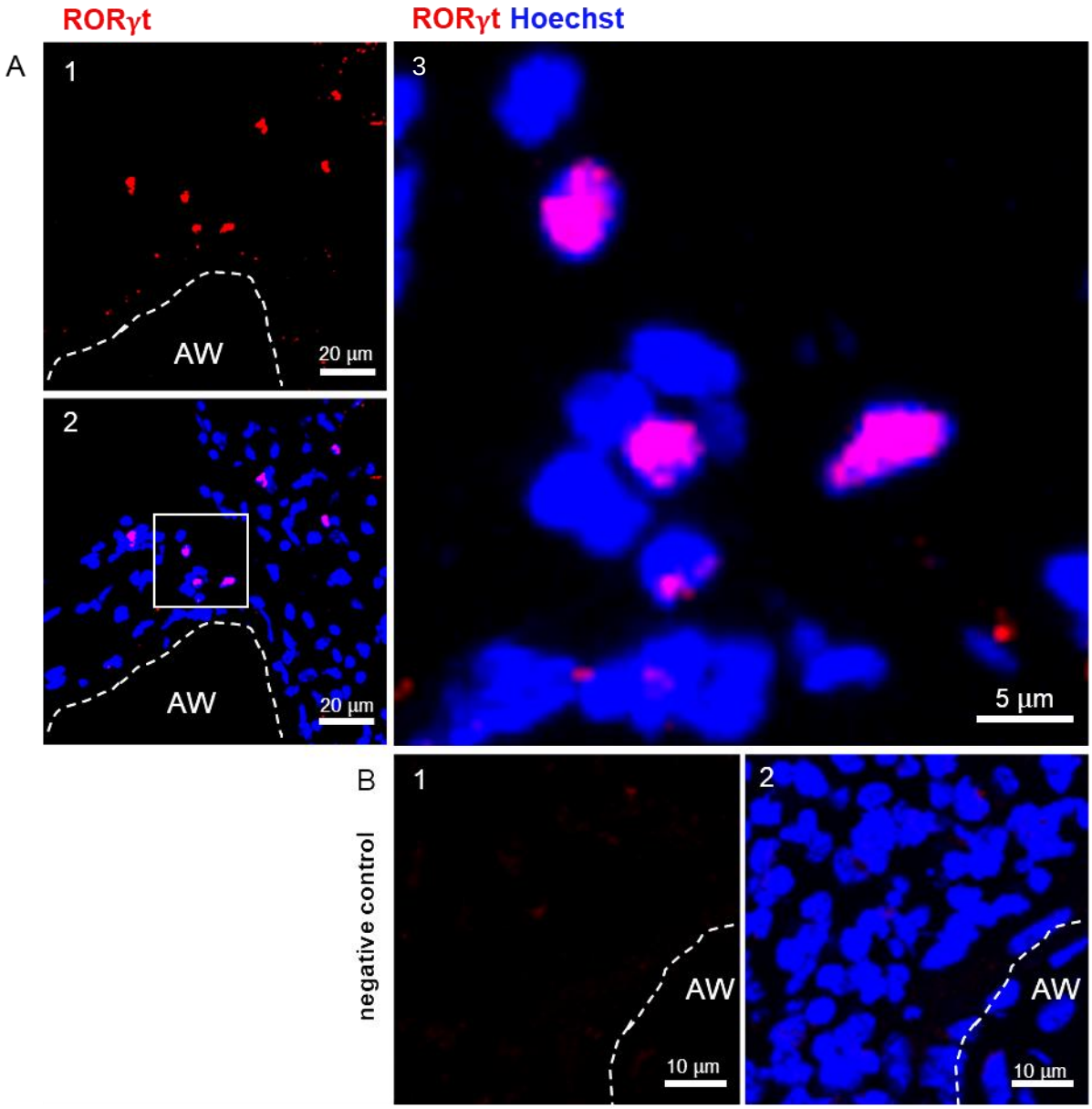

Fig. 6.13: Analysis of subcellular localization of the fluorescence signal of pulmonary RORγt$^+$ cells. 300 µm lung sections of HDM-immunized C57BL/6 mice (n=2) were incubated with a RORγt antibody [A1] and Hoechst DNA dye was added [A2]. The frame indicates the magnified area in [A3]. Controls were incubated with the secondary antibody and Hoechst [B1-2]. Z-stacks were generated with the laser scanning confocal microscope and analyzed, using Imaris software. Representative images are shown. White lines mark the borders of the airways. AW=airway lumen.

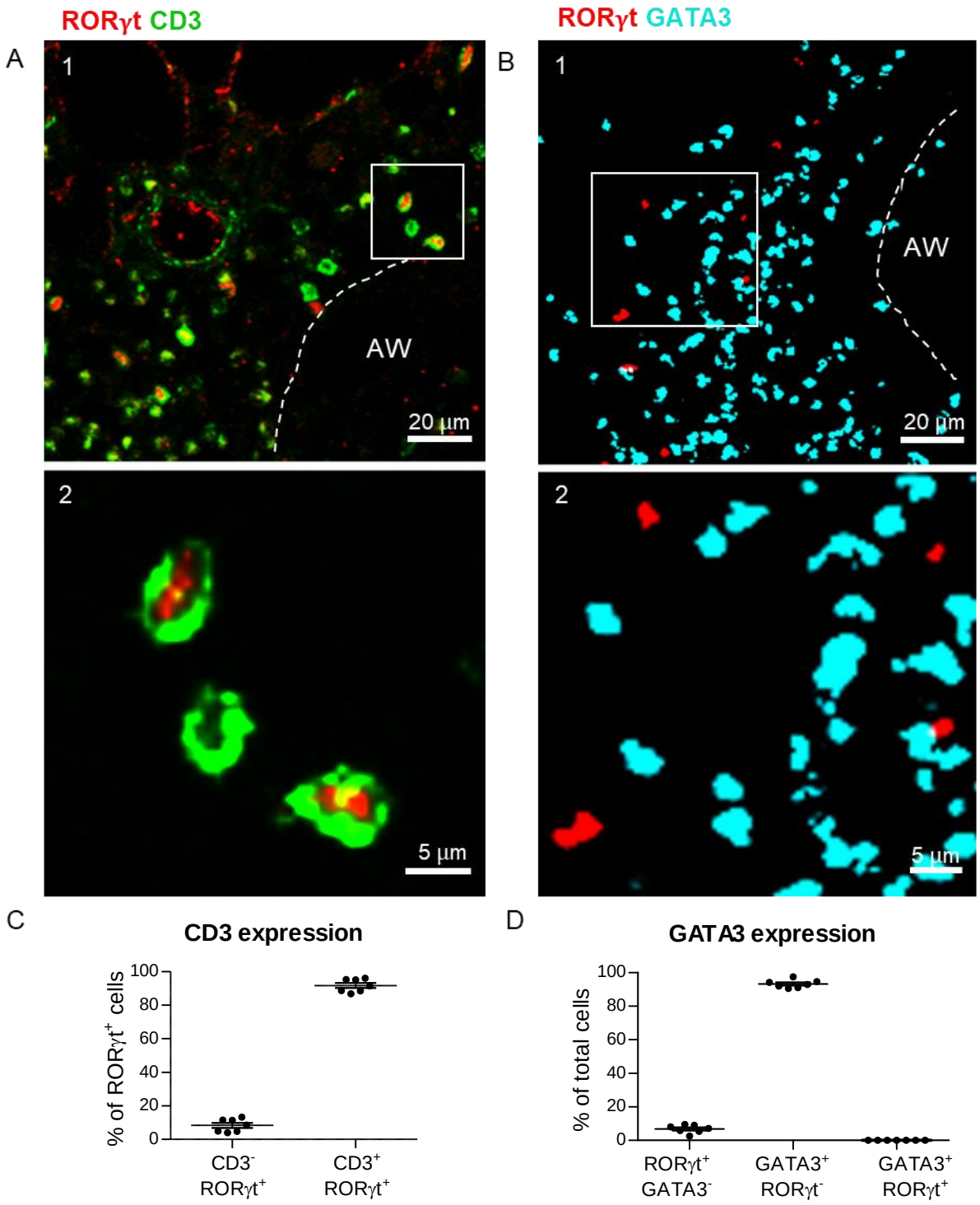

Fig. 6.14: Analysis of pulmonary RORγt⁺ cells with regard to the CD3 or GATA3 expression.
300 µm lung sections of HDM-immunized C57BL/6 mice (n=2) were incubated with a RORγt (red) antibody and CD3 (green) antibody [A1]. The frame indicates the magnified area in [A2]. Percentages were determined by counting RORγt⁺ cells expressing CD3 (78 cells in total). Lung sections were also incubated with RORγt and GATA3 (turquoise) antibodies [B1]. The frame indicates the magnified area in [B2]. White lines mark the borders of the airways. AW=airway lumen. Percentages were determined by counting RORγt⁺ or GATA3⁺ cells [C,D] (n=7 Z-stacks; 1036 cells in total). Mean and SEM shown.

6.3.4 Prenatal antibiotics do not influence the localization of RORγt$^+$ cells

In order to visualize airways and blood vessel, αSMA was added to the RORγt imaging approach. The anatomical structures of potential localization were divided into large airways, small airways/blood vessels, and pleura/alveoli region. Before using the tissue samples of control-HDM and P0-HDM mice for analysis, lung sections of two HDM-immunized C57BL/6 wt mice that were generated for establishing the pulmonary RORγt IHC protocol. For the two mice analyzed, a major proportion of 78 % RORγt$^+$ cells localized at large airways. A smaller proportion of 22 % were found at small airways/blood vessels. Less than 1 % localized at the alveolar/pleura region (Fig. 6.15 A-C). Being interested, in whether antibiotics exposure could influence the localization of potential IL-17A producers, sections of control-HDM and P0-HDM mice were incubated with the RORγt antibody. RORγt$^+$ cells in lung sections of control-HDM mice showed a similar localization pattern as the two test mice before: 74 % RORγt$^+$ cells localized at large airways, 29 % localized at small airways/blood vessels, and less than 1 % localized at alveoli/pleura region (Fig. 6.16). RORγt$^+$ cells of P0-HDM mice showed a similar localization pattern compared to the control-HDM mice: 75 % of RORγt$^+$ cells localized at large airways, 24 % localized at small airways/blood vessels, and less than 1 % at alveoli/pleura region (Fig. 6.16).

Taken together, the majority of RORγt$^+$ cells localized to large airways. In this IHC approach, antibiotics exposure did not shift the pattern of RORγt$^+$ cell localization.

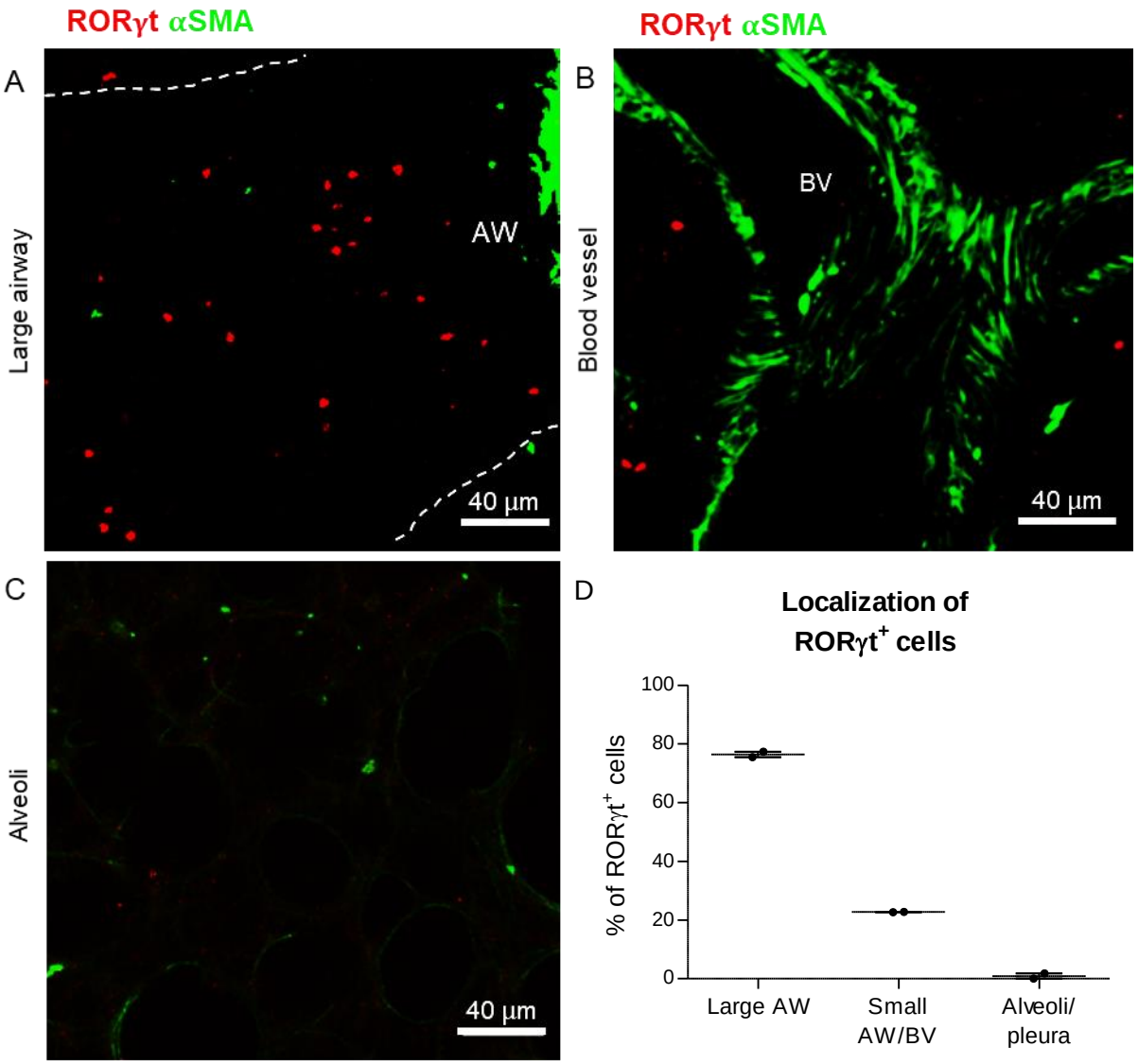

Fig. 6.15: Analysis of the anatomical localization of pulmonary RORγt⁺ cells.
300 µm lung sections of HDM-immunized C57BL/6 mice (n=2) were incubated with a RORγt (red) antibody. For visualization of airways and blood vessels, αSMA (green) antibody was added. Alveoli were visible by tissue autofluorescence [C]. Z-stacks were generated with the laser scanning confocal microscope and analyzed, using Imaris software. Representative images are shown [A-C]. White lines mark the border of the airway. AW=airway lumen; BV=blood vessel. Percentages of RORγt⁺ cell localization at large airways, small airways/blood vessels, and alveoli/pleura region were determined by counting [D] (106 cells in total). Mean and SEM shown.

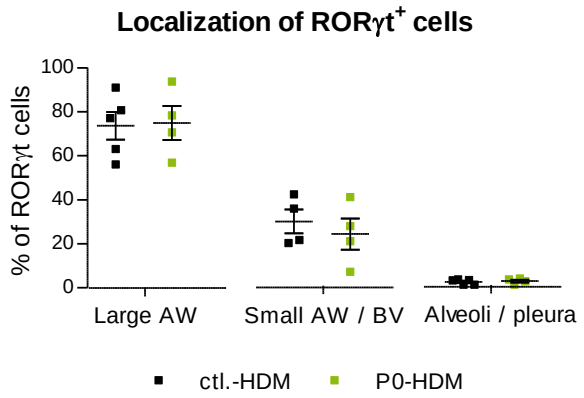

Fig. 6.16: Analysis of pulmonary RORγt⁺ cells with regard to the anatomical localization, comparing control- and P0-HDM mice. 300 µm lung sections of C57BL6 control-HDM mice (n=5) and P0-HDM mice (n=4) were incubated with a RORγt antibody. Z-stacks were generated with the confocal microscope and analyzed, using Imaris software. Percentages of RORγt⁺ cells were analyzed by counting cells at large airways, small airways/blood vessels, and alveoli/pleura region (868 cells in total). ctl.=control. Mean and SEM shown.

6.3.5 Prenatal antibiotics do not influence the proportion or localization of RORγt⁺ αβT cells, γδT cells, and ILCs

In a similar approach to the intracellular cytokine analysis (Fig. 6.6), the subpopulations of RORγt-expressing cells were identified. Antibodies to CD3 and TCRβ were added to distinguish αβT cells ($CD3^+TCR\beta^+$), γδT cells ($CD3^+TCR\beta^-$), and ILC3 ($CD3^-TCR\beta^-$). The approach was tested in sections of two HDM-immunized C57BL/6 wt mice. The largest population of RORγt⁺ cells consisted of 58 % αβT cells, the second largest population of 30 % γδT cells, and the smallest population of 12 % ILC3 (Fig. 6.17 E). A representative overview of individual cells and overview of a large airway is visible (Fig. 6.17 A-D). Also individual panel images of the overview are provided in the supplement section of the thesis (Supplement Fig. 10.4). Control-HDM and P0-HDM mice were analyzed in terms of the RORγt⁺ subpopulations. Similar to the two tested mice, subpopulations of RORγt⁺ cells in lung sections of control-HDM mice comprised of 60 % αβT cells, 32 % γδT cells, and 8 % ILC3. For P0-HDM mice, the subpopulations were essentially similar to control-HDM mice, comprising of 61 % αβT cells, 31 % γδT cells and 7 % ILC3 (Fig. 6.18).

In summary, in this *in situ* analysis, the proportions of the three subpopulations identified as αβT cells, γδT cells and ILCs were not influenced by prenatal antibiotics as observed for intracellular cytokine staining (Fig. 6.6 C).

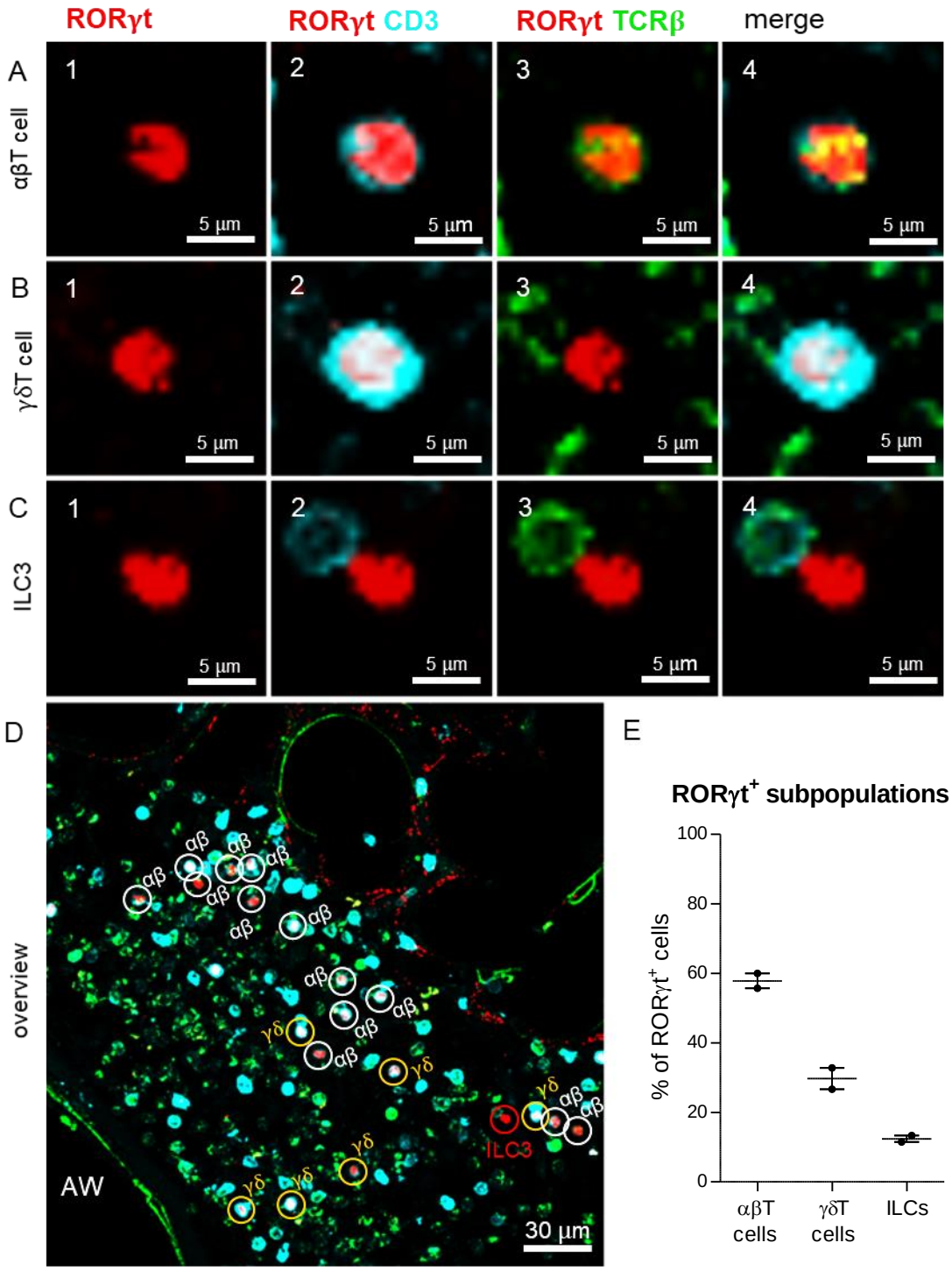

Fig. 6.17: Analysis of pulmonary RORγt⁺ subpopulations αβT cells, γδT cells, and ILCs.
300 µm lung sections of HDM-immunized C57BL/6 mice (n=2) were incubated with RORγt (red), CD3 (turquoise), and TCRβ (green) antibodies. RORγt⁺ populations included $CD3^+TCR\beta^+$ αβT cells [A1-4], $CD3^+TCR\beta^-$ γδT cells [B1-4], and $CD3^-TCR\beta^-$ ILC3 [C1-4]. Z-stacks were generated with the laser scanning confocal microscope and analyzed, using Imaris software. A representative overview of a large airway is shown [D]. AW=airway lumen. Percentages of αβT cells, γδT cells, and ILC3 were determined by counting [E] (106 cells in total). Mean and SEM shown.

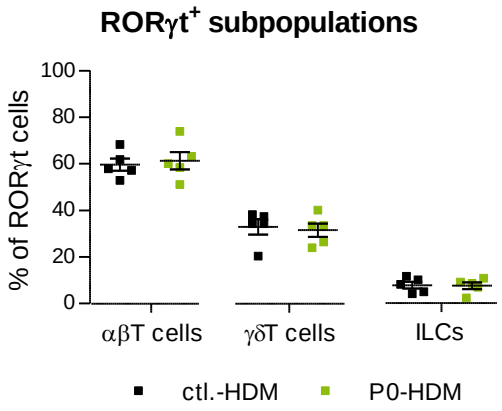

Fig. 6.18: Analysis of pulmonary RORγt⁺ subpopulations αβT cells, γδT cells, and ILC3, comparing control- and P0-HDM mice. 300 µm lung sections of C57BL/6 control-HDM mice (n=5) and P0-HDM mice (n=5) were incubated with RORγt, CD3, and TCRβ antibodies. RORγt⁺ subpopulations included $CD3^+TCR\beta^+$ αβT cells, $CD3^+TCR\beta^-$ γδT cells, and $CD3^-TCR\beta^-$ ILC3. Z-stacks were generated with the confocal microscope and analyzed, using Imaris software. Percentages of αβT cells, γδT cells, and ILC3 were determined by counting (large airways: 548 cells in total; small airways: 162 cells in total). ctl.=control. Mean and SEM shown.

Because the localization of the three subpopulations could be reliably assigned by tissue autofluorescence, the Z-stacks acquired for RORγt⁺ subpopulation identification were reanalyzed for the localization of the subpopulations. At large airways, the RORγt⁺ cells of control-HDM mice were 63 % αβT cells, 30 % γδT cells, and 7 % ILC3. Similar to control-HDM mice, 70 % αβT cells, 22 % γδT cells, and 7 % ILC3 were found at large airways of P0-HDM mice (Fig. 6.19 A). Analyzing RORγt⁺ cells at small airways of control-HDM mice, 64 % were αβT cells, 27 % γδT cells, and 8 % ILC3. Similar to control-HDM mice, 66 % αβT cells, 25 % γδT cells, and 9 % ILC3 were found at small airways of P0-HDM mice. The results are graphed in Fig. 6.19 B.

Taken together, antibiotics exposure did not alter the distribution of RORγt⁺ subpopulations at large and small airways. In this IHC approach, an equal distribution of the subpopulations was found at both localizations.

6.3.6 Prenatal antibiotics do not influence the frequency of contacts between RORγt⁺ cells and CD11c⁺ DCs

Because an increase in epithelial permeability was measured, which could potentially increase the interaction rate of proinflammatory DCs with IL-17A⁺ cells, HDM-immunized mice were analyzed for RORγt-contacting DCs. An antibody to CD11c, which is a cell surface protein

expressed by DCs, was added to the RORγt antibody and the fluorescence signals were analyzed in terms of proximity. A representative overview is given with additional enlarged 3D views of RORγt$^+$ cells and DCs in contact to each other (Fig. 6.20 A,B). For two mice analyzed, the mean contact rate was 60 % (Fig. 6.20 C). Next, the approach was applied to lung sections of control-HDM and P0-HDM mice. Analyzing lung sections of control-HDM mice, 71 % of RORγt$^+$ cells were in proximity to CD11c$^+$ DCs (Fig. 6.21). For P0-HDM lung sections, the contact rate was 71 %, which was essentially similar to control-HDM mice.

Taken together, the high contact rate of RORγt$^+$ cells and CD11c$^+$ DCs did not show further enhancement, if mice had been exposed to antibiotics *in utero*.

A

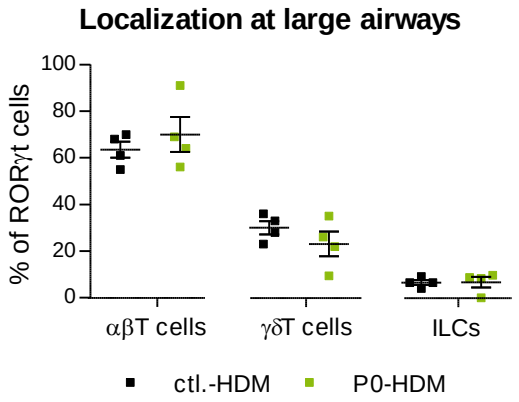

B

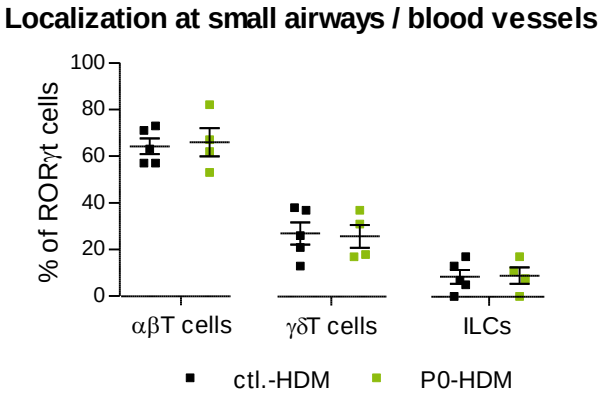

Fig. 6.19: Analysis of pulmonary RORγt$^+$ subpopulations αβT cells, γδT cells, and ILCs with regard to the anatomical localization, comparing control- and P0-HDM mice. 300 µm lung sections of C57BL/6 control-HDM mice (n=5) and P0-HDM mice (n=4) were incubated with RORγt, CD3, and TCRβ antibodies. Z-stacks were generated with the confocal microscope and analyzed, using Imaris software. Percentages of RORγt$^+$ cells were determined by counting of αβT cells (CD3$^+$TCRβ$^+$), γδT cells (CD3$^+$TCRβ$^-$), and ILC3 (CD3$^-$TCRβ$^-$) at large airways [A] and at small airways/blood vessels [B] (480 cells in total). ctl.=control. Mean and SEM shown.

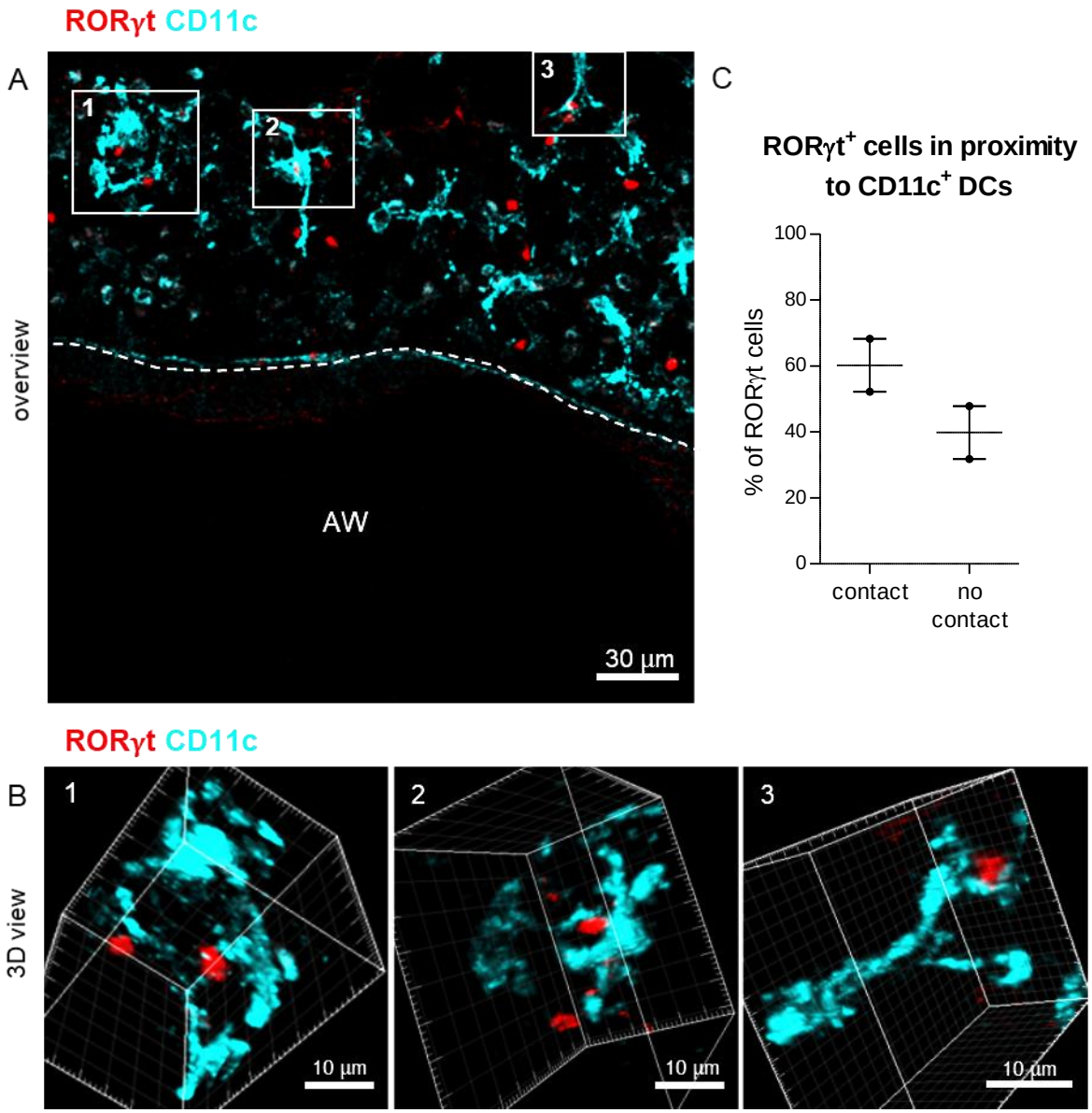

Fig. 6.20: Analysis of pulmonary RORγt$^+$ cells with regard to their localization in relation to CD11c$^+$ DCs. 300 µm lung sections of HDM-immunized C57BL/6 mice (n=2) were incubated with RORγt (red) and CD11c (turquoise) antibodies. Z-stacks were generated with the confocal microscope and analyzed, using Imaris software. A representative overview of a large airway is given [A]. The white line marks the border of the airway. AW=airway lumen. The framed areas are visible enlarged and in 3D views in [B1-3]. The percentages of contacts were determined by counting RORγt cells in contact with CD11c$^+$ DCs [C] (90 cells in total). Mean and SEM shown.

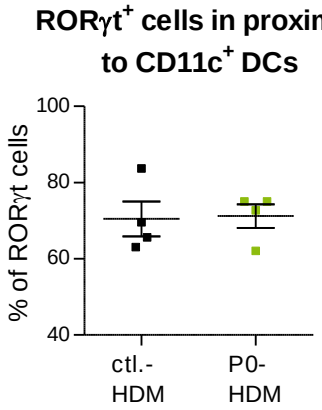

Fig. 6.21: Analysis of pulmonary RORγt$^+$ cells with regard to their localization in relation to CD11c$^+$ DCs, comparing control- and P0-HDM mice. 300 µm lung sections of C57BL/6 control-HDM (n=4) and P0-HDM mice (n=4) were incubated with RORγt and CD11c antibodies. Z-stacks were generated with the confocal microscope and analyzed, using Imaris software. Percentages of contacts between RORγt$^+$ cells and DCs were determined by counting (356 cells in total). ctl.=control. Mean and SEM shown.

CD11c is known to be expressed by monocyte-derived (mo)DCs, CD11b$^+$ conventional (c)DCs, and by CD103$^+$ cDCs. While CD103$^+$ cDCs have been rather linked to tolerogenic responses, moDCs and cDCs have been shown to contribute to antigen presentation under inflammatory conditions of allergic asthma. [32, 199] By adding a label for langerin, a protein expressed by CD103$^+$ cDC, the DCs in contact with RORγt$^+$ cells were further specified in one HDM-immunized C57BL/6 wt mouse. The DCs in proximity of RORγt$^+$ cells for this one mouse did not express langerin as visible in the overview (Fig. 6.22).

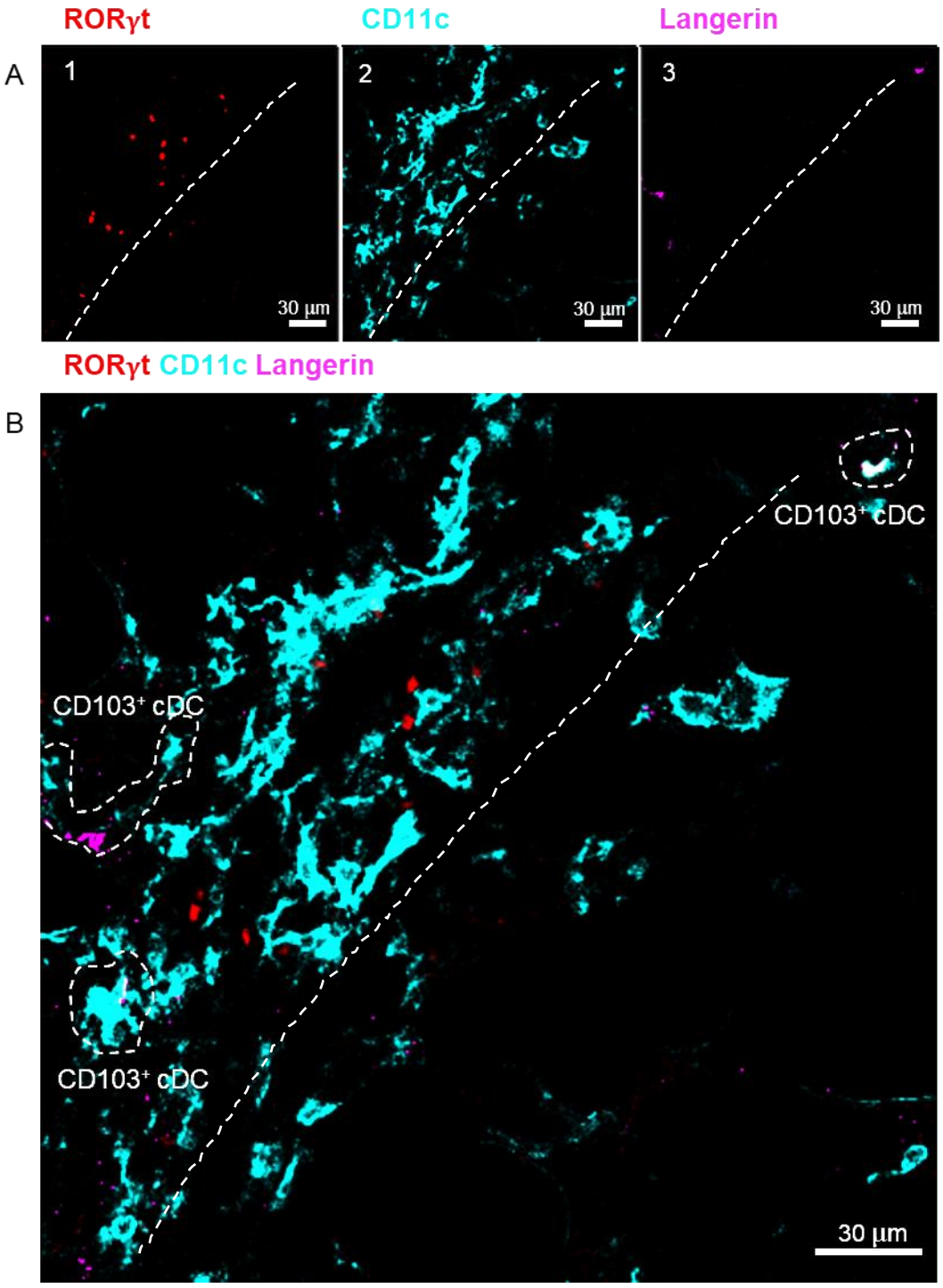

Fig. 6.22: Specification of the CD11c⁺ DC type in proximity to RORγt⁺ cells.
300 µm lung sections of one HDM-immunized C57BL/6 mouse were incubated with RORγt (red), CD11c turquoise) and langerin (pink) antibodies. Z-stacks were generated with the laser scanning confocal microscope and analyzed, using Imaris software. Individual overviews of RORγt [A1], CD11c [A2], and langerin [A3] are given with an overview of the three channels merged [B]. The white lines mark the DCs positive for langerin or the border of the airway.

7 Discussion

The impact prenatal antibiotics exposure had on the asthma phenotype was analyzed. The finding of the Deshmukh laboratory in Cincinnati that naïve P0 mice showed early life alterations in immune responses in terms of susceptibility to newborn pneumonia was indicative that P0 mice have early life alterations that might persist long-term and therefore influence asthma development. [197] However, prenatal antibiotics exposure in this study did not influence the lung function measured by baseline R_{RS} or HDM-driven, inflammatory R_{RS}. No alterations were found in terms of inflammatory immune cells present in the airway lumen or inflammatory T_H2 or T_H17 cytokines. Changes found included a trend of decrease in epithelial barrier function at baseline and an increased capacity of cells to produce IL-17A upon HDM-immunization. The IL-17A-producing cells were identified as γδT cells. The elevated frequencies in IL-17A$^+$ cells had no impact on neutrophil recruitment, since BAL fluid neutrophils were not elevated. A tendency of higher variability in mucus-related gene expression was found for P0-HDM mice.

7.1 Prenatal maternal microbiota disruption is not sufficient to induce severe experimental asthma

P0-HDM mice showed minor changes in terms of the asthma phenotype, while P14-HDM mice exhibited profound changes with increase in R_{RS}, increase in IL-17A$^+$ cells, and increase in neutrophils. (unpublished data, Lewkowich laboratory) While some data suggest that microbiota can cross the placental barrier during pregnancy, sparse data are available on the role of intrauterine microbiota shaping adequate immune responses. However, data by Gomez de Aguero *et al.* (2016) suggested that microbial products may prepare fetal immune cells for the extrauterine environment. It is commonly acknowledged that the vast microbial colonization of the intestine and other body cavities with large quantities of microbiota is induced perinatally and postnatally by transfer to the offspring, activating immune cell proliferation and differentiation. [200]

Antibiotic-mediated microbiota disruption most likely affected both P0 and P14 mice: the dysbiotic mother passed on the bacterial taxa present at the time of birth, presumably introducing long-term alteration in microbiota diversity and composition. Since the microbial disruption continued until 14 days after birth, alterations of P14 mice were more profound, which could subsequently have determined the mode of asthma development. The idea that microbiota can play a role in asthma pathogenesis is supported by the finding that asthmatics show altered intestinal and pulmonary microbiota composition. However, dysbiosis can also be a consequence of the disease. [201] For

future experiments, it could be of interest to analyze the composition and diversity of long-term microbiota at the time when sensitization is induced, comparing control *vs*. P0 *vs*. P14 mice. In terms of composition and abundance it would be of interest, if P0 mice' microbiome is more similar to control mice or to P14 mice: microbiota similar to control mice would suggest that microbiota was influential to the mode of asthma development. Microbiota similar to P14 mice would suggest that the microbiota cannot solely determine the mode of asthma development. A likely explanation for this would be that microbial disruption may have prevented from development of adequate tolerogenic immune responses expected to occur subsequently after birth. If microbiota of P0 mice recovered in time to induce microbiota-dependent tolerogenic immune responses, P14 mice may not have escaped impaired postnatal immune development and were therefore more susceptible to severe experimental asthma later in life. A critical postnatal time window has been suggested during which tolerogenic responses to microbiota develop: germ-free mice that were co-housed with SPF mice directly after birth had less proinflammatory cytokines and more T_{Reg} cells compered to germ-free mice inoculated with caecum content after three weeks of life. [153] In a similar study, germ-free rats were colonized with two species of commensals after birth. These rats showed less LPS-specific IgG upon LPS challenge compared to germ-free rats colonized with commensals at an older age. [154] Possibly in line with this is the finding that newborn children exposed to farming environment and mice exposed to farm dust in early life show more tolerogenic responses and are protected from inflammation later in life. [160] For future experiments addressing immune development after birth, changes could be addressed by measuring and comparing individual factors that have been identified to contribute to tolerogenic responses postpartum.

One of the factors that contribute to early life tolerogenic responses are SCFAs, which have been shown to induce tolerogenic responses and protect mice from experimental asthma. [191] SCFAs have pleiotropic functions on diverse cell types and tissues. Although little evidence suggests that SCFAs accumulate in the lung, they may act on lung immunity by activation of pulmonary epithelial and immune cells. [191, 202-204] Another factor contributing to postnatal shaping of the microbiota and possibly mediating tolerogenic responses before adaptive immunity has fully developed are maternal IgA. [205-207] In the mammalian gland, many IgA-producing plasma cells are found during pregnancy and postpartum. [208] Mice only show the first own IgA-producing plasma cells after weaning at 4-5 weeks of age. [209] Germ-free mice have reduced IgA, since a certain density of microbiota was shown to be necessary in order to induce IgA production by plasma cells. [210] Blocking maternal IgA might be an approach to identify early life responses that determine long-term immunity and the asthma phenotype. Analyzing the duration of exposure that is necessary to induce severe asthma could give a read out on whether adaptive immunity is affected: if only

long postnatal exposure until P14 is sufficient to induce severe, the development of adaptive immune responses could be affected.

Data from human children suggest that environmental factors like lactation, [172] high fiber diet, [173] older siblings, [174] pets, [175] and a farming environment [176] lower the risk to develop asthma. Critical in the development of tolerance are antigen-specific T_{Reg} cells, contributing to tolerance throughout life by suppression of proinflammatory responses towards specific antigens. Commensals like *Clostridium* species were positively correlated with the number of T_{Reg} cells. [211] Also SCFA levels have been identified to play a role in T_{Reg} cell expansion and function: smaller numbers of T_{Reg} cells were found in mice that lack the SCFA receptor G-coupled receptor 43. [212] Another way how SCFAs were shown to affect T_{Reg} cell frequency and function was by SCFA-mediated inhibition of the histone deacetylases (HDAC): butyrate-mediated HDAC inhibition was shown to directly facilitate T_{Reg} expansion. [213] In allograft experiments, the presence of SCFAs increased the suppressive capacities of T_{Reg} cells. [214] In the context of this study it could be that SCFA-producing bacterial taxa of P0 mice recovered faster than SCFA-producing bacteria of P14 mice. A lack of antigen-specific T_{Reg} cells or other SCFA-dependent anti-inflammatory immune responses could have impaired immune responses of P14 mice, leading to severe asthma.

Fig 7.1 summarizes some aspects that potentially play a role in long-term microbiota composition or immunity of P14 *vs*. P0 or control mice and could be of interest for future experimental approaches.

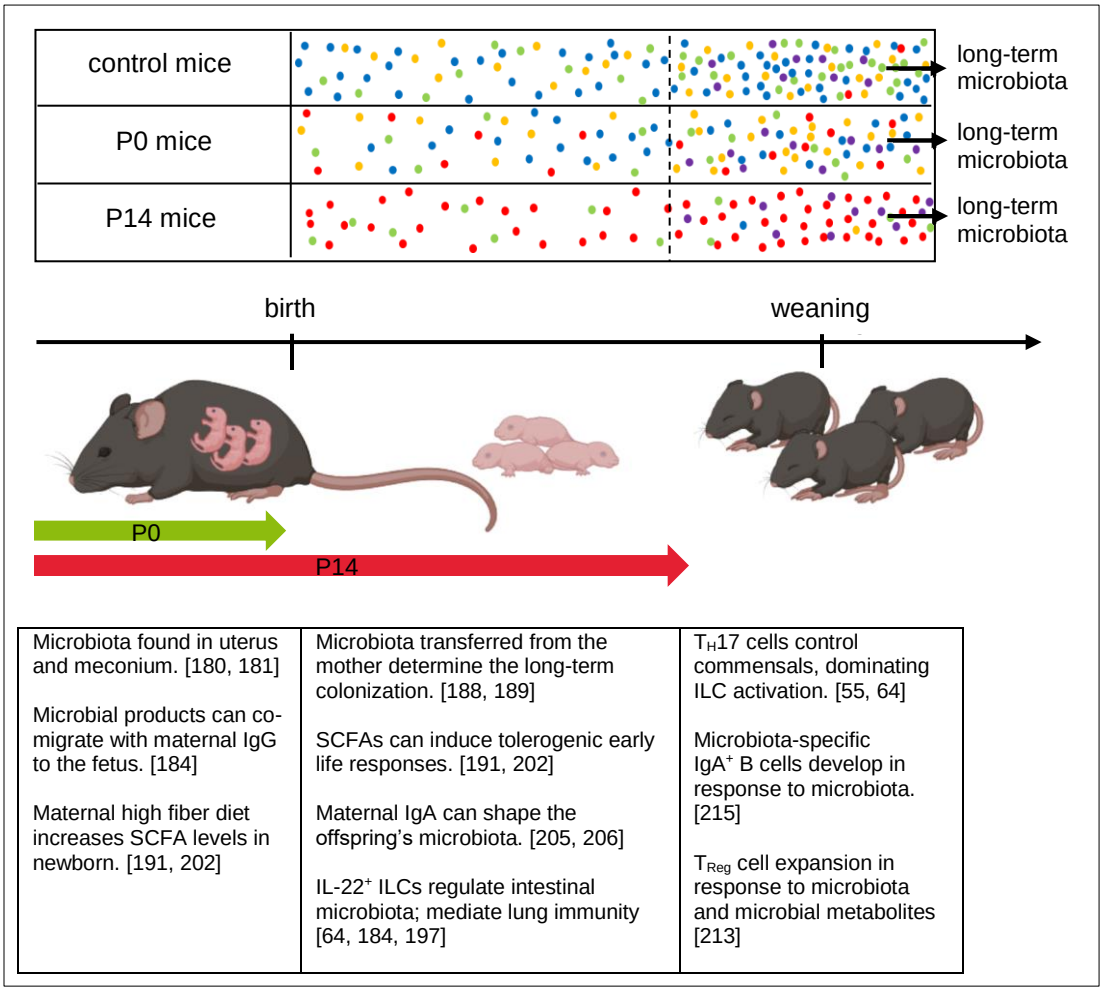

Fig. 7.1: Schematic overview of the potential long-term microbiota composition changes and immune developmental steps that could be impacted by antibiotics exposure. Maternal exposure to antibiotics potential changes on the long-term microbial composition in terms of bacterial taxa, represented by the colored dots (top part). Blue, green, and yellow dots represent beneficial taxa, red dots represent taxa associated with adverse effects, and purple dots represent new taxa that appear during weaning time. In the lower part a selection of microbiota-dependent immune developmental steps that occur subsequently before and after birth are listed.

7.2 Potential effects of antibiotics on microbiota and potential microbiota-independent effects

The three antibiotics used in this study inhibit distinct bacterial protein synthesis pathways: ampicillin is an antibiotic that interferes with the synthesis of the bacterial wall of Gram-positive and Gram-negative bacteria, [216] gentamicin interferes with the ribosomal protein synthesis of many Gram-negative and some Gram-positive bacteria, [217] vancomycin is an inhibitor of bacterial

cell wall synthesis of Gram-positive bacteria. [218] The three antibiotics used show rather limited capacities to influence the fetus or newborn directly: ampicillin is taken up by the gastrointestinal tract and can pass to the placenta by diffusion. [219] However, no embryo toxicity or congenital abnormalities have been reported for ampicillin, which is frequently used during pregnancy. [220] Gentamicin and vancomycin are poorly absorbed by the gastrointestinal tract and were not likely to have reached the uterus or the newborn mice *via* lactation. [221, 222] The antibiotics in this study were given orally. However, if administered intravenously, both gentamicin and vancomycin can cross the placental barrier by diffusion, where gentamicin can potentially cause minor congenital abnormalities, while vancomycin can potentially cause nephrotoxicity to the fetus. [223-225] On the other hand, both gentamicin and vancomycin are recommended by the American College of Obstetricians and Gynecologists for chorioamnionitis. [226] In terms of general health, no differences in body weight were observed for P0 treatment, which would have been an indicator for a general health disadvantage (Supplement Fig. 10.5).

Presumably, a broad spectrum of bacteria were targeted by the antibiotics, shifting the maternal microbiota composition even during the short duration of exposure for P0 mice. Because the data on newborn pneumonia was carried out with the same experimental approach and these mice showed shifts in microbiota, it is very likely that the mice of this project also showed similar alterations in microbiota. The changes observed by the Deshmukh laboratory on newborn pneumonia mice during the first two weeks of life were less *Lactobacillales*, *Enterobacteriales*, *Clostridales*, and *Bacillares*. At the same time, an increase in *Actinomycetales* and *Bacteroida* was observed. [197]

Taken together, broad effects of antibiotics were likely to impact the maternal microbiota rather than directly affecting the fetus.

7.3 Pre-sensitization phase of experimental allergic asthma

An intact epithelial barrier serves in maintenance of tolerance, keeping particles and microbes from the lumen at distance from immune cells. P0-PBS mice that had not been immunized and therefore can be considered naïve, showed a non-significant increase in epithelial permeability, since more intravascular FITC-albumin entered the lumen (Fig. 6.2). This is interesting, since some data suggest that inflammatory diseases like asthma, food allergy or inflammatory bowel disease are connected to increase in epithelial permeability. [227, 228] Epithelial barrier function is regulated by tight junctions between cells. Direct links between microbiota and epithelial barrier function have been shown: several studies showed that SCFAs can induce the expression or

assembly of tight junctions. [203, 229] Interestingly, an upregulation of adhesion genes and tight junction genes was shown in response to human milk oligosaccharides, enabling the colonization of the intestine with SCFA-producing microbiota such as *bifidobacteria infantilis* and *lactobacillus (rhamnosus GG*). [230] Also direct sensing of microbiota can influence epithelial barrier function: intestinal epithelial cells can upregulate tight junctions by direct sensing of commensals *via* TLRs. [233] TLR2 has been reported to play a role in microbiota sensing and epithelial barrier function in the intestine. [233] Interestingly, mice that lack TLR2 and 4 fed with high fat diet were highly susceptible to pulmonary edema, linking intestinal dysbiosis to severe pulmonary epithelial barrier dysfunction. [234] In the future it would be interesting to analyze SCFA levels of offspring mice, since SCFAs can induce tight junction expression and assembly. [204, 235] Also, it would be interesting to see, if microbial reconstitution or supplementation with SCFAs would reduce asthma symptoms of P14-HDM mice. Mechanisms whereby epithelial barrier function influences allergen sensitization were reviewed by Georas *et al*. (2014). [236] The authors suggested that more and larger allergens could enter the tissue and activate immune cells and antigen uptake by DCs, while small molecules would rather induce tolerogenic responses. Fig. 7.2 is an adapted overview on tolerogenic *versus* inflammatory responses dependent on epithelial permeability. [236-238]

A limitation of this study is that the overall fluorescence intensity of the recovered BAL fluid was very low in comparison to the serum fluorescence intensity (0.66-1.12 %). Therefore this experimental approach requires repetition and could potentially be completed with *in vitro* experiments to evaluate epithelial permeability and tight junction integrity.

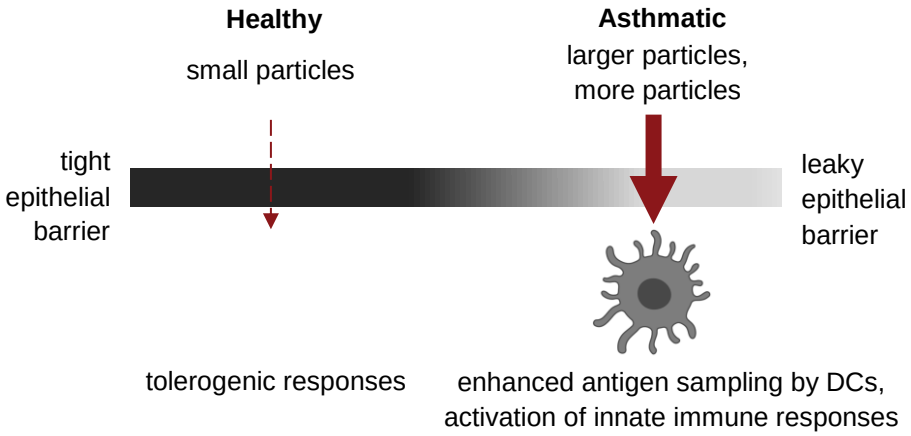

Fig. 7.2: Hypothetical contribution of epithelial barrier dysfunction to the sensitization phase adapted from Georas *et al*. (2014). [236] Impaired epithelial barrier may contribute to DC priming during asthma pathogenesis. While fewer, small particles rather induce tolerogenic responses, large and more particles could activate DC maturation and activate innate immune responses.
(Elsevier license number: 4846630683773)

7.4 Initiation of allergic airway inflammation – polarization of T helper cells

Although in this study the initiation phase of experimental allergic asthma was not investigated, it is possible to draw conclusions on the initiation in hindsight by analyzing the outcome of T cell differentiation. In terms of T_H2 responses, clear and substantial increases in T_H2 responses were observed for all asthmatic animals, regardless to the exposure to antibiotics. This was evident by the detection of T_H2 cytokines like IL-4, IL-5, and IL-13 but also by the recruitment of eosinophils (Fig. 6.4, 6.5). At the same time, no further intensification of T_H2 responses was observed for P0- or P14-HDM mice.

In an OVA-induced experimental asthma mouse model exposed postnatally to vancomycin from E0 to P49, Russell *et al*. (2012) found an increase in T_H2 responses and increase in R_{RS}, eosinophils, and antigen-specific IgE. The authors found that only vancomycin but not streptomycin could induce the more severe T_H2-driven asthma. Analyzing the microbiota showed that vancomycin markedly shifted the microbiota composition in comparison to streptomycin-treated or control mice. [239] In terms of immune cells, T_{Reg} cells were reduced in these animals. Low T_{Reg} cell quantities correlated with a reduction in *Clostridium* species, which confirmed data by another study that also used vancomycin exposure and found reduced T_{Reg} cells. [211] Although the model used by Russell *et al*. was an OVA-driven asthma mouse model and the antibiotics exposure duration was longer and did not include prenatal exposure, the data by Russell *et al*. suggested that the shifts in microbiota were responsible for alterations seen in the asthma phenotype, possibly by reduction of protective *Clostridium* species. The combination of antibiotics and/or the time frame of antibiotics exposure could be responsible for the mode of asthma development. Recently, Alhasan *et al*. (2019) exposed pregnant mice to increasing doses of vancomycin and found that offspring mice immunized with OVA developed a more severe asthma phenotype. Although the authors did not measure R_{RS}, BAL fluid cells were significantly elevated, if high vancomycin doses were given. Also a reduction of *Clostridiales* and *Prevotella* species was found along with reduced concentrations of SCFAs measured in caecum contents of the asthmatic offspring mice. Overall, the authors showed that prenatal antibiotics can impact the asthma phenotype, if high doses of vancomycin are given during pregnancy. [240]

It remains to be investigated how microbiota and/or reduced microbial products could contribute to the mode of asthma development and whether the long-term alterations in microbiota determine asthma development as indicated by epidemiological data or whether the early life microbiota alterations determine later asthma development. One way by which the mode of asthma

development could be influenced by the microbiota at the time of sensitization is by the activation of DCs that induced a polarization of naïve T cells towards T_H17 responses. Recently reviewed by Vroman *et al.* (2015), factors like C3 and serum amyloid A were found to induce T_H17 responses, while the complement factor C5a negatively correlated with T_H17 responses in an asthma mouse model of severe asthma. [130, 241] On the other hand, factors like TSLP and IL-33 have been described to rather promote T_H2 responses. [126] It is possible, that factors that determine DC maturation are dependent on the microbiota. Although the increased IL-17A$^+$ cells observed for both P0- and P14-HDM mice were not identified as αβT cells but as γδT cells for P0 mice or ILC3 for P14 mice, DCs could have been activated to secrete cytokines like IL-23. In terms of activation, both ILC3 and γδT cells are not dependent on adaptive immunity but can be activated within the tissues by cytokines. [242] Both populations are activated by IL-23, while T_H17 cells rather depend on IL-6 signaling and proliferate antigen-specifically. [243, 244] ILC3 and γδT cells develop around E10-E14 of pregnancy, while αβT cells only develop after birth. [245]

Because ILCs and γδT cells develop during embryogenesis, dysbiosis of the mother could have led to altered microbes or microbial metabolites co-migrating with maternal IgG to the uterus and changed the priming of γδT cells or ILCs *in utero*: Gomez de Aguero *et al*. showed that during pregnancy fetal ILCs upregulate the expression of AhR in response to microbial metabolites. In response, intestinal IL-22$^+$ ILCs were activated to proliferate and regulate the microbiota after birth. [184] The changes in priming of these cells may persist long-term and participate in determination of the asthma phenotype during sensitization. A lack of ILC3 influx to the newborn lung, using the same antibiotics mouse model as in this study was connected to increased susceptibility to newborn pneumonia, linking maternal dysbiosis and lung immunity. [197] Possibly, alterations of the newborn mice lasted long-term, leading to altered frequencies of γδT cells or ILCs. Using a mouse model of experimental psoriasis, Zanvit *et al*. (2015) exposed newborn mice to antibiotics from P0 to P21 and found that experimental psoriasis induced later in life was more severe. The disease severity was mediated by γδT cells. The increased disease severity was explained by profound alterations in microbial composition of the neonatal antibiotic-treated mice, which lasted into adulthood. The authors also found that antibiotics-treatment of adult mice ameliorated the symptoms. The data by Zanvit *et al*. suggest that the early life shifts in microbiota induced by antibiotics can cause a more severe inflammatory disease later in life, mediated by γδT cells. [246]

Taken together, while in section 7.3 an altered epithelial permeability was discussed to play a potential role in the mode of asthma development, this section focused on the cells potentially dependent on the microbiota. The question remains open, whether γδT cells and ILC3 could

possibly have been primed in early life or even during pregnancy, since they develop during embryogenesis. Also early life anti-inflammatory immune responses could have been impaired due to altered microbiota and microbial metabolites. On the other hand, shifts in long-term microbiota could possibly have changed DC maturation at the time of sensitization, which determined IL-17A$^+$ cell activation at the time of sensitization.

7.5 Chronic phase of experimental allergic asthma

During the chronic phase of allergic asthma, the innate and adaptive immune responses to specific allergens have fully developed and effector cells and -molecules have induced remodeling of the airways, increase in mass and contractibility of smooth muscle cells, and increase in goblet cells and mucin expression. [109, 110] Two systemic and two topical HDM-treatments led to full development of TH2 responses, including elevated TH2 cytokines, BAL fluid immune cells, and elevated RRS (Fig. 6.3, 6.4, 6.5). However, in terms of TH2 responses, no differences were observed in comparison to the control mice. In terms of BAL fluid cells, the numbers of immune cells found for P0-HDM mice even showed a statistically non-significant reduction (Fig. 6.4). However, the reduction could have been due to technical issues with pale Diff Quick stainings, which made it more difficult to detect the least frequent populations, neutrophils and lymphocytes.

While T_H2 responses remained similar for control- and P0-HDM mice, IL-17A$^+$ cell frequencies were increased. The IL-17A cytokine concentrations of whole lung cell suspensions measured by ELISA somewhat contradicted the flow cytometry measurements (Fig. 6.5 D). A possible explanation could be the different methodical approaches of cell restimulation in both assays. For the cytokine concentration measurements, cells were restimulated with HDM, possibly mostly stimulating antigen-specific $\alpha\beta$T cells. For the analysis of intracellular cytokines, cells were stimulated with PMA/ionomycin, stimulating all potential cytokine-producing cells. Therefore one method could have restimulated one cell type while the other cell types were potentially stimulated by the other method. On the other hand, both methods of restimulation showed the potential number of IL-17A-producing cells, not the numbers that were actual active in the lung. Therefore from the experiments one can conclude that *in vivo* not more production takes place but there is a difference in terms of potential IL-17A producers, identified as $\gamma\delta$T cells. However, due to the lack of stimulus they may not actually secrete IL-17A.

While postnatal dysbiosis led to BAL fluid neutrophilia of P14-HDM mice, the changes caused by prenatal antibiosis of P0-HDM mice were insufficient to induce neutrophilia. Although neutrophil recruitment by IL-17A has been reported during infection and in severe asthma of humans and mice, [135, 136] the elevation in IL-17A$^+$ cells observed in this study was not sufficient to cause

neutrophilia. Possibly, the longer postnatal antibiotics exposure of P14 mice induced additional factors for neutrophil activation and recruitment.

In terms of mucus production, being a cardinal symptom of chronic asthma, some more variability for P0-HDM mice in comparison to control mice was observed for *Muc5ac* and *Gob5* expression (Fig. 6.9). Given this tendency, P14-HDM mice should be analyzed for mucus-related gene expression, which would be a plausible explanation for the increased R_{RS} observed for these mice. [247]

Blockade of IL-17A cytokine

Blocking of the cytokine IL-17A led to reduced R_{RS}, which highly suggests that IL-17A contributed to R_{RS}. However, this effect was visible in spite of the fact that the overall R_{RS} of P0-HDM mice was not elevated in comparison to control-HDM mice, which is in line with the knowledge that asthma is not a sole T_H2-driven disease but that also T_H17 responses contribute to the disease, independently to the antibiotics gavage. [130, 241] From the data of this project the reduction of several components may be indicative of the role that IL-17A had on the reduction of R_{RS}: In terms of BAL fluid cells, no reduction of inflammatory cells was observed. Additionally, T_H2 cytokines IL-4, IL-5, IL-13 remained comparable to HDM mice. However, a reduction of IL-13$^+$ cells was observed, although the cytokine levels measured by ELISA were not reduced. This could be due to the different methods of restimulation, which were discussed in section 7.5. Since synergistic effects of IL-13 and IL-17A have been reported previously, it could be that the reduction of IL-17A cytokine caused the reduction of IL-13$^+$ cells directly. [130, 131] A reduction in mucin gene expression was also observed. IL-17A has previously been described to contribute to excessive mucus secretion in allergic airway inflammation. [132, 247] The reduction in mucin expression following IL-17A blockade could be indicative of the origin of severe R_{RS} found for P14-HDM mice. Although other IL-17A-dependent factors like smooth muscle layer increase could have contributed, excessive mucus secretion should be considered.

Microscopy approach of potential IL-17A producers

The microscopy approach aimed to investigate the IL-17A$^+$ cells *in situ* in order to see, if differences seen in flow cytometry could be substantiated by microscopy. Also the data on ILC3 influx into the lungs in the newborn pneumonia study indicated that the recruitment of these cells can be altered in P0 mice in terms of numbers and possibly in terms of localization. Because of the way the sections were generated, a quantification analysis of RORγt$^+$ cells could not be

performed without a bias since RORγt$^+$ cells mostly localized to large airways and therefore sections generated at the lateral parts of the lobes were more likely to have fewer numbers due to the fact that fewer large airways were found. In order to eliminate this bias, serial lung sections would have been necessary, comparing corresponding sections of control- and P0-HDM mice. Therefore the primary aim was not to quantify cell numbers but to identify and investigate the relative distribution of pulmonary RORγt$^+$ cells.

First, the identification and reliability of the imaging approach were investigated. The nuclear localization of the signal and the positivity for CD3, as well as the negativity for GATA3 were strong indicators for signal specificity (6.13, 6.14). Notably, the comparison of the RORγt signal to the transcription factor GATA3 showed about tenfold more GATA3$^+$ cells, being in line with the expectation of a strong T_H2 dominance, reflected by the results on cytokine concentration measurements and the frequency of cytokine-producing cells (Fig. 6.5, 6.6). The observation that P0-HDM mice showed increased IL-17A$^+$ γδT cells measured by flow cytometry could not be confirmed by the IHC approach (Fig. 6.18). One plausible explanation for this result might be that the populations quantified by both techniques were not entirely identical. Because PMA/ionomycin is a strong stimulant, it is likely that cells detected by flow cytometry were not included in the IHC analysis due to low RORγt expression level in unstimulated conditions. Another possible explanation would be that IL-17A is not solely depending on the transcription factor RORγt. In fact, Yang *et al.* (2008) showed that RORγt -/- cells do not have complete loss of IL-17A production and only combined RORγt and RORα knockout sufficiently eliminated IL-17A production. [248] RORα involved in IL-17A production was not detected by the IHC approach but could have been detected by the flow cytometry approach, since IL-17A$^+$ cells were analyzed. However, according to the available literature both transcription factors should be expressed by the same cells. [248] A limitation of the flow cytometry approach was the low number of cells in the final gate, which was due to overall less IL-17A$^+$ cells in comparison to IL-13$^+$ cells. Therefore verification of the flow cytometry measurements is necessary.

The localization of RORγt$^+$ cells close to large and small airways and blood vessels was consistent with the described localization of pulmonary immune cell populations. [75] Being interested in RORγt$^+$ cells and/or the subpopulations clustering at specific localizations like small airways, the RORγt$^+$ ILC3, αβT cell and γδT cells were analyzed in terms of their localization. Severe asthma has been associated with inflammation of the small airways previously, with high frequency of neutrophils, small airway plugging, and remodeling of small airways. [249, 250] Given the assumption that high local cytokine concentrations can contribute to the inflammation such as recruitment of immune cells and airway remodeling, an increase in IL-17A$^+$ cells at small airways would have

been of profound interest. However, the distribution of the RORγt$^+$ cell subpopulations was similar, comparing both treatment groups: large airways were the predominant localization site of all three populations, while fewer RORγt$^+$ cells were found at small airways or blood vessels. A limitation of the approach is that few RORγt cell numbers at small airways were very low and therefore generating Z-stacks was rather time consuming. To investigate small differences, analyzing higher cell numbers would have been necessary, since the technique is not feasible for large quantity analysis. Taken together the data indicate that the effects of IL-17A rather dependent on the activation than on the localization, which could be different in a different model.

Interestingly, independent to the antibiotics exposure, many RORγt$^+$ cells localized close to CD11c$^+$ DCs under inflammation. Possibly it could be interesting to apply the approach to P14-HDM mice, and possibly it could be interesting to look at the sensitization phase rather than looking at the chronic phase of the disease. Manual image acquisition and analysis as performed in this study is very time consuming. To increase the number of images analyzed in a certain time, an unsupervised quantification approach would greatly facilitate the analysis of RORγt$^+$ cells and DCs under inflammatory conditions. [251] In a first step towards the goal, imaging/quantification could be established and in a second step the subpopulations could be analyzed, asking, whether one of the three RORγt$^+$ subpopulations is more likely to interact with DCs under inflammation. In a third step this approach could be applied to one of the antibiotics exposure models.

8 Conclusion and future perspective

The hypothesis of the thesis that prenatal antibiotics exposure, similar to postnatal antibiotics exposure, induces a severe asthma phenotype could not be substantiated. Furthermore, we hypothesized that IL-17A$^+$ cells show altered pattern of localization at large or small airways, and altered interaction with DCs, which could not be found. In hindsight, the overall minor changes seen are in line with the published data on immune cell priming that occurs in response to the major influx of microbiota during and after birth, suggesting that the dysbiosis of P0 mice could be rescued by microbial colonization after birth. The experimental setups of both P0 and P14 experiments were identical and only differed in the duration of maternal exposure. The combined results of the two projects provide valuable data that link the prenatal and postnatal phase with long-term immunity. The established microscopy approach is a valuable tool for *in situ* analysis of potential IL-17A producers. This study favors the concept that all IL-17A-producing cells localize in the same area and the activation signals are more important for their function than their localization. Possibly under other conditions, an altered distribution of these cells is important for their function, which should be investigated. Fig. 7.3 integrates the results gained from both antibiotics exposure studies. For the future perspective, some important questions could be followed up on experimental asthma of mice exposed to antibiotics: What is the long-term microbiota composition of P0 mice at the point of sensitization in comparison to P14 mice and control mice? Does epithelial permeability during the pre-sensitization phase or excessive mucus production during inflammation contribute to asthma severity of P14 mice? Are early life tolerogenic responses impacted by the microbial disruption and how long after birth must the disruption of microbiota be continued to induce a severe experimental asthma phenotype?

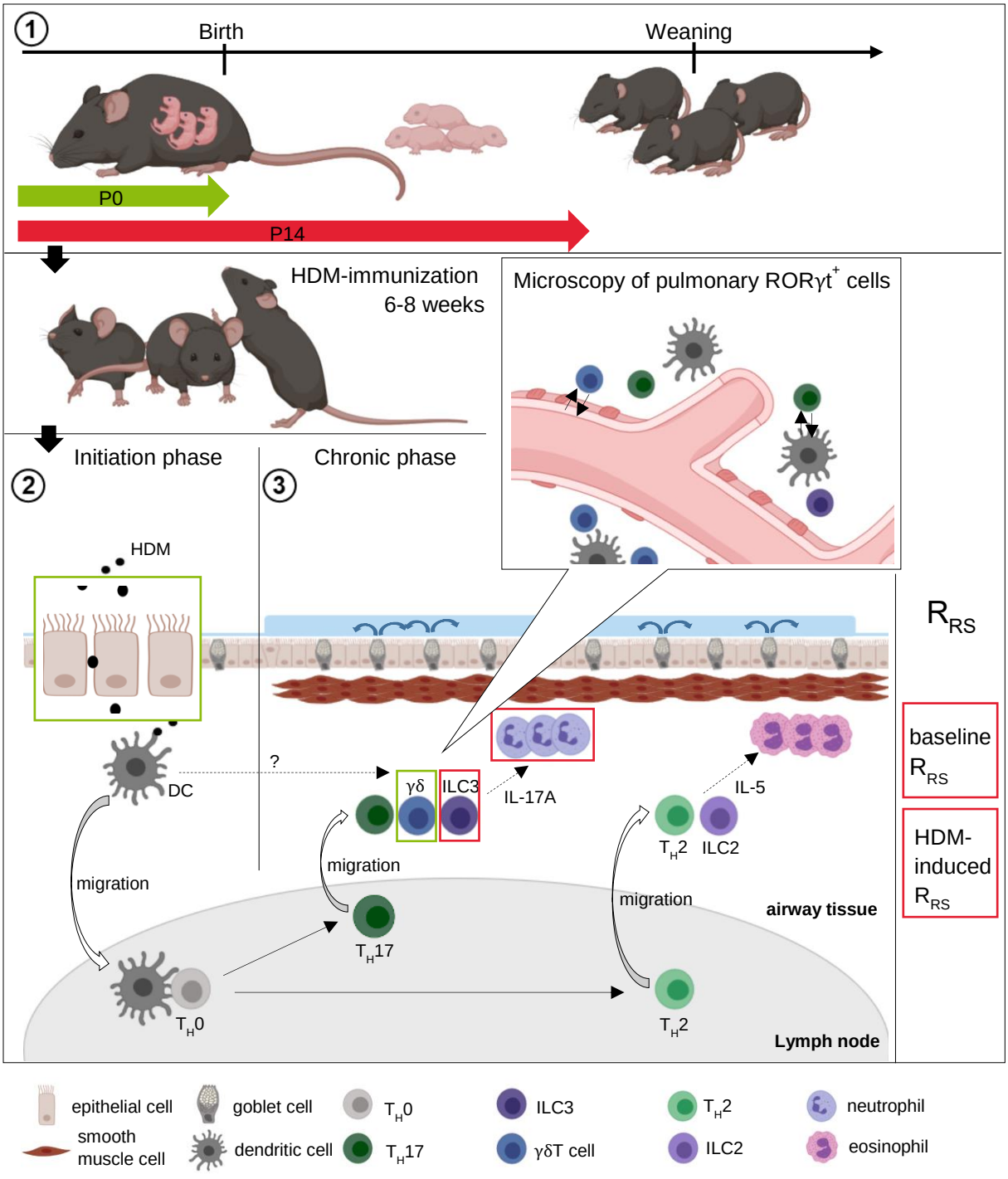

Fig. 7.3: Schematic overview of the working hypothesis, integrating the results of P0 and P14 exposure experiments, adapted from Vroman *et al.* (2015). [126] Prenatal or postnatal antibiotics exposure (1) influence the immunity of the offspring mice that may have preexisting epithelial barrier dysfunction (2). Indicated by red frames, upon HDM treatment, P14 mice develop severe asthma, with alterations in IL-17A$^+$ ILC3, neutrophilia, and R_{RS}. (unpublished data, Lewkowich laboratory) Green frames indicate the alterations in basal lung function and asthma phenotype seen for P0 mice (3). T_H2 responses for both exposure studies were comparable to control mice.

9 References

1. Mitchell, G.F., Co-evolution of parasites and adaptive immune responses. Immunol. Today, 1991. **12**(3): p. A2-5.
2. Elvington, M., M.K. Liszewski, and J.P. Atkinson, Evolution of the complement system: from defense of the single cell to guardian of the intravascular space. Immunological reviews, 2016. **274**(1): p. 9-15.
3. Dias Da Silva, W. and I.H. Lepow, Complement as a mediator of inflammation. II. Biological properties of anaphylatoxin prepared with purified components of human complement. J. Exp. Med., 1967. **125**(5): p. 921-46.
4. Dunkelberger, J.R. and W.C. Song, Complement and its role in innate and adaptive immune responses. Cell. Res., 2010. **20**(1): p. 34-50.
5. Hanada, T. and A. Yoshimura, Regulation of cytokine signaling and inflammation. Cytokine Growth Factor Rev., 2002. **13**(4-5): p. 413-21.
6. Gasteiger, G., et al., Cellular Innate Immunity: An Old Game with New Players. J. Innate Immun., 2017. **9**(2): p. 111-125.
7. Takeuchi, O. and S. Akira, Pattern recognition receptors and inflammation. Cell, 2010. **140**(6): p. 805-20.
8. Medzhitov, R., Toll-like receptors and innate immunity. Nature Rev. Immunol., 2001. **1**: p. 135-145.
9. Inohara, N., *et al.*, An induced proximity model for NF-kappa B activation in the Nod1/RICK and RIP signaling pathways. J. Biol. Chem., 2000. **275**(36): p. 27823-31.
10. Gordon, S., *Phagocytosis: The Legacy of Metchnikoff. C*ell, 2016. **166**(5): p. 1065-1068.
11. Zhou, L., et al., Macrophages polarization is mediated by the combination of PRR ligands and distinct inflammatory cytokines. Int. J. Clin. Exp. Pathol., 2015. **8**(9): p. 10964-74.
12. Zimmerli, S., *et al*., Phagosome-lysosome fusion is a calcium-independent event in macrophages. J. Cell. Biol., 1996. **132**(1-2): p. 49-61.
13. Bar-On, L. and S. Jung, Defining in vivo dendritic cell functions using CD11c-DTR transgenic mice. Methods Mol. Biol., 2010. **595**: p. 429-42.
14. Lanzavecchia, A., Mechanisms of antigen uptake for presentation. Curr. Opin. Immunol., 1996. **8**(3): p. 348-54.
15. Reis e Sousa, C., Activation of dendritic cells: translating innate into adaptive immunity. Curr. Opin. Immunol., 2004. **16**(1): p. 21-5.
16. Seth, S., *et al*., CCR7 essentially contributes to the homing of plasmacytoid dendritic cells to lymph nodes under steady-state as well as inflammatory conditions. J. Immunol., 2011. **186**(6): p. 3364-72.
17. Futosi, K., S. Fodor, and A. Mócsai, Neutrophil cell surface receptors and their intracellular signal transduction pathways. International immunopharmacology, 2013. **17**(3): p. 638-650.
18. Travers, J. and M.E. Rothenberg, Eosinophils in mucosal immune responses. Mucosal Immunol., 2015. **8**(3): p. 464-75.
19. Webb, L.M., *et al*., Binding to heparan sulfate or heparin enhances neutrophil responses to interleukin 8. Proc. Natl. Acad. Sci. U S A, 1993. **90**(15): p. 7158-62.
20. Chertov, O., *et al*., Identification of human neutrophil-derived cathepsin G and azurocidin/CAP37 as chemoattractants for mononuclear cells and neutrophils. J. Exp. Med., 1997. **186**(5): p. 739-47.
21. Desai, J.V. and M.S. Lionakis, The role of neutrophils in host defense against invasive fungal infections. Curr. Clin. Microbiol. Rep., 2018. **5**(3): p. 181-189.

22. Solberg, C.O. and K.B. Hellum, Neutrophil granulocyte function in bacterial infections. Lancet, 1972. **2**(7780): p. 727-30.
23. Gleich, G.J., *et al*., Cytotoxic properties of the eosinophil major basic protein. J. Immunol., 1979. **123**(6): p. 2925-7.
24. Sanmugalingham, D., *et al*., Interleukin-5 enhances eosinophil adhesion to bronchial epithelial cells. Clin. Exp. Allergy, 2000. **30**(2): p. 255-63.
25. Giembycz, M.A. and M.A. Lindsay, Pharmacology of the eosinophil. Pharmacol. Rev., 1999. **51**(2): p. 213-340.
26. Hepworth, M.R., *et al*., Mast cells orchestrate type 2 immunity to helminths through regulation of tissue-derived cytokines. Proc. Natl. Acad. Sci. USA, 2012. **109**(17): p. 6644-6649.
27. Uyttenhove, C., R.J. Simpson, and J. Van Snick, Functional and structural characterization of P40, a mouse glycoprotein with T-cell growth factor activity. Proc. Natl. Acad. Sci. U S A, 1988. **85**(18): p. 6934-8.
28. Siriganian, R.P., Mast cell signal transduction from the high-affinity IgE receptor. Curr. Op. Immunol., 2003. **14**(6): p. 639-646.
29. Li, E., *et al*., Mast cell-mediated changes in smooth muscle contractility during mouse giardiasis. Infect. Immun., 2007. **75**(9): p. 4514-8.
30. Gasteiger, G., *et al*., Tissue residency of innate lymphoid cells in lymphoid and nonlymphoid organs. Science (New York, N.Y.), 2015. **350**(6263): p. 981-985.
31. Ignacio, A., C.N.S. Breda, and N.O.S. Camara, Innate lymphoid cells in tissue homeostasis and diseases. World journal of hepatology, 2017. **9**(23): p. 979-989.
32. Mortha, A., *et al*., Microbiota-dependent crosstalk between macrophages and ILC3 promotes intestinal homeostasis. Science, 2014. **343**(6178): p. 1249288.
33. Sonnenberg, G.F. and D. Artis, Innate lymphoid cells in the initiation, regulation and resolution of inflammation. Nat. Med., 2015. **21**(7): p. 698-708.
34. Spits, H., *et al*., Innate lymphoid cells--a proposal for uniform nomenclature. Nat. Rev. Immunol., 2013. **13**(2): p. 145-9.
35. Moro, K., *et al*., Innate production of T(H)2 cytokines by adipose tissue-associated c-Kit(+)Sca-1(+) lymphoid cells. Nature, 2010. **463**(7280): p. 540-4.
36. Neill, D.R., *et al*., Nuocytes represent a new innate effector leukocyte that mediates type-2 immunity. Nature, 2010. **464**(7293): p. 1367-70.
37. Saenz, S.A., *et al.*, IL25 elicits a multipotent progenitor cell population that promotes T(H)2 cytokine responses. Nature, 2010. **464**(7293): p. 1362-6.
38. Yasuda, K., *et al*., Contribution of IL-33-activated type II innate lymphoid cells to pulmonary eosinophilia in intestinal nematode-infected mice. Proc. Natl. Acad. Sci. U S A, 2012. **109**(9): p. 3451-6.
39. Artis, D. and H. Spits, The biology of innate lymphoid cells. Nature, 2015. **517**(7534): p. 293-301.
40. Yoshida, H., *et al*., IL-7 receptor alpha+ CD3(-) cells in the embryonic intestine induces the organizing center of Peyer's patches. Int. Immunol., 1999. **11**(5): p. 643-55.
41. Eberl, G., *et al*., An essential function for the nuclear receptor RORgamma(t) in the generation of fetal lymphoid tissue inducer cells. Nat. Immunol., 2004. **5**(1): p. 64-73.
42. Buchmann, K., Evolution of Innate Immunity: Clues from Invertebrates via Fish to Mammals. Front. Immunol., 2014. **5**: p. 459.
43. Worbs, T, Hammerschmidt, S.I., Förster, R., Dendritic cell migration in health and disease. Nature. Rev. Immunol., 2017. **17**: p. 30-48.
44. Cella, M., F. Sallusto, and A. Lanzavecchia, Origin, maturation and antigen presenting function of dendritic cells. Curr. Opin. Immunol., 1997. **9**(1): p. 10-6.
45. Ingulli, E., *et al*., In vivo detection of dendritic cell antigen presentation to CD4(+) T cells. J. Exp. Med., 1997. **185**(12): p. 2133-41.

46. Konig, R., L.Y. Huang, and R.N. Germain, MHC class II interaction with CD4 mediated by a region analogous to the MHC class I binding site for CD8. Nature, 1992. **356**(6372): p. 796-8.
47. Russ, B., *et al*., T cell immunity as a tool for studying epigenetic regulation of cellular differentiation. Frontiers in Genetics, 2013. **4**(218).
48. van Panhuys, N., TCR Signal Strength Alters T–DC Activation and Interaction Times and Directs the Outcome of Differentiation. Frontiers in Immunology, 2016. **7**(6).
49. von Andrian, U.H. and T.R. Mempel, Homing and cellular traffic in lymph nodes. Nat. Rev. Immunol., 2003. **3**(11): p. 867-78.
50. Pernis, B., G. Chiappino, and D.S. Rowe, Cells producing IgD immunoglobulins in human spleen. Nature, 1966. **211**(5047): p. 424-5.
51. Bourgois, A., E.R. Abney, and R.M. Parkhouse, Mouse immunoglobulin receptors on lymphocytes: identification of IgM and IgD molecules by tryptic cleavage and a postulated role for cell surface IgD. Eur. J. Immunol., 1977. **7**(4): p. 210-3.
52. Tonegawa, S., Somatic generation of antibody diversity. Nature, 1983. **302**(5909): p. 575-81.
53. MacLennan, I.C., Germinal centers. An. Rev. Immunol., 1994. **12**: p. 117-39.
54. Tudor, D., *et al*., Isotype modulates epitope specificity, affinity, and antiviral activities of anti-HIV-1 human broadly neutralizing 2F5 antibody. Proc. Natl. Acad. Sci. U S A, 2012. **109**(31): p. 12680-5.
55. Ivanov, II, *et al*., Induction of intestinal Th17 cells by segmented filamentous bacteria. Cell, 2009. **139**(3): p. 485-98.
56. Hsieh, C.S., *et al*., Development of TH1 CD4+ T cells through IL-12 produced by Listeria-induced macrophages. Science, 1993. **260**(5107): p. 547-9.
57. Romagnani, S., T-cell subsets (Th1 versus Th2). Ann. Allergy Asthma Immunol., 2000. **85**(1): p. 9-18; quiz 18, 21.
58. Finkelman, F.D., *et al*., Stat6 regulation of in vivo IL-4 responses. J. Immunol., 2000. **164**(5): p. 2303-10.
59. Silva-Filho, J.L., Caruse-Neves, C., Pinheiro, A.A.S., IL-4:an important cytokine in determining the fate of T cells. Biophys. Rev., 2014. **6**(1): p. 111-18.
60. Else, K.J., *et al*., Cytokine-mediated regulation of chronic intestinal helminth infection. J. Exp. Med., 1994. **179**(1): p. 347-51.
61. Walker, J.A., McKenzie, A.N.J., TH2 cell development and function, Nature Rev. Immunol. 2018. **18**: p. 121-133.
62. Junttila, I.S., Tuning the Cytokine Responses: An Update on Interleukin (IL)-4 and IL-13 Receptor Complexes. Front. Immunol., 2018. **9**(888).
63. Hwang, E.S., Transcriptional regulation of T helper 17 cell differentiation. Yonsei Med. J., 2010. **51**(4): p. 484-491.
64. Mao, K., *et al.*, Innate and adaptive lymphocytes sequentially shape the gut microbiota and lipid metabolism. Nature, 2018. **554**(7691): p. 255-259.
65. Corthay, A., How do regulatory T cells work? Scandin. J. Immunol., 2009. **70**(4): p. 326-336.
66. Born, W.K., *et al*., gammadelta T Cells and B Cells. Adv. Immunol., 2017. 134: p. 1-45.
67. Meraviglia, S., *et al.*, gammadelta T cells cross-link innate and adaptive immunity in Mycobacterium tuberculosis infection. Clin. Dev. Immunol., 2011. **2011**: p. 587315.
68. Benveniste, P.M., *et al.*, Generation and molecular recognition of melanoma-associated antigen-specific human gammadelta T cells. Sci. Immunol., 2018. **3**(30).
69. Wesch, D., *et al*., Modulation of gammadelta T cell responses by TLR ligands. Cell Mol. Life Sci., 2011. **68**(14): p. 2357-70.

70. Zarin, P., *et al.*, Gamma delta T-cell differentiation and effector function programming, TCR signal strength, when and how much? Cell Immunol., 2015. **296**(1): p. 70-5.
71. Fahl, S.P., F. Coffey, and D.L. Wiest, Origins of gammadelta T cell effector subsets: a riddle wrapped in an enigma. J. Immunol., 2014. **193**(9): p. 4289-94.
72. Kirby, A.C., *et al*., Pulmonary dendritic cells and alveolar macrophages are regulated by gammadelta T cells during the resolution of S. pneumoniae-induced inflammation. J. Pathol., 2007. **212**(1): p. 29-37.
73. Harding, R., K.E. Pinkerton, and C. Plopper, The Lung: Development, Aging and the Environment. 2003. **410**.
74. Courtice, F.C., Lymph flow in the lungs. Br Med Bull, 1963. **19**: p. 76-9.
75. Kretschmer, S., et al., Visualization of intrapulmonary lymph vessels in healthy and inflamed murine lung using CD90/Thy-1 as a marker. PLoS One, 2013. 8(2): p. e55201.
76. Lloyd, C.M. and J.R. Murdoch, Tolerizing allergic responses in the lung. Mucosal Immunol., 2010. **3**(4): p. 334-44.
77. Coleman, M.M., *et al*., Alveolar macrophages contribute to respiratory tolerance by inducing FoxP3 expression in naive T cells. Am J. Respir. Cell. Mol. Biol., 2013. **48**(6): p. 773-80.
78. Khare, A., *et al*., Cutting edge: inhaled antigen upregulates retinaldehyde dehydrogenase in lung CD103+ but not plasmacytoid dendritic cells to induce Foxp3 de novo in CD4+ T cells and promote airway tolerance. J. Immunol., 2013. **191**(1): p. 25-9.
79. van Schayck, C.P. and H.A. Smit, The prevalence of asthma in children: a reversing trend. Eur. Respir. J., 2005. 26(4): p. 647-50.
80. Wang, Y.L., *et al*., Role of airway epithelial cells in development of asthma and allergic rhinitis. Resp. Med., 2008. **102**(7): p. 949-955.
81. Holgate, S.T., *et al*., Epithelial-mesenchymal interactions in the pathogenesis of asthma. J. Allergy Clin. Immunol., 2000. **105**(2 Pt 1): p. 193-204.
82. Adgate, J.L., *et al*., Allergen levels in inner city homes: baseline concentrations and evaluation of intervention effectiveness. J. Expo. Sci. Environ. Epidemiol., 2008. **18**(4): p. 430-40.
83. Holgate, S.T, The airway epithelium is central to the pathogenesis of asthma. Allerg. Intern., 2008. **57**(1): p. 1-10.
84. Guilbert, T.W., *et al*., Decreased lung function after preschool wheezing rhinovirus illnesses in children at risk to develop asthma. J. Allergy Clin. Immunol., 2011. **128**(3): p. 532-8 e1-10.
85. Jackson, D.J., *et al*., Evidence for a causal relationship between allergic sensitization and rhinovirus wheezing in early life. Am J. Respir. Crit. Care Med., 2012. **185**(3): p. 281-5.
86. Gauderman, W.J., *et al*., Association of Improved Air Quality with Lung Development in Children. New England Journal of Medicine, 2015. **372**(10): p. 905-913.
87. Rank, M.A., *et al*., IL-33-activated dendritic cells induce an atypical TH2-type response. J. Allergy Clin. Immunol., 2009. **123**(5): p. 1047-1054.
88. Gough, L., *et al*., The cysteine protease activity of the major dust mite allergen Der p 1 selectively enhances the immunoglobulin E antibody response. J. Exp. Med., 1999. **190**(12): p. 1897-902.
89. Wan, H., *et al.*, Der p 1 facilitates transepithelial allergen delivery by disruption of tight junctions. J. Clin. Invest., 1999. **104**(1): p. 123-33.
90. Oboki, K., *et al*., IL-33 is a crucial amplifier of innate rather than acquired immunity. Proc. Natl. Acad. Sci. U S A, 2010. **107**(43): p. 18581-6.
91. Martinez-Gonzalez, I., C.A. Steer, and F. Takei, Lung ILC2s link innate and adaptive responses in allergic inflammation. Trends Immunol., 2015. **36**(3): p. 189-95.
92. del Rio, M.L., *et al*., CD103- and CD103+ bronchial lymph node dendritic cells are specialized in presenting and cross-presenting innocuous antigen to CD4+ and CD8+ T cells. J. Immunol., 2007. **178**(11): p. 6861-6.

93. Sunttila, I.S., Tuning the cytokine responses: an update on interleukine (IL)-4 and IL-13 receptor complexes. Front. Immunol., 2018. **9**: p. 888.
94. Punnonen, J. and J.E. de Vries, IL-13 induces proliferation, Ig isotype switching, and Ig synthesis by immature human fetal B cells. J. Immunol., 1994. **152**(3): p. 1094-102.
95. Oettgen, H.C., Regulation of the IgE isotype switch: new insights on cytokine signals and the functions of epsilon germline transcripts. Curr. Opin. Immunol., 2000. **12**(6): p. 618-23.
96. Poulsen, L.K. and L. Hummelshoj, Triggers of IgE class switching and allergy development. Ann. Med., 2007. **39**(6): p. 440-56.
97. Sehra, S. *et al*., TH9 cells are required for tissue mast cell accumulation during allergic inflammation. J. Allergy. Clin. Immunol., 2015. **136**: p. 433-440.
98. Kearly, J. *et al*., IL-9 governs allergen-induced mast cell numbers in the lung and chronic remodeling of the airways. Am. J. Respir. Crit. Care Med., 2011. **183**(7): p. 865-875.
99. Yurt, R.W., R.W. Leid, Jr., and K.F. Austen, Native heparin from rat peritoneal mast cells. J. Biol. Chem., 1977. **252**(2): p. 518-21.
100. Schneider, E., *et al*., Histamine-producing cell-stimulating activity. Interleukin 3 and granulocyte-macrophage colony-stimulating factor induce de novo synthesis of histidine decarboxylase in hemopoietic progenitor cells. J. Immuno.l, 1987. **139**(11): p. 3710-7.
101. Plaut, M., *et al*., Mast cell lines produce lymphokines in response to cross-linkage of Fc epsilon RI or to calcium ionophores. Nature, 1989. **339**(6219): p. 64-7.
102. Amin, K., The role of mast cells in allergic inflammation. Respir. Med., 2012. **106**(1): p. 9-14.
103. Miller, H.R. and A.D. Pemberton, Tissue-specific expression of mast cell granule serine proteinases and their role in inflammation in the lung and gut. Immunology, 2002. **105**(4): p. 375-90.
104. Abrink, M., M. Grujic, and G. Pejler, Serglycin is essential for maturation of mast cell secretory granule. J Biol Chem, 2004. **279**(39): p. 40897-905.
105. Hart, H, Regulation of the inflammatory response in asthma by mast cell products. Immunol. Cell. Biol., 2001. **79**(2): p. 149-153.
106. Gregory, G.D., *et al*., Mast cell IL-4 expression is regulated by Ikaros and influences encephalitogenic Th1 responses in EAE. J. Clin. Invest., 2006. **116**(5): p. 1327-36.
107. Amin, K., *et al*., The extracellular deposition of mast cell products is increased in hypertrophic airways smooth muscles in allergic asthma but not in nonallergic asthma. Allergy, 2005. **60**(10): p. 1241-7.
108. Margulis, A., *et al*., Mast cell-dependent contraction of human airway smooth muscle cell-containing collagen gels: influence of cytokines, matrix metalloproteases, and serine proteases. J. Immunol., 2009. **183**(3): p. 1739-50.
109. Shore, S.A., Direct effects of Th2 cytokines on airway smooth muscle. Curr. Opin. Pharmacol., 2004. **4**(3): p. 235-240.
110. Atherton, H.C., G. Jones, and H. Danahay, IL-13-induced changes in the goblet cell density of human bronchial epithelial cell cultures: MAP kinase and phosphatidylinositol 3-kinase regulation. Am. J. Physiol. Lung Cell. Mol. Physiol., 2003. **285**(3): p. L730-9.
111. Hovenberg, H.W., *et al*., MUC5AC, but not MUC2, is a prominent mucin in respiratory secretions. Glycoconj. J., 1996. **13**(5): p. 839-47.
112. Nielsen, P.A., *et al*., Identification of a major human high molecular weight salivary mucin (MG1) as tracheobronchial mucin MUC5B. Glycobiology, 1997. **7**(3): p. 413-9.
113. Okuda, K., W.J., *et al.*, Localization of secretory mucins MUC5AC and MUC5B in normal/healthy human airways. Am. J. Respir. Crit. Care Med., 2018. **199**(6): p. 715-727.

114. Ordonez, C.L., *et al*., Mild and moderate asthma is associated with airway goblet cell hyperplasia and abnormalities in mucin gene expression. Am. J. Respir. Crit. Care Med., 2001. **163**(2): p. 517-23.
115. Wan, H., *et al*., Foxa2 regulates alveolarization and goblet cell hyperplasia. Development, 2004. **131**(4): p. 953-64.
116. Zhen, G., *et al*., IL-13 and epidermal growth factor receptor have critical but distinct roles in epithelial cell mucin production. Am J. Respir. Cell. Mol. Biol., 2007. **36**(2): p. 244-53.
117. Yu, H., *et al*., Interleukin-13 induces mucin 5AC production involving STAT6/SPDEF in human airway epithelial cells. Cell. Commun. Adhes., 2010. **17**(4-6): p. 83-92.
118. Barnes, P.J., Neuroeffector mechanisms: the interface between inflammation and neuronal responses. J. Allergy Clin. Immunol., 1996. **98**(5 Pt 2): p. S73-81
119. Carroll, N.G., C. Cooke, and A.L. James, Bronchial blood vessel dimensions in asthma. Am. J. Respir. Crit. Care. Med., 1997. **155**(2): p. 689-95.
120. Fitzpatrick, A.M., *et al*., Features of severe asthma in school-age children: Atopy and increased exhaled nitric oxide. J. Allergy. Clin. Immunol., 2006. **118**(6): p. 1218-25.
121. Reddel, H.K., *et al*., An official American Thoracic Society/European Respiratory Society statement: asthma control and exacerbations: standardizing endpoints for clinical asthma trials and clinical practice. Am J. Respir. Crit. Care Med., 2009. **180**(1): p. 59-99.
122. Adcock, I.M., *et al*., Steroid resistance in asthma: mechanisms and treatment options. Curr. Allergy Asthma Rep., 2008. **8**(2): p. 171-8.
123. Chakir, J., *et al*., Airway remodeling-associated mediators in moderate to severe asthma: effect of steroids on TGF-beta, IL-11, IL-17, and type I and type III collagen expression. J. Allergy Clin. Immunol., 2003. **111**(6): p. 1293-8.
124. Al-Ramli, W., *et al*., T(H)17-associated cytokines (IL-17A and IL-17F) in severe asthma. J. Allergy Clin. Immunol., 2009. **123**(5): p. 1185-7.
125. Schleich, F., *et al.*, Heterogeneity of phenotypes in severe asthmatics. The Belgian Severe Asthma Registry (BSAR). Respir. Med., 2014. **108**(12): p. 1723-32.
126. Vroman, H., B. van den Blink, and M. Kool, Mode of dendritic cell activation: the decisive hand in Th2/Th17 cell differentiation. Implications in asthma severity? Immunobiology, 2015. **220**(2): p. 254-61.
127. Veldhoen, M., *et al*., TGFbeta in the context of an inflammatory cytokine milieu supports de novo differentiation of IL-17-producing T cells. Immunity, 2006. **24**(2): p. 179-89.
128. Lee, JY., *et al*., Serum amyloid A proteins induce pathogenic Th17 cells and promote inflammatory disease. Cell, 2020. **180**(1): p. 79-91.
129. Mitzutani, N., *et al.*, Complement-induced IL-17 plays a role in an IgE-mediated late-phase asthmatic response and airways hyperresponsiveness via neutrophilic inflammation in mice. J. Immunol., 2012. **188**(11): p. 5694-5705.
130. Lajoie, S., *et al.*, Complement-mediated regulation of the IL-17A axis is a central genetic determinant of the severity of experimental allergic asthma. Nat. Immunol., 2010. **11**(10): p. 928-35.
131. Hall, S.L., *et al.*, IL-17A enhances IL-13 activity by enhancing IL-13-induced signal transducer and activator of transcription 6 activation. J. Allergy. Clin. Immunol., 2017. **139**(2): p. 462-471 e14.
132. Fujisawa, T., *et al*., Regulation of airway MUC5AC expression by IL-1beta and IL-17A; the NF-kappaB paradigm. J. Immunol., 2009. **183**(10): p. 6236-43.
133. Pelletier, M., *et al*., Evidence for a cross-talk between human neutrophils and Th17 cells. Blood, 2010. **115**(2): p. 335-43.
134. Stoppelnburg, A.J. *et al*., Local IL-17A potentiates early neutrophil recruitment to the repiratory tract during severe RSV infection. Plos ONE, 2013. **8**(10): p. 1-10.
135. McAllister, F., *et al.*, Role of IL-17A, IL-17F, and the IL-17 receptor in regulating growth-related oncogene-alpha and granulocyte colony-stimulating factor in bronchial epithelium:

implications for airway inflammation in cystic fibrosis. J. Immunol., 2005. **175**(1): p. 404-12.
136. Fossiez, F., *et al*., T cell interleukin-17 induces stromal cells to produce proinflammatory and hematopoietic cytokines. J. Exp. Med., 1996. **183**(6): p. 2593-603.
137. Zosky, G.R. and P.D. Sly, Animal models of asthma. Clin. Exp. Allergy, 2007. **37**(7): p. 973-88.
138. Tsitoura, D.C., *et al*., Mechanisms preventing allergen-induced airways hyperreactivity: role of tolerance and immune deviation. J. Allergy Clin. Immunol., 2000. **106**(2): p. 239-46.
139. Stevenson, C.S. and M.A. Birrell, Moving towards a new generation of animal models for asthma and COPD with improved clinical relevance. Pharmacol. Ther., 2011. **130**(2): p. 93-105.
140. Gregory, L.G. and C.M. Lloyd, Orchestrating house dust mite-associated allergy in the lung. Trends Immunol., 2011. **32**(9): p. 402-11.
141. Yasue, M., *et al.*, Comparison of sensitization to crude and purified house dust mite allergens in inbred mice. Lab. Anim. Sci., 1998. **48**(4): p. 346-52.
142. Atochina, E.N., *et al*., Attenuated allergic airway hyperresponsiveness in C57BL/6 mice is associated with enhanced surfactant protein (SP)-D production following allergic sensitization. Respir. Res., 2003. **4**: p. 15.
143. Sahu, N., *et al*., Modeling susceptibility versus resistance in allergic airway disease reveals regulation by Tec kinase Itk. PLoS One, 2010. **5**(6): p. e11348.
144. Birrell, M.A., A.J. Van Oosterhout, and M.G. Belvisi, Do the current house dust mite-driven models really mimic allergic asthma? Eur. Respir. J., 2010. **36**(5): p. 1220-1.
145. Cates, E.C., *et al.*, Intranasal exposure of mice to house dust mite elicits allergic airway inflammation via a GM-CSF-mediated mechanism. J. Immunol., 2004. **173**(10): p. 6384-92.
146. Shinagawa, K. and Kojima, M, Mouse model of airway remodeling: strain differences. Am. J. Respir. Crit. Care Med., 2003.**168**(8): p. 959-967.
147. Piyadasa, H., *et al.*, Biosignature for airway inflammation in a house dust mite-challenged murine model of allergic asthma. Biol. Open, 2016. **5**(2): p. 112-21.
148. Gronlund, M.M., *et al*., Fecal microflora in healthy infants born by different methods of delivery: permanent changes in intestinal flora after cesarean delivery. J. Pediatr. Gastroenterol Nutr., 1999. **28**(1): p. 19-25.
149. Moossavi, S., *et al*., Composition and Variation of the Human Milk Microbiota Are Influenced by Maternal and Early-Life Factors. Cell Host Microbe, 2019. **25**(2): p. 324-335.e4.
150. Sender, R., S. Fuchs, and R. Milo, Revised Estimates for the Number of Human and Bacteria Cells in the Body. PLoS Biol, 2016. **14**(8): p. e1002533.
151. Palmer, C., et al., Development of the human infant intestinal microbiota. PLoS Biol., 2007. **5**(7): p. e177.
152. Kurokawa, K., *et al*., Comparative metagenomics revealed commonly enriched gene sets in human gut microbiomes. DNA Res., 2007. **14**(4): p. 169-81.
153. Hansen, C.H., *et al*., Patterns of early gut colonization shape future immune responses of the host. PLoS One, 2012. **7**(3): p. e34043.
154. Karlsson, M.R., *et al*., Neonatal colonization of rats induces immunological tolerance to bacterial antigens. Eur. J. Immunol., 1999. **29**(1): p. 109-18.
155. Bach, J.F., The effect of infections on susceptibility to autoimmune and allergic diseases. New Engl. J .Med., 2002. **347**(12): p. 911-20.
156. Strachan, D.P., Hay fever, hygiene, and household size. Bmj, 1989. **299**(6710): p. 1259-60.
157. Romagnani, S., Human TH1 and TH2 subsets: regulation of differentiation and role in protection and immunopathology. Int. Arch. Allergy Immunol., 1992. **98**(4): p. 279-85.

158. von Mutius, E., *et al.*, Exposure to endotoxin or other bacterial components might protect against the development of atopy. Clin. Exp. Allergy, 2000. **30**(9): p. 1230-4.
159. Scudellari, M., *News Feature:* Cleaning up the hygiene hypothesis*.* Proc. Natl. Acad. Sci. U S A, 2017. **114**(7): p. 1433-1436.
160. Stein, M., *et al*., Innate Immunity and Asthma Risk in Amish and Hutterite Farm Children. New Engl. J. Med., 2016. 375: p. 411-421.
161. Arrieta, M.C., *et al.*, Early infancy microbial and metabolic alterations affect risk of childhood asthma. Sci. Transl. Med., 2015. **7**(307): p. 307ra152.
162. Dominguez-Bello, M.G., *et al*., Delivery mode shapes the acquisition and structure of the initial microbiota across multiple body habitats in newborns. Proc. Natl. Acad. Sci. U S A, 2010. **107**(26): p. 11971-5.
163. West, C.E., D.J. Videky, and S.L. Prescott, Role of diet in the development of immune tolerance in the context of allergic disease*.* Curr. Opin. Pediatr., 2010. **22**(5): p. 635-41.
164. Bener, A., *et al.*, Role of breast feeding in primary prevention of asthma and allergic diseases in a traditional society*.* Eur. Ann. Allergy Clin. Immunol., 2007. **39**(10): p. 337-43.
165. McKeever, T.M., *et al.*, The importance of prenatal exposures on the development of allergic disease: a birth cohort study using the West Midlands General Practice Database. Am. J. Respir. Crit .Care Med., 2002. **166**(6): p. 827-32.
166. Kozyrskyj, A.L., P. Ernst, and A.B. Becker, Increased risk of childhood asthma from antibiotic use in early life*.* Chest, 2007. **131**(6): p. 1753-9.
167. Marra, F., *et al*., Antibiotic use in children is associated with increased risk of asthma. Pediatrics, 2009. **123**(3): p. 1003-10.
168. Martel, M.J., *et al.*, Determinants of the incidence of childhood asthma: a two-stage case-control study. Am. J .Epidemiol., 2009. **169**(2): p. 195-205.
169. Rusconi, F., *et al*., Paracetamol and antibiotics in childhood and subsequent development of wheezing/asthma: association or causation? Int. J. Epidemiol., 2011. **40**(3): p. 662-7.
170. Stensballe, L.G., *et al.*, Use of antibiotics during pregnancy increases the risk of asthma in early childhood. J. Pediatr., 2013. **162**(4): p. 832-838.e3.
171. Makino, H., *et al*., Mother-to-infant transmission of intestinal bifidobacterial strains has an impact on the early development of vaginally delivered infant's microbiota. PLoS One, 2013. **8**(11): p. e78331.
172. Dogaru, C.M., *et al*., Breastfeeding and childhood asthma: systematic review and meta-analysis. Am. J. Epidemiol., 2014. **179**(10): p. 1153-67.
173. Seyedrezazadeh, E., *et al.*, Fruit and vegetable intake and risk of wheezing and asthma: a systematic review and meta-analysis. Nutr. Rev., 2014. **72**(7): p. 411-28.
174. Laursen, M.F., *et al.*, Having older siblings is associated with gut microbiota development during early childhood*.* BMC microbiology, 2015. **15**: p. 154-154.
175. Holscher, B., *et al.*, Exposure to pets and allergies in children*.* Pediatr. Allergy Immunol., 2002. **13**(5): p. 334-41.
176. Genuneit, J., Exposure to farming environments in childhood and asthma and wheeze in rural populations: a systematic review with meta-analysis*.* Pediatr. Allergy Immunol., 2012. **23**(6): p. 509-18.
177. Enders, R.H., *et al.*, Placental amino acid uptake. III. Transport systems for neutral amino acids. Am. J. Physiol., 1976. **230**(3): p. 706-10.
178. Hill, E.P. and L.D. Longo, Dynamics of maternal-fetal nutrient transfer. Fed. Proc., 1980. **39**(2): p. 239-44.
179. Malek, A., Role of IgG antibodies in association with placental function and immunologic diseases in human pregnancy. Expert. Rev. Clin. Immunol., 2013. **9**(3): p. 235-49.
180. Ardissone, A.N., *et al.*, Meconium microbiome analysis identifies bacteria correlated with premature birth*.* PLoS One, 2014. **9**(3): p. e90784.
181. Hu, J., *et al.*, Diversified microbiota of meconium is affected by maternal diabetes status*.* PLoS One, 2013. **8**(11): p. e78257.

182. Jimenez, E., *et al.*, Is meconium from healthy newborns actually sterile? Res. Microbiol., 2008. **159**(3): p. 187-93.
183. Lauder, A.P., *et al.*, Comparison of placenta samples with contamination controls does not provide evidence for a distinct placenta microbiota. Microbiome, 2016. **4**(1): p. 29.
184. Gomez de Aguero, M., *et al.*, The maternal microbiota drives early postnatal innate immune development. Science, 2016. **351**(6279): p. 1296-302.
185. Wang, J., *et al.*, Aryl hydrocarbon receptor/IL-22/Stat3 signaling pathway is involved in the modulation of intestinal mucosa antimicrobial molecules by commensal microbiota in mice. Innate Immun., 2018. **24**(5): p. 297-306.
186. Bouskra, D., *et al*., Lymphoid tissue genesis induced by commensals through NOD1 regulates intestinal homeostasis. Nature, 2008. **456**(7221): p. 507-10.
187. Falk, P.G., *et al*., Creating and maintaining the gastrointestinal ecosystem: what we know and need to know from gnotobiology. Microbiol Mol Biol Rev, 1998. **62**(4): p. 1157-70.
188. Nuriel-Ohayon, M., H. Neuman, and O. Koren, Microbial Changes during Pregnancy, Birth, and Infancy. Front. Microbiol., 2016. **7**: p. 1031.
189. Sakwinska, O., *et al*., Does the maternal vaginal microbiota play a role in seeding the microbiota of neonatal gut and nose? Benef. Microbes, 2017. **8**(5): p. 763-778.
190. Roduit, C., *et al.*, High levels of butyrate and propionate in early life are associated with protection against atopy. Allergy, 2019. **74**(4): p. 799-809.
191. Trompette, A., *et al.*, Gut microbiota metabolism of dietary fiber influences allergic airway disease and hematopoiesis. Nat. Med., 2014. **20**(2): p. 159-66.
192. Lindh, E., Increased risistance of immunoglobulin A dimers to proteolytic degradation after binding of secretory component. J. Immunol., 1975. **114**(1 Pt 2): p. 284-6.
193. Rogier, E.W., *et al*., Lessons from mother: Long-term impact of antibodies in breast milk on the gut microbiota and intestinal immune system of breastfed offspring. Gut microbes, 2014. **5**(5): p. 663-668.
194. Corthesy, B., Role of secretory IgA in infection and maintenance of homeostasis. Autoimmun. Rev., 2013. **12**(6): p. 661-5.
195. Crabbe, P.A., *et al*., Immunohistochemical observations on lymphoid tissues from conventional and germ-free mice. Lab. Invest., 1970. **22**(5): p. 448-57.
196. Fagundes, C., *et al*., Transient TLR Activation Restores Inflammatory Response and Ability To Control Pulmonary Bacterial Infection in Germfree Mice. J. Immunol. (Baltimore, Md. : 1950), 2011. **188**: p. 1411-20.
197. Gray, J., *et al.*, Intestinal commensal bacteria mediate lung mucosal immunity and promote resistance of newborn mice to infection. Sci. Transl. Med., 2017. **9**(376).
198. Villey, I., R. de Chasseval, and J.P. de Villartay, RORgammaT, a thymus-specific isoform of the orphan nuclear receptor RORgamma / TOR, is up-regulated by signaling through the pre-T cell receptor and binds to the TEA promoter. Eur. J. Immunol., 1999. **29**(12): p. 4072-80.
199. van Rijt, L.S. and B.N. Lambrecht, Dendritic cells in asthma: a function beyond sensitization. Clin. Exp. Allergy, 2005. **35**(9): p. 1125-34.
200. Amenyogbe, N., T.R. Kollmann, and R. Ben-Othman, Early-Life Host–Microbiome Interphase: The Key Frontier for Immune Development. Front. in Ped., 2017. **5**(111).
201. Hufnagl, K., *et al.*, Dysbiosis of the gut and lung microbiome has a role in asthma. Seminars in Immunopathology, 2020. **42**(1): p. 75-93.
202. Tan, J., *et al.*, Dietary Fiber and Bacterial SCFA Enhance Oral Tolerance and Protect against Food Allergy through Diverse Cellular Pathways. Cell Rep., 2016. **15**(12): p. 2809-24.
203. Ohata, A., M. Usami, and M. Miyoshi, Short-chain fatty acids alter tight junction permeability in intestinal monolayer cells via lipoxygenase activation. Nutrition, 2005. **21**(7-8): p. 838-47.

204. Peng, L., *et al*., Butyrate enhances the intestinal barrier by facilitating tight junction assembly via activation of AMP-activated protein kinase in Caco-2 cell monolayers. The Journal of nutrition, 2009. **139**(9): p. 1619-1625.
205. Mirpuri, J., *et al.*, Proteobacteria-specific IgA regulates maturation of the intestinal microbiota. Gut Microbes, 2014. **5**(1): p. 28-39.
206. Roger, L.C., et al., Examination of faecal Bifidobacterium populations in breast- and formula-fed infants during the first 18 months of life. Microbiology, 2010. **156**(Pt 11): p. 3329-41.
207. Rogier, E.W., *et al.*, Secretory antibodies in breast milk promote long-term intestinal homeostasis by regulating the gut microbiota and host gene expression. Proc. Natl. Acad. Sci., 2014. **111**(8): p. 3074-3079.
208. Roux, M.E., *et al*., Origin of IgA-secreting plasma cells in the mammary gland. J. Exp. Med., 1977. **146**(5): p. 1311-1322.
209. Harris, N.L., *et al.*, Mechanisms of Neonatal Mucosal Antibody Protection. The Journal of Immunology, 2006. **177**(9): p. 6256-6262.
210. Hapfelmeier, S., *et al.*, Reversible microbial colonization of germ-free mice reveals the dynamics of IgA immune responses. Science, 2010. **328**(5986): p. 1705-9.
211. Atarashi, K., *et al.*, Induction of colonic regulatory T cells by indigenous Clostridium species. Science, 2011. **331**(6015): p. 337-41.
212. Smith, P.M., *et al*., The microbial metabolites, short-chain fatty acids, regulate colonic Treg cell homeostasis. Science, 2013. **341**(6145): p. 569-73.
213. Davie, J.R., Inhibition of histone deacetylase activity by butyrate. J. Nutr., 2003. **133**(7 Suppl): p. 2485s-2493s.
214. Furusawa, Y., *et al.*, Commensal microbe-derived butyrate induces the differentiation of colonic regulatory T cells. Nature, 2013. **504**(7480): p. 446-50.
215. Weng, M. and W.A. Walker, The role of gut microbiota in programming the immune phenotype. J. Dev. Or. Health Disease, 2013. **4**(3): p. 203-214.
216. ROY, C., *et al*., β-Lactamases and snsceptibility phenotypes to β-lactam antibiotics in Escherichia coli strains. Journal of Antimicrobial Chemotherapy, 1992. **29**(5): p. 593-594.
217. Wilson, D.N., Ribosome-targeting antibiotics and mechanisms of bacterial resistance. Nat. Rev. Microbiol., 2014. **12**(1): p. 35-48.
218. Watanakunakorn, C., The antibacterial action of vancomycin. Rev. Infect. Dis., 1981. **3** suppl: p. S210-5.
219. MacAulay, M.A., M. Abou-Sabe, and D. Charles, Placental transfer of ampicillin. Am. J. Obstet. Gynecol., 1966. **96**(7): p. 943-50.
220. Czeizel, A.E., *et al.*, A population-based case-control teratologic study of ampicillin treatment during pregnancy. Am. J. Obstet. Gynecol., 2001. **185**(1): p. 140-7.
221. Craig, W.A., Optimizing aminoglycoside use. Crit. Care Clin., 2011. **27**(1): p. 107-21.
222. Geraci, J.E., *et al*., Some laboratory and clinical experiences with a new antibiotic, vancomycin. Antibiot. Annu., 1956: p. 90-106.
223. Nahum, G.G., K. Uhl, and D.L. Kennedy, Antibiotic use in pregnancy and lactation: what is and is not known about teratogenic and toxic risks. Obstet. Gynecol., 2006. **107**(5): p. 1120-38.
224. Nichoga, L.A., A.M. Skosyreva, and S.D. Voropaeva, Transplacental passage of gentamicin and its effect on the fetus. Antibiotiki, 1982. **27**(12): p. 46-50.
225. Joshi, M.D., *et al.*, Evaluation of Fetal and Maternal Vancomycin-Induced Kidney Injury during Pregnancy in a Rat Model. Antimicrob. Agents Chemother., 2019. **63**(10).
226. American College of Obstetricians and Gynecologists. 2017.
227. Gon, Y. and S. Hashimoto, Role of airway epithelial barrier dysfunction in pathogenesis of asthma. Allergol. Int., 2018. **67**(1): p. 12-17.
228. Heyman, M., Gut barrier dysfunction in food allergy. Eur. J. of Gastroent. Hep., 2005. **17**(12).

229. Peng, L., *et al*., Butyrate enhances the intestinal barrier by facilitating tight junction assembly via activation of AMP-activated protein kinase in Caco-2 cell monolayers*.* J. Nutr., 2009. **139**(9): p. 1619-25.
230. Ewaschuk, J.B., *et al*., Secreted bioactive factors from Bifidobacterium infantis enhance epithelial cell barrier function. Am. J. Physiol. Gastrointest. Liver Physiol., 2008. **295**(5): p. G1025-34.
231. Khonsari, S., *et al.*, A comparative study of bifidobacteria in human babies and adults*.* Biosci. Microbiota Food Health, 2016. **35**(2): p. 97-103.
232. Le Huerou-Luron, I., S. Blat, and G. Boudry, Breast- v. formula-feeding: impacts on the digestive tract and immediate and long-term health effects*.* Nutr. Res. Rev., 2010. **23**(1): p. 23-36.
233. Cario, E., Barrier-protective function of intestinal epithelial Toll-like receptor 2*.* Mucosal Immunology, 2008. 1 Suppl **1**: p. S62-6.
234. Ji, Y., et al., Diet-induced alterations in gut microflora contribute to lethal pulmonary damage in TLR2/TLR4-deficient mice. Cell Rep., 2014. **8**(1): p. 137-149.
235. Valenzano, M.C., *et al*., Remodeling of Tight Junctions and Enhancement of Barrier Integrity of the CACO-2 Intestinal Epithelial Cell Layer by Micronutrients*.* PloS one, 2015. **10**(7): p. e0133926-e0133926.
236. Georas, S.N. and F. Rezaee, Epithelial barrier function: at the front line of asthma immunology and allergic airway inflammation. J. Allergy Clin. Immunol., 2014. **134**(3): p. 509-520.
237. Menard, S., N. Cerf-Bensussan, and M. Heyman, Multiple facets of intestinal permeability and epithelial handling of dietary antigens. Mucosal Immunol, 2010. **3**(3): p. 247-59.
238. Perrier, C. and B. Corthesy, Gut permeability and food allergies*.* Clin. Exp. Allergy, 2011. **41**(1): p. 20-8.
239. Russell, S.L., *et al*., Early life antibiotic-driven changes in microbiota enhance susceptibility to allergic asthma*.* EMBO Rep, 2012. **13**(5): p. 440-7.
240. Alhasan, M.M., *et al.*, Antibiotic use during pregnancy increases offspring asthma severity in a dose-dependent manner*.* Allergy, 2020. **75**(8): p. 1979-1990.
241. Schmudde, I., *et al.*, C5a receptor signalling in dendritic cells controls the development of maladaptive Th2 and Th17 immunity in experimental allergic asthma. Mucosal Immunol., 2013. **6**(4): p. 807-25.
242. Sutton, C.E., L.A. Mielke, and K.H. Mills, IL-17-producing γδ T cells and innate lymphoid cells*.* Eur. J. Immunol., 2012. **42**(9): p. 2221-31.
243. Jones, G.W., *et al*., Loss of CD4+ T cell IL-6R expression during inflammation underlines a role for IL-6 trans signaling in the local maintenance of Th17 cells*.* J. Immunol., 2010. **184**(4): p. 2130-9.
244. Sutton, C.E., L.A. Mielke, and K.H. Mills, IL-17-producing gammadelta T cells and innate lymphoid cells*.* Eur. J. Immunol., 2012. **42**(9): p. 2221-31.
245. Vermijlen, D. and I. Prinz, Ontogeny of Innate T Lymphocytes - Some Innate Lymphocytes are More Innate than Others*.* Front. Immunol., 2014. **5**: p. 486-486.
246. Zanvit, P., *et al.*, Antibiotics in neonatal life increase murine susceptibility to experimental psoriasis. Nat. Commun., 2015. **6**: p. 8424.
247. Evans, C.M., *et al.*, The polymeric mucin Muc5ac is required for allergic airway hyperreactivity*.* Nat. Commun., 2015. **6**: p. 6281.
248. Yang, X.O., *et al.*, T helper 17 lineage differentiation is programmed by orphan nuclear receptors ROR alpha and ROR gamma. Immunity, 2008. **28**(1): p. 29-39.
249. Kuyper, L.M., *et al.*, Characterization of airway plugging in fatal asthma*.* Am. J. Med., 2003. **115**(1): p. 6-11.
250. Wenzel, S.E., *et al.*, Evidence that severe asthma can be divided pathologically into two inflammatory subtypes with distinct physiologic and clinical characteristics. Am. J. Respir. Crit. Care Med., 1999. **160**(3): p. 1001-8.

251. Li, W., R.N. Germain, and M.Y. Gerner, High-dimensional cell-level analysis of tissues with Ce3D multiplex volume imaging. Nat. Protoc., 2019. **14**(6): p. 1708-1733.

10 Appendix

10.1 Supplement

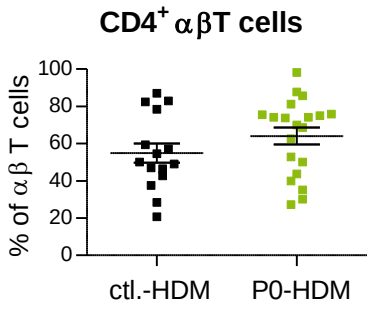

Fig. 10.1: Analysis of the CD4⁺ subpopulation of αβT cells.
Lung tissue of C57BL/6 control or P0 mice treated with PBS or HDM was harvested and single cell suspensions were restimulated with PMA (50 ng/mL) and ionomycin (0.5 µg/mL), intracellularly stained for IL-13 and IL-17A. The cells were analyzed by flow cytometry. Lymphocytes identified by CD90.2 expression were analyzed regarding their IL-17A positivity. To further differentiate IL-17A⁺ populations of HDM-immunized mice, CD3 and TCRβ expression was analyzed to identify CD3⁺TCRβ⁺ αβT cells to identify CD4⁺ T cells. ctl.=control. Mean and SEM shown. Student T test.

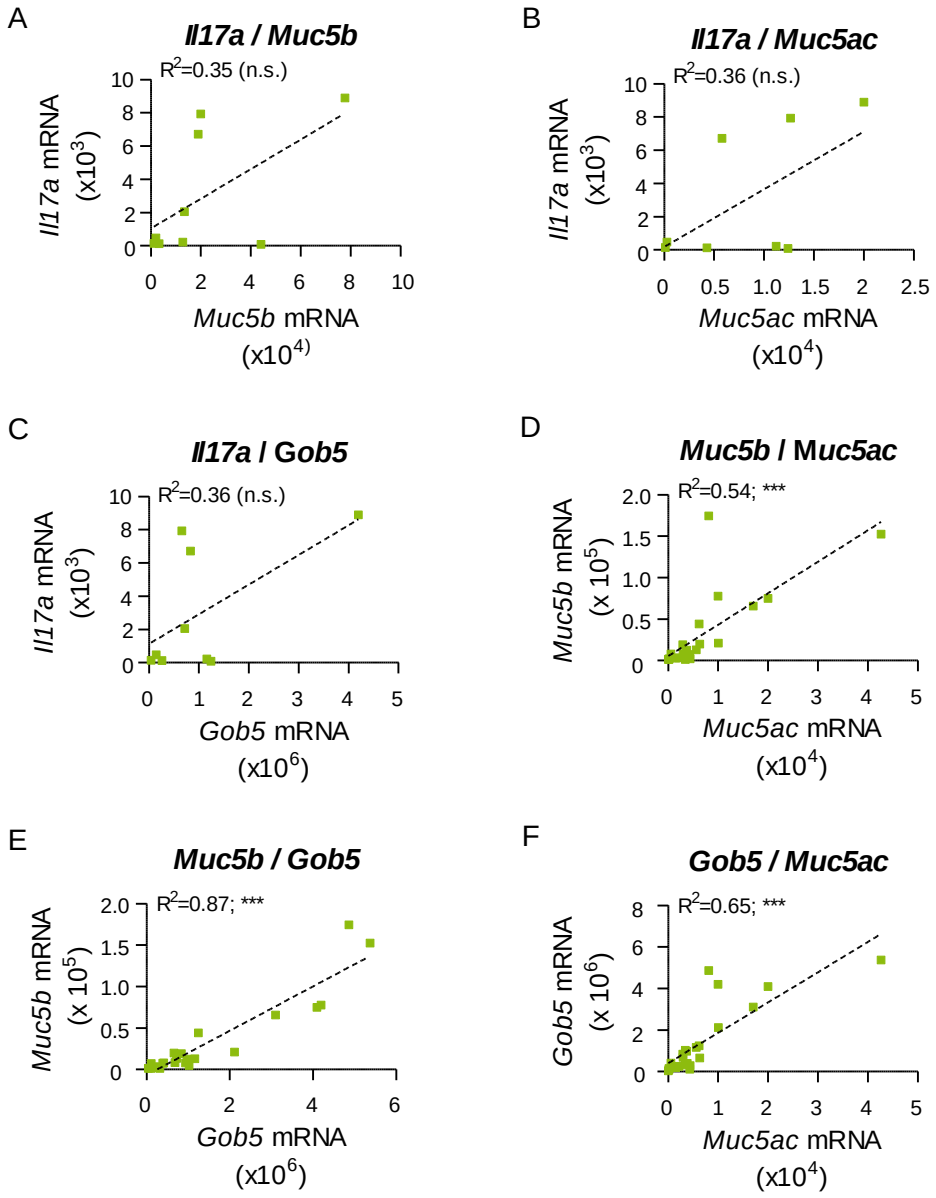

Fig. 10.2: Correlation analysis of *Il17a* and mucus gene expression of P0-HDM mice.
For P0-HDM mice, *Il17a* mRNA was correlated with *Muc5b* [A], *Muc5ac* [B], and *Gob5* [C]. The tree mucus-related genes were also correlated: *Muc5b* mRNA was correlated with *Muc5ac* [D], and with *Gob5* mRNA [E]. *Gob5* mRNA was correlated with *Muc5ac* [F]. Pearson correlation (***p < 0.001).

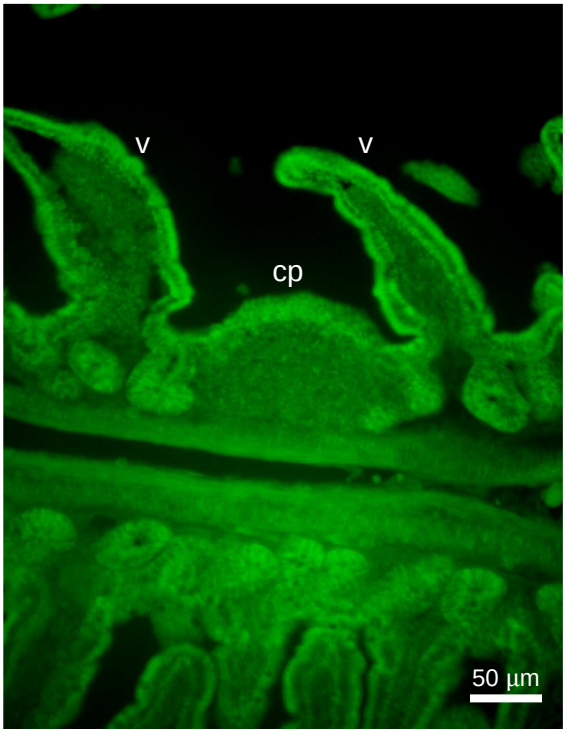

Fig. 10.3: Intestinal cryptopatch surrounded by villi, visible by tissue autofluorescence.
18 µm cryosection of intestinal tissue visible by tissue-intrinsic autofluorescence. The crypt-like appearance of cryptopatches was the morphological characteristic for the identification of the anatomical structures intestinal RORγt^{+} expectedly localized to. The cryptopatch is surrounded by intestinal villi. cp=cryptopatch. v=villus.

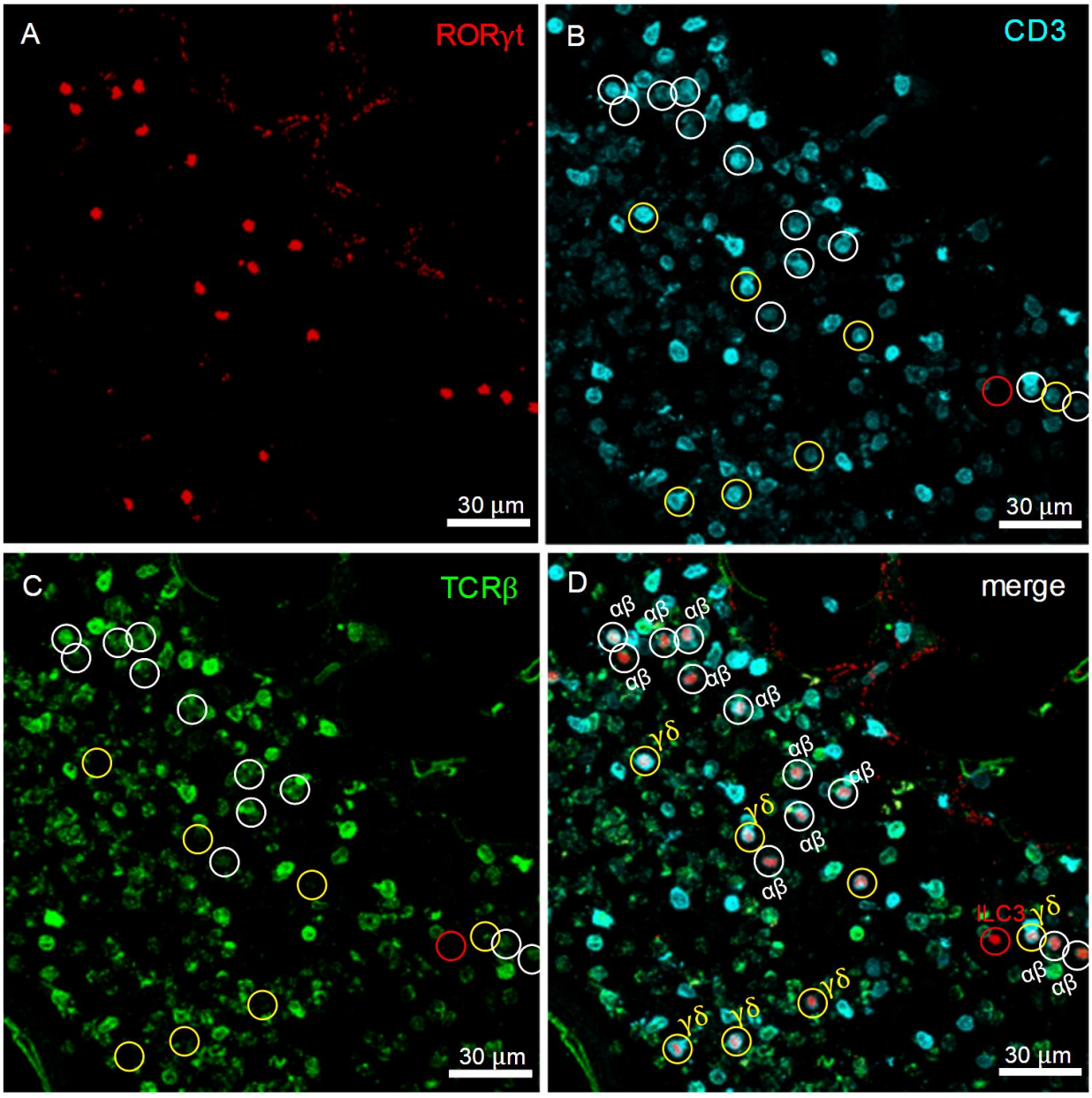

Fig. 10.4: Analysis of pulmonary RORγt-expressing cells in regard of the subpopulations that express RORγt. 300 µm lung sections of C57BL/6 HDM-immunized mice (n=2) were incubated with a RORγt [A], CD3 [B], and TCRβ [C] antibodies. A merged overview is shown [D]. Z-stacks were generated with the laser scanning confocal microscope and analyzed using Imaris software. White circles mark αβT cells, yellow circles mark γδT cells, and the red circle marks an ILC3.

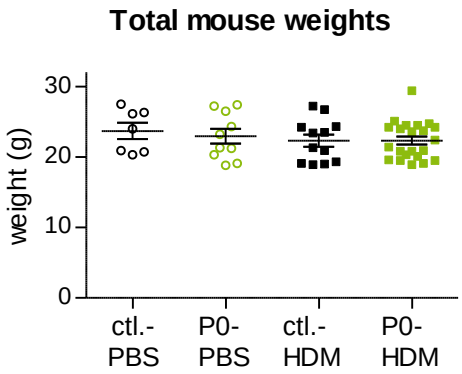

Fig. 10.5: Total mouse weights at the time of lung-function measurements.
Before lung function measurements were performed, the body weight of C57BL/6 control and P0 mice treated with PBS or HDM was noted.

10.2 Abbreviations

Table 10.1: Abbreviations

ACK	Ammonium-Chloride-Potassium
AF	Alexa Fluor
AhR	Aryl hydrocarbon receptor
APC	Allophycocyanin
BAL	Bronchoalveolar lavage
BCR	B cell receptor
BSA	Bovine Serum Albumin
BV	Brilliant Violet
C3	Complement 3
CCHMC	Cincinnati Children's Medical Center
CD	Cluster of differentiation
Cp	Crossing point
DC	Dendritic cell
DNA	Desoxyribonucleic acid
dNTP	Deoxyriobonucleotide triphosphate
3D	3 dimensional
DTT	Dithiothreitol
E	Embryonic day
ELISA	Enzyme-linked Immunoabsorbance Assay
FBS	Fetal Bovine Serum
FITC	Albumin-fluorescin isothiocanate conjugate

continued

FoxP 3	Forkhead-box protein
GATA3	GATA binding protein
GFP	Green fluorescence protein
HDM	House dust mite
HRP	Horseradish Peroxidase
i.t	*intratracheal*
i.v	*intravenous*
IACUC	Institutional Animal Care and Use Committee
Ig	Immunoglobulin
Ig	Immunoglobulin
IHC	Immunohistochemistry
IL	Interleukin
ILC	Innate lymphoid cell
Inc	Incorporate
L-Glut	L-Glutamine
LSM	Laser scanning microscope
mAb	Monoclonal antibody
MHC	Major histocompatibility complex
Muc	Mucin
NOD	Nucleotide-binding oligomerization domain
OCT	Optimal cutting temperature
OD	Optical density
OVA	Ovalbumin
P	Postnatal day
pAb	Polyclonal antibody
Pe	Phycoerythrin
PBS	Phosphate buffered saline
PCR	Polymerase chain reaction
Pen	Penicillin
PFA	Paraformaldehyde
PMA	Phorbol 12-myristate 13-acetate
PRR	Pattern recognition receptor
R	Receptor
RA	Retinoic acid
Rbbt	Rabbit
RNA	Ribonucleic acid
ROR	Retinoid-related orphan receptor
ROS	Reactive oxygen species
R_{RS}	Respiratory system resistance
RT	Room temperature
RT-qPCR	Real time-quantitative PCR
S	Ribosomal protein

continued

SCFAs	Short-chain fatty acids
SM	Smooth muscle
αSMA	α-smooth muscle actin
SPF	Specific-pathogen free
Strep	Streptomycin
syr. hamster	Syrian hamster
TCR	T cell receptor
TGF-β	Transforming growth factor-β
T_H	T helper cell
TLR	Toll-like receptors
Tm	Melting temperature
T_{Reg}	Regulatory T cells
TSLP	Thymic stromal lymphopoeitin
USDA	United States Department of Agriculture
USP	United States Pharmacopeia
wt	wildtype

10.3 List of figures

Fig. 10.5: Total mouse weights at the time of lung-function measurements.

10.4 List of tables

Acknowledgements

I would like to thank the following people for their support during the experimental phase and the writing of this thesis:

First, I would like to thank Prof. Dr. Peter König for his mentorship, support with experimental planning, results discussion, and thesis writing.

Second, I would like to thank the second referee of this thesis, Prof. Dr. Jens Mittag.

I would like to thank Ian Lewkowich for his mentorship and providing the possibility to work in his laboratory at the Department of Immunobiology, CCHMC, Cincinnati, for one year.

Julie Hargis did the flexiVent measurements, Dasom Kim did the RT-qPCR analysis, and Ian Lewkowich helped with the flow cytometry experiments and evaluation.

I would like to thank Inken Schmudde, Jaclyn McAlees, Hanna Ulrich, Sophia Eggert, and Adrienne Wilburn for helping with the experiments, data analysis or thesis writing.

Finally, I would like to thank my family for their constant support.